Title
ELECTROCHROMATOGRAPHIC SEPARATIONS OF RAEE EARTHS

Authors
Nady, Louie
Vermeulen, Theodore R.

Publication Date
1970-05-01

UCRL-19526

c.2

ELECTROCHROMATOGRAPHIC SEPARATIONS OF RARE EARTHS

Louie Nady* and Theodore R. Vermeulen

May 1970

AEC Contract No. W-7405-eng-48

*Filed as a Ph.D. Thesis

LAWRENCE RADIATION LABORATORY
UNIVERSITY of CALIFORNIA BERKELEY

UCRL-19526 c.2

DISCLAIMER

ELECTROCHROMATOGRAPHIC SEPARATIONS OF RARE EARTHS

Contents

Abstract v

Notation vii

I. Electrochromatography. 1

Criteria for Apparatus Design. 2

"Ribbon" Separation Units. 9

Block Units. 11

Concentration-Polarization Separations 25

Continuous Ligand Electrochromatography. 33

References 38

II. Mobility of Trivalent-Monovalent Cation Mixtures on Ion Exchangers 41

Introduction 41

Particle Conductivity vs. Bed Conductivity 42

Ion Mobility from Particle Conductivity. 43

Apparatus. 44

Results on Single-Counter-Ion Systems. 50

Mobilities and Diffusivities 61

Results for Mixtures of Ions 63

References 69

III. Sorption of Simple and Complexed Ions by Ion Exchangers 70

Introduction 70

Theory of Donnan Uptake and Complexing 71

The second advance is the development and operation of a continuous preparative-scale ligand electrochromatograph. Continuous separation is achieved in this unit as a result of transverse electrophoretic migration of uncomplexed rare earth ions across a laminar flow of complexing agent in a packed bed. Selective complex formation with the ion mixture (with a resultant marked mobility change for the complexed species) causes the net electrophoretic migration rates to differ for each component, hence separates them. Zones of relatively pure Ce^{+++} and La^{+++}, in different runs, have been achieved from mixtures of the two ions, using EDTA as the ligand.

NOTATION

$a\pm$	activity of electrolyte in solution
$\bar{a}\pm$	activity of electrolyte in resin phase
a_w	activity of water in solution phase
$\bar{a}_w$	activity of water in resin phase
C_i	equivalent concentration of i in solution
$\bar{C}_i$	equivalent concentration of i in resin phase
C_i^*	equivalent concentration of total complexed ions containing i species
Co	total equivalent concentration of uncomplexed ions being separated in ligand electrochromatograph
C_o^*	total equivalent concentration of complexed ions in ligand electrochromatograph
C_p	heat capacity
D	effective dispersion coefficient
D_A	axial dispersion coefficient
D_R	radial dispersion coefficient
d_p	particle diameter
D_i	ion diffusivity in solution
$\bar{D}_i$	ion diffusivity in resin phase
E	voltage
E'	E/E_{Ze}, reduced voltage variable
f	the ratio of the mobility of Ce^{+++} on resin in Ag^+ form to the mobility of Ce^{+++} on resin in Ce^{+++} form.
F	Faraday constant

g ratio of mobility of Ag^+ on resin in Ce^{+++} form to the mobility of Ag^+ on resin in Ag^+ form

h distance in direction perpendicular to transition between components in a ligand electrochromatograph

H length of electrochromatograph

i current

$K_1, K_2 \ldots K_n$ Bjerrum stability constants

k_b specific electrical bed conductivity

k_h effective thermal conductivity

K_m $= k_b/k_s$, ratio of bed conductivity to solution conductivity

k_p specific electrical particle conductivity

K_p $= k_p/k_s$, ratio of particle conductivity to solution conductivity

k_s specific electrical solution conductivity

ℓ half the distance between cooling faces

m_i molality of i in solution

$\bar{m}_i$ molality of i in resin phase

$\bar{M}_n$ $= \bar{m}_A \bar{K}_n$, a constant given by the product of the resin phase counter ion molality and the resin phase Bjerrum stability constant

N_{ij}^i net equivalent transport of component i across the i-ij transition

$\bar{Q}$ equivalent resin capacity

R gas constant

r_j^i equilibrium parameter

R_j^i $= (X_j \phi_i)/(X_i \phi_j)$, a modified equilibrium parameter for ligand electrochromatograph

S $Co/\overset{*}{Co}$, ratio of total concentration of uncomplexed process ions to total concentration of complexed process species

t time

t_i effective transference number

T temperature

T' $T-T_o^*$, reduced temperature

U_e electrophoretic velocity

U_e^w electro-osmotic flow velocity

U_i mobility of i in solution

$\bar{U}_i$ mobility of i resin phase

U_c convective velocity of fluid through electrochromatograph unit

U_{ij}^i electrophoretic migration velocity of an i-ij transition

U_p net velocity of uncomplexed species perpendicular to transitions

V_{AY} molar volume of electrolyte AY

V_w molar volume of water

$(V_m)_H$ swollen volume in the m-form for a quantity of resin that has a 1.0 gm H-form dry weight

$(V_{md})_H$ volume of dry resin in the m-form for a quantity of resin that has a 1.0 gm H-form dry weight

w width of electrochromatograph unit

W $= k_b/k_h$, ratio of specific electrical conductivity to thermal conductivity

$(W_m)_H$ volume of water sorbed by a resin in the m-form for a quantity of resin that has a 1.0 gm H-form dry weight

X_i equivalent fraction of i of total uncomplexed process ions

Y_i equivalent fraction of i of total complexed process ions

$\bar{Y}_i$ equivalent fraction of i on resin

Z_c direction of convective flow in electrochromatograph unit

$\tilde{Z}_c$ dimensionless, normalized convective distance

Z_e direction of electrophoretic flow in electrochromatograph unit

$\tilde{Z}_e$ dimensionless, normalized electrophoretic distance

Z_f feed distance

Z_i valence of ion i

Z'_e $= z_e/Z_e$, reduced variable

α_h $= k_n/\rho C_p$, constant, ratio of thermal conductivity to the product of density and heat capacity

α^i_j resin selectivity coefficient for ions i and j

$\gamma\pm$ activity coefficient for electrolyte in solution

$\bar{\gamma}\pm$ activity coefficient for electrolyte in resin phase

$\in$ volume-fraction of a packed bed not occupied by the particles

ξ $= (U_p/D)(\frac{C^*_o}{C_o+C^*_o})\,[h - (U_p C_o t)/(C_o+C^*_o)]$, dimensionless variable

θ angle between transition path and coordinate in direction of convective flow

$\bar{\Lambda}_i$ equivalent conductivity of i in the resin phase

ν_i stoichiometric coefficient of i

ν sum of stoichiometric coefficients of electrolyte

ϕ_i $= (Y_i C^*_o + X_i C_o)/(C^*_o + C_o)$, the point value equivalent fraction of i (in both complexed and uncomplexed form)

ρ density

$\bar{\sigma}_i$ total uptake of i by resin (including complexed and uncomplexed species)

τ residence time

ψ_i $= C_i D_i + \bar{C}_i \bar{D}_i$, modified concentration parameter for solution and resin phases

ELECTROCHROMATOGRAPHY

Electrochromatography may be described as a separation process combining the techniques of electrophoresis and chromatography to achieve an enhanced separation. Such a process may be either continuous or batch. For the preparative scale continuous operation is often desirable.

Continuous electrophoresis is the separation of electrically charged species of different mobilities from a continuous feedstream, by application of a direct-current voltage perpendicular to the direction of flow. The charged species each travel at the same velocity as the bulk liquid in the direction of fluid flow, but at different velocities in the transverse (electro-migration) direction. The path thus traced out by each ion will have different angles with respect to the fluid streamline, allowing the separated species to be continuously collected along the end of the apparatus.

When the fluid stream moves through a porous adsorptive medium, with a d-c electric field imposed at right angles to the flow, electrochromatography results. The separation is determined by the chromatographic velocity (less than the fluid velocity) in the direction of fluid flow; and by the fluid-phase and adsorbent-phase mobilities, as well as by the distribution ratios for the ions between the fluid and the sorbent, in the direction of current flow. Caplan[1] has shown that the presence of an adsorptive medium, such as an ion exchanger, can enhance or diminish a prospective separation, depending on the particular system.

Criteria for Apparatus Design

The major requirements to be met for successful separations via electrophoresis or electrochromatography fall into four categories.[2]

1. Finding conditions (solution composition, resin composition and structure) that will give selective migration with enhancement rather than diminution of selectivity in the event adsorption occurs. For electrochromatographic separations, however, ionic mobility data on sorbent materials such as ion exchangers is especially lacking. Estimates of ionic mobilities on such sorbents as ion-exchange resins or membranes can be made for exchangers in one ionic form from reported self-diffusivities.[3-18] Resin ionic mobilities are however strongly affected by the presence of other ionic species;[11,19,20] at present no adequate approach has yet been developed for estimating individual ionic mobilities on exchangers in mixed ionic form.

2. Obtaining stabel flow conductions by use of an "anti-convectant," i.e. a porous medium such as a packed bed using small spheres or granules, addition of a water-soluble polymer, or imposition of a vertical density gradient. Such steps may not be sufficient, due to interference from channeling caused by irregularity of packing, or from electro-osmotic flow, or temperature gradients.

3. Controlling the temperature rise. Heat produced by the passage of current is one of the most serious factors limiting electrochromatographic separations, especially on the preparative scale. The need to provide adequate cooling (to prevent the stabilized flow from being disrupted by dissolved air bubbles, thermal gradients, or at the limit, by the liquid

boiling) requires cooling and tends to limit the size (the distance between cooling faces) as well as the voltage and the electrolyte concentration.

4. Transverse spreading by molecular diffusion and eddy dispersion.

Apparatus Types

The need to control the maximum temperature rise in the system has resulted in two main types of apparatus for electrophoresis and electrochromatography:

First, multicomponent "ribbon" separation units--apparatus capable of separating small quantities of mixtures which may contain few or many species. In general, such units operate with high voltages and low currents.

Second, "block" separation units--apparatus designed to separate larger quantities of a mixture into two (or at most three) species or fractions. Such units generally use low to moderate voltages and high currents.

Figure 1 illustrates the two types of apparatus with their most characteristic types of separation. Ribbon units are characterized by a large distance Z_e for electromigration, such as is needed to separate several components into distinct zones. To achieve a large horizontal movement of ions in a reasonable time, large voltage gradients must be used. The resulting high level of Joule heating necessitates a narrow distance between the cooling faces, shown as the thickness w in Fig. 1. The small cross-sectional area and the required residence time combine

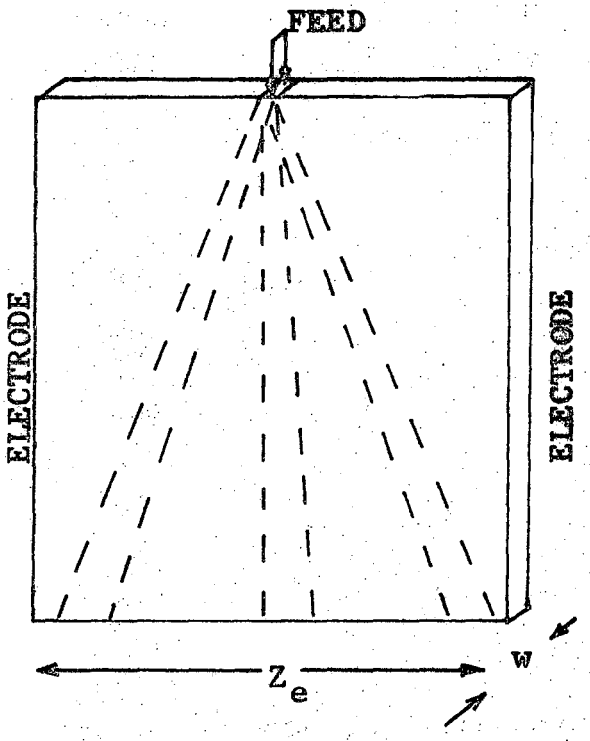

a) "Trace" Unit

(Z_e >> W)

cooling at faces

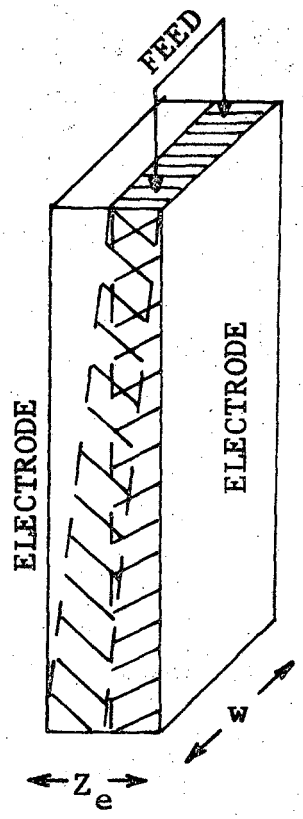

b) "Bulk" Unit

($W > Z_e$)

cooling at

electrodes

Fig. 1. Typical electrophoresis or electrochromatograph apparatus.

to limit the throughput in such units, with no scale-up possible except by modular replication of the original apparatus. In the case of block-unit separations, only two or three components or fractions are separated, and the separation distance and the required voltages are less. Hence, adequate cooling can be achieved by circulation of a cooled electrolyte adjacent to the electrodes. (At sufficiently low concentrations, adiabatic operation may be possible.) Now the thickness of the apparatus w is not limited, and scale-up can readily be accomplished by extending this dimension.

Modes of Operation

Both types of units have generally been operated in the trace fashion; that is, "background" or "elutant" electrolyte is fed to the unit along with the mixture to be separated with pretty much the same effect as in trace chromatography. This background electrolyte allows the ions of the mixture to separate into distinct zones, with the background electrolyte providing the necessary electrical conduction between zones. This background electrolyte unfortunately also permeates the zones of separated components and must subsequently be removed by some method.

Figure 2a shows a typical result for a ribbon unit operated in the trace mode. Block units operated in the trace mode (Fig. 2b) will often have the two zones overlap somewhat (due to the larger amounts of feed mixture) but will again have background electrolyte present in and around the two desired zones.

A more desirable potential operation for preparative applications is in "bulk" mode; that is, as shown in Fig. 2c, to have one separated

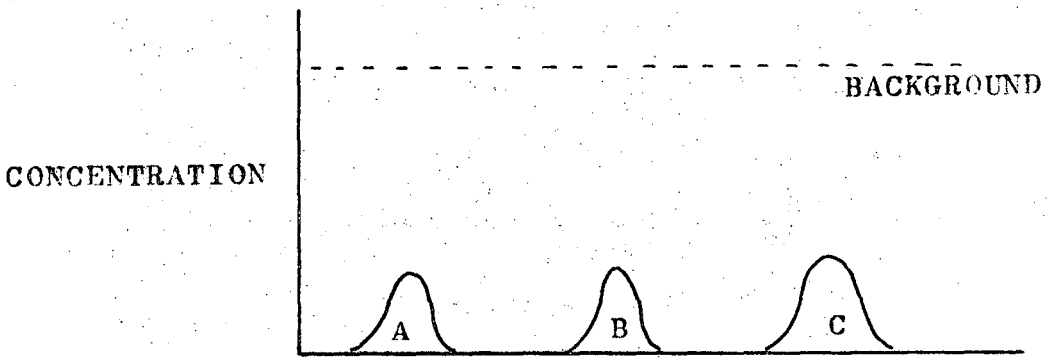

A. RIBBON UNIT IN TRACE MODE

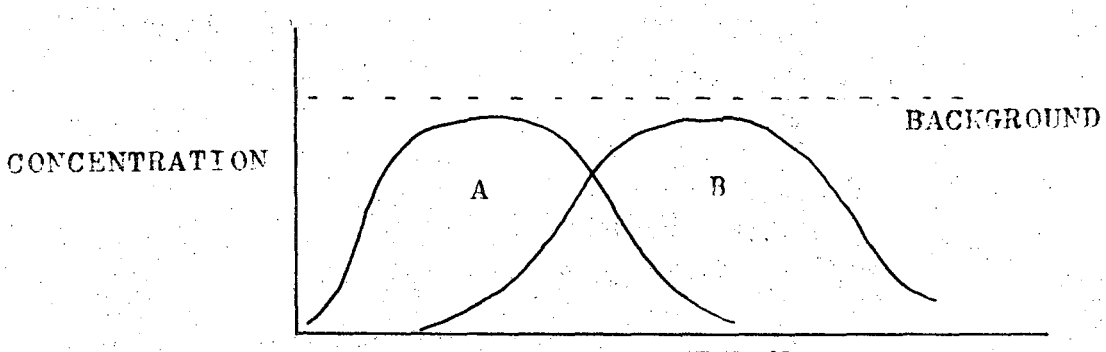

B. BLOCK UNIT IN TRACE MODE

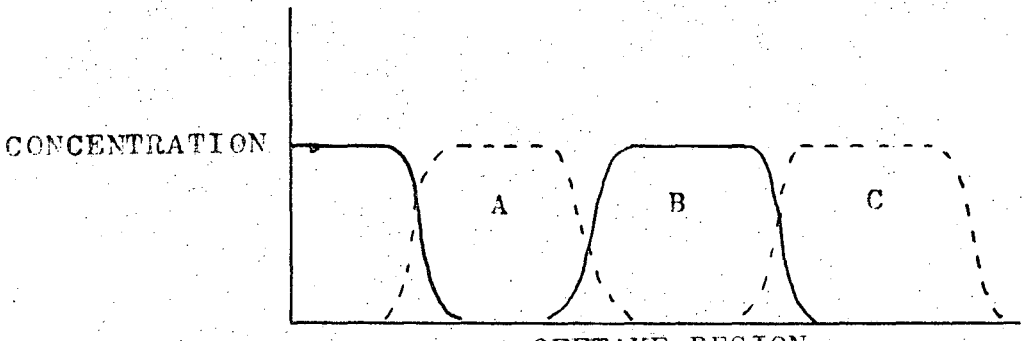

C. BULK MODE OF OPERATION

Fig. 2. Offtake patterns for trace and bulk modes of operation.

component follow the other without the presence of a background electrolyte in or between the desired zones. To maintain electrical conductivity, other ions may be required to bracket the separated zones; such ions, however, would not permeate the separated zones. The overlap regions between components are recycled, and only pure components collected. Such operations admit feed solution over a large part of the entrance cross-section, and hence provide broad zones of separated components.

Table I gives some of the advantages and disadvantages of the two types of units operated in the two modes.

For electrochromatographic separations, additional consideration of the sorbent must be made. For continuous electrochromatographic separations, there must be either a difference in mobility of the ions on the sorbent or a large selectivity between the ions by the sorbent, or both. The only sorbents effective are those which leave the sorbed species in a mobile--that is, ionic--form, such as ionic-exchange resins. For the resins, mobility ratios and selectivity generally increase with increasing crosslinkage. However, the actual mobilities decrease, especially for multivalent ions. Thus the rate of separation, which depends in part on the ionic mobilities on the resin, becomes very slow. In addition, most standard resins are not very selective between similar ions, such as the rare earths. Soluble complexing agents provide an alternate means of enhancing the relative mobilities, if they are selective and also produce a marked change in mobility for the ions which become complexed. The separation in such a case depends on the electrophoretic migration

Table I

Objectives for separation	Ribbon		Block	
	Trace	Bulk	Trace	Bulk
Ability to separate many components	+	+	0	0
Products reasonably concentrated	-	+	0	+
Easy scale-up	-	-	+	+
Low power consumption per unit solute recovered	-	+	0	+
Low voltage (minimizes safely precautions needed)	-	-	+	+

in the solution and the selectivity of the complexing agent for the ions. Complexing agents can generally be found that are very selective within any given ion group. In the separation of rare earths, for instance, EDTA and similar compounds have been found to exhibit a very large selectivity between ions.[38]

From the points discussed in the previous section, the conclusion can be drawn that while a ribbon column is indispensible for analytical work, the optimal preparative-scale separation is achieved on a block unit operated in the bulk mode using soluble complexing agents as the chromatographic sorbent.

"Ribbon" Separation Units

Historically, electrophoresis and electrochromatography have been of interest primarily as an analytic technique. Thus most units that have been developed are of ribbon type. Most such units, both in terms of type and of actual number in use in analytic laboratories, employ filter-paper curtains as the supporting medium for flow. Curtain units and other ribbon designs have been reviewed by Pucar.[21]

Filter-Paper Curtain Units

Such units are operated in one of three manners: Single-direction batch, two-dimensional batch, and continuous. Temperature rise is often controlled by fluid evaporation from the paper, its moisture content being replenished from electrolyte solutions at each end. Cooling can also be achieved by clamping cooled glass or plastic plates (cooled by water or gas circulated outside) to each side of the filter paper.

In discontinuous single-direction electrophoresis, a rectangular filter sheet is wetted and placed on a horizontal support. The ends are dipped into separate containers of electrolyte containing an electrode. The sample to be separated is introduced as a spot on this wetted sheet, and voltage is applied.

Discontinuous two-dimensional electrochromatography is conducted similarly, except that after the electrophoresis step an eluting solution is passed through the filter paper to produce a chromatographic separation perpendicularly to the electrophoretic migration.

Continuous paper electrophoresis units are mounted vertically, or at an angle, to allow gravity flow of fluid down the paper curtain. Typical units are shown in Figs. 2, 3, and 4. The electric field is applied perpendicular to the flow, though a uniform field is not always provided. Fig. 2 is an example of such a resulting non-uniform field. The voltage in this case is applied to the end corners of the paper only, resulting in curved lines of force for the electric field. Figure 3 shows the most common type of rectangular paper curtain, with a relatively uniform applied field. Figure 4 is an example of the type of geometry possible for the paper curtains besides the rectangular shapes. Commercial paper-electrophoresis units are those marketed by Beckman (Model CP) and by Microchemical Specialties Co. (Kirk-Misco "Variable Angle Plate" Spectrolators).

Packed Beds:

In these units the paper curtain is replaced by a flat rectangular bed packed with beads or granules or polystyrene, ion-exchange resin, adsorbent gels, or with other porous media. Cooling is accomplished by

jacketing the faces of the units. Such units generally have a somewhat larger throughput capacity than the filter-curtain units. The beds are thicker than the filter sheets, but must be operated at lower power levels because of the larger paths for heat removal. A commercial unit of this type is the JMK-Stubbings apparatus available from Fisher Scientific.

Free-Flow Units:

Free flow between closely and precisely spaced horizontal glass or plastic sheets provides a means of achieving stable flow. In units using this means for preventing convection, cooling jackets are provided above and below the flow section. The unit developed by Blakebrough and Brookes[23] is shown in Fig. 5. Commercial units of this type include the "Pheroplan" developed by Barrollier, Watzke, and Gibian[22] and Elphor model "FF" available from Brinkman Instruments.

Block Units

These units may be scaled-up from ribbon-type systems, or may utilize selective counter-ion transport through ion-exchange membranes.

Free-Flow Units

Dobry and Finn[30] attempted to scale-up free-flow electrophoresis from milliliters to liters per hour. Figure 6 gives a schematic representation of their apparatus. The mixture to be separated is introduced at the bottom of the column; the separated zones are collected in slits at the top. Flow in the separation chamber, as well as in the electrode compartments, is upward, and is stabilized by the addition of Methocel,

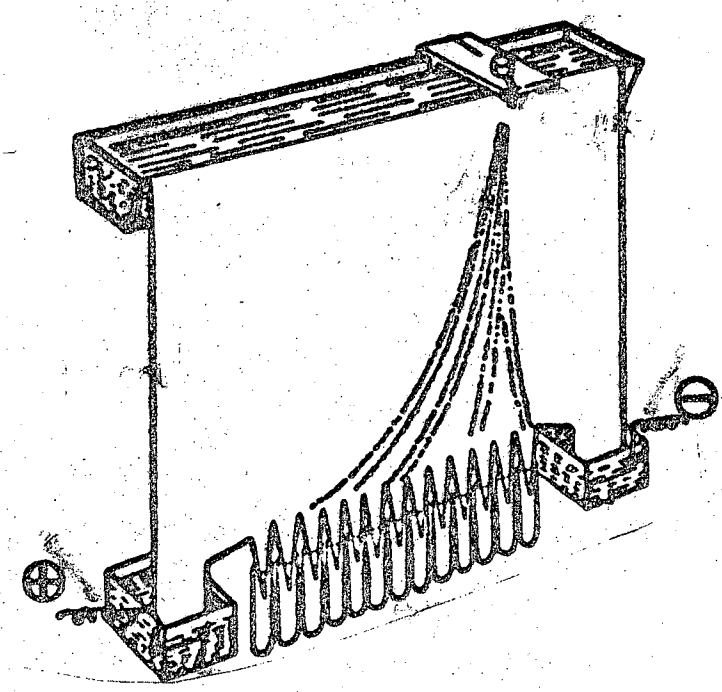

Fig. 2. Durrum paper-sheet apparatus, with trough for elutant, inlet wick for feed; electrode containers and collecting vessels at the base.

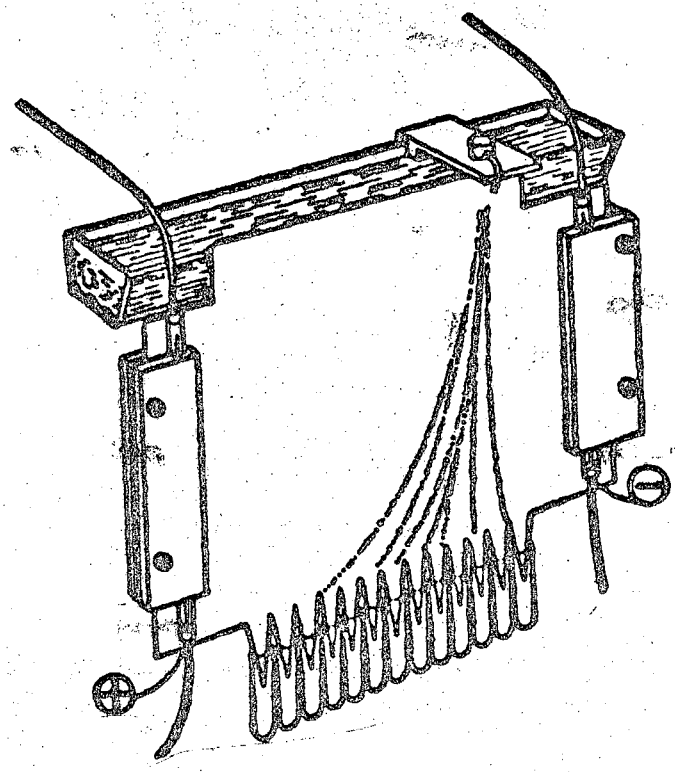

Fig. 3. Durrum apparatus with membrane-covered electrode, allowing continuous flow of coolant and rectangular voltage gradient across paper sheet.

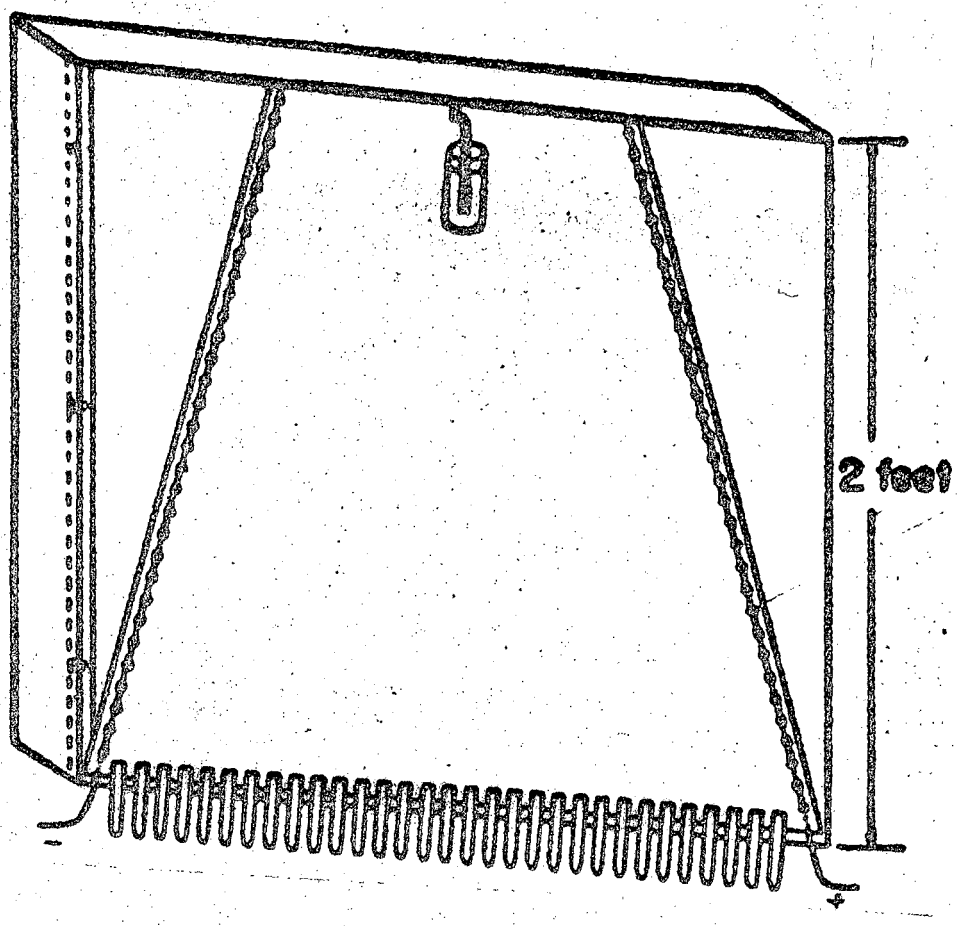

Fig. 4. Strain's apparatus. Separation sheet trimmed to trapezoid shape lies on a sloping block of polystyrene foam; platinum wire electrodes along the sides.

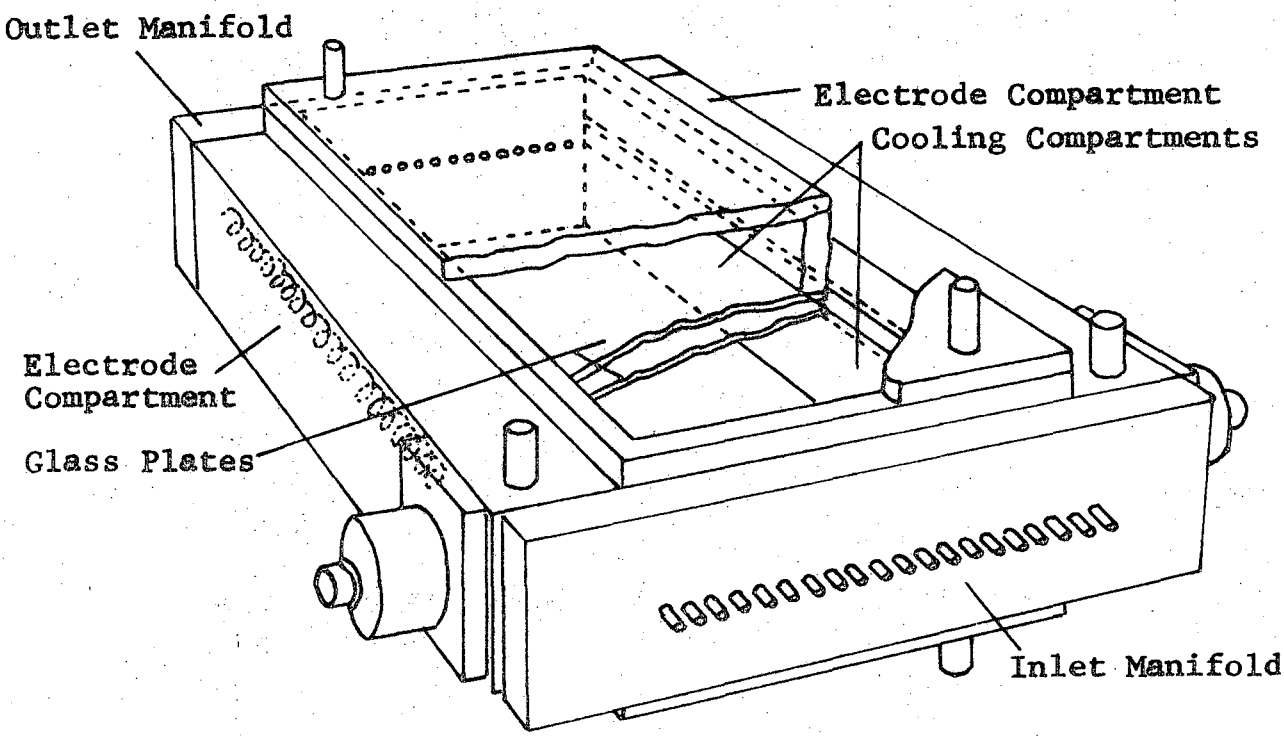

Fig. 5. Blakebrough-Brookes apparatus for free-flow electrophoresis.

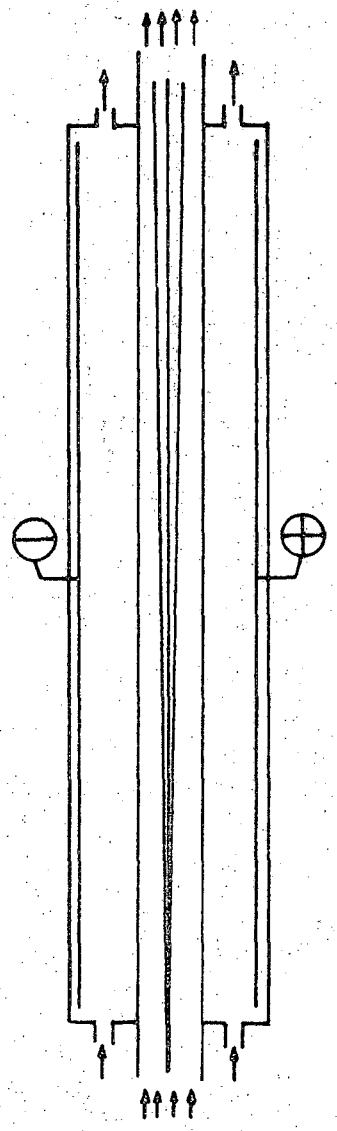

Fig. 6. Dobry-Finn apparatus with upward laminar flow of high-viscosity solution.

polyvinylalcohol, or Dextran to the background solution. By operating at low power densities (low concentrations), the temperature rise for the liquid per pass through the column will remain less than 1°C.

Density gradients to stabilize flow were first employed by Philpot.[24] Mel[25] also applied this technique in the apparatus shown in Fig. 7. The liquid flow is in the horizontal direction, with layers of increasing density (from top to bottom) introduced at one end through separate inlets. The density gradient is established using increasing amounts of sucrose, 0 to 7.5% top to bottom. Mixture to be separated is introduced in one such layer. The electric field is applied perpendicular to this flow by platinum electrodes placed above and below the flow chamber. The electrode compartment is separated from the flow chamber by permeable membranes. In both the above units, no special consideration is given to cooling; operation is restricted to low electrolyte concentrations and low voltage gradients.

Packed-Bed Unit

A preparative cylindrical electrochromatograph (ECG), modelled after existing packed electrophoresis units, has been developed at Berkeley[33-36] and is shown in Fig. 8. Cylindrical geometry was selected for scale-up because of the relative ease of construction and the absence of edge effects. The prototype units is 9 inches in diameter and 48 inches high. The annular bed is separated from the inner and outer electrodes by porous ceramic diaphragms, and is packed with uniform spherical particles of small diameter. Mixture to be separated enters in a narrow band of hypodermic needles at the top of the column and is collected at

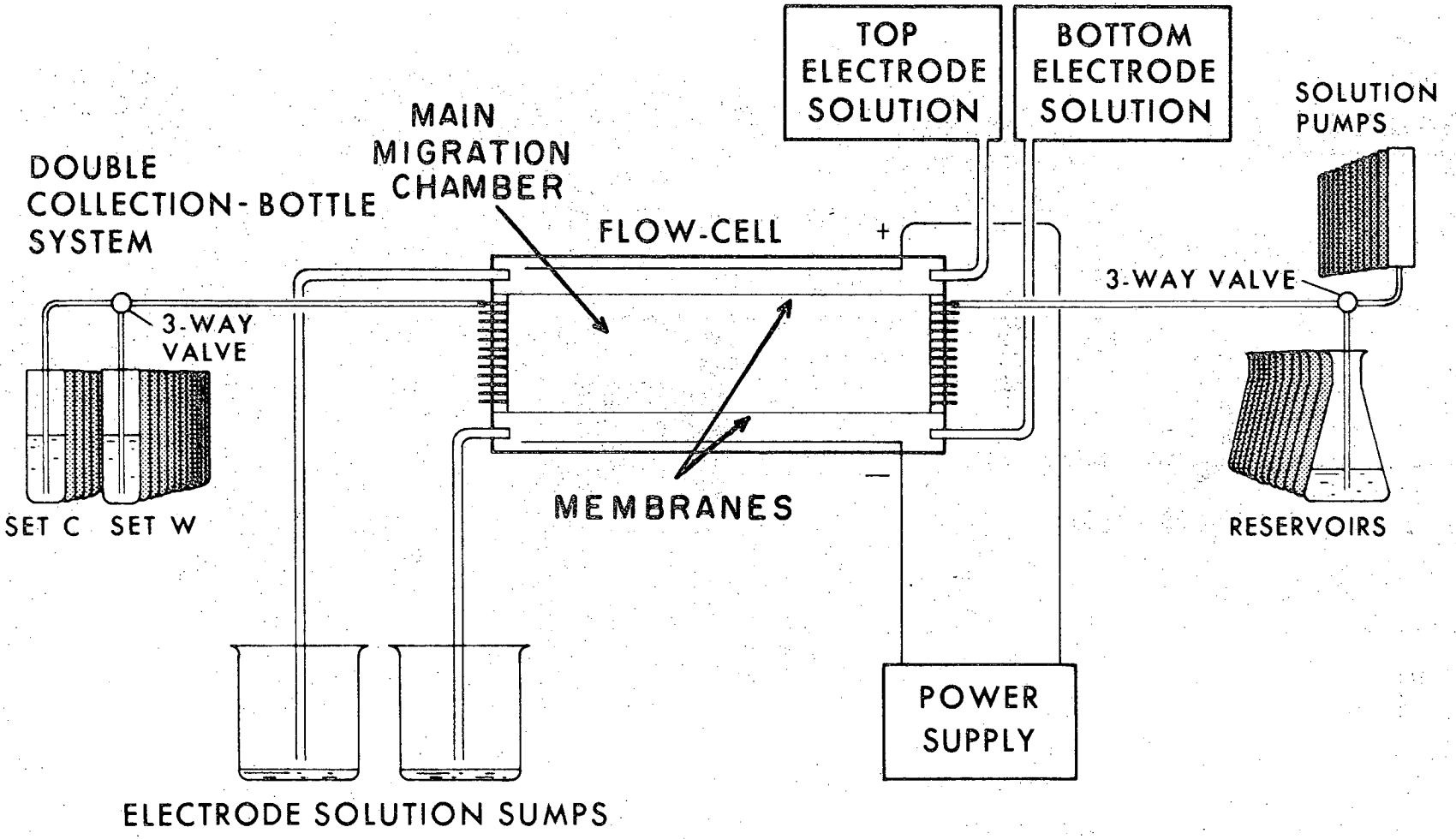

Fig. 7. Stable-flow free-boundary (STAFLO) apparatus, by Mel.

MU-29018

UCRL-19526

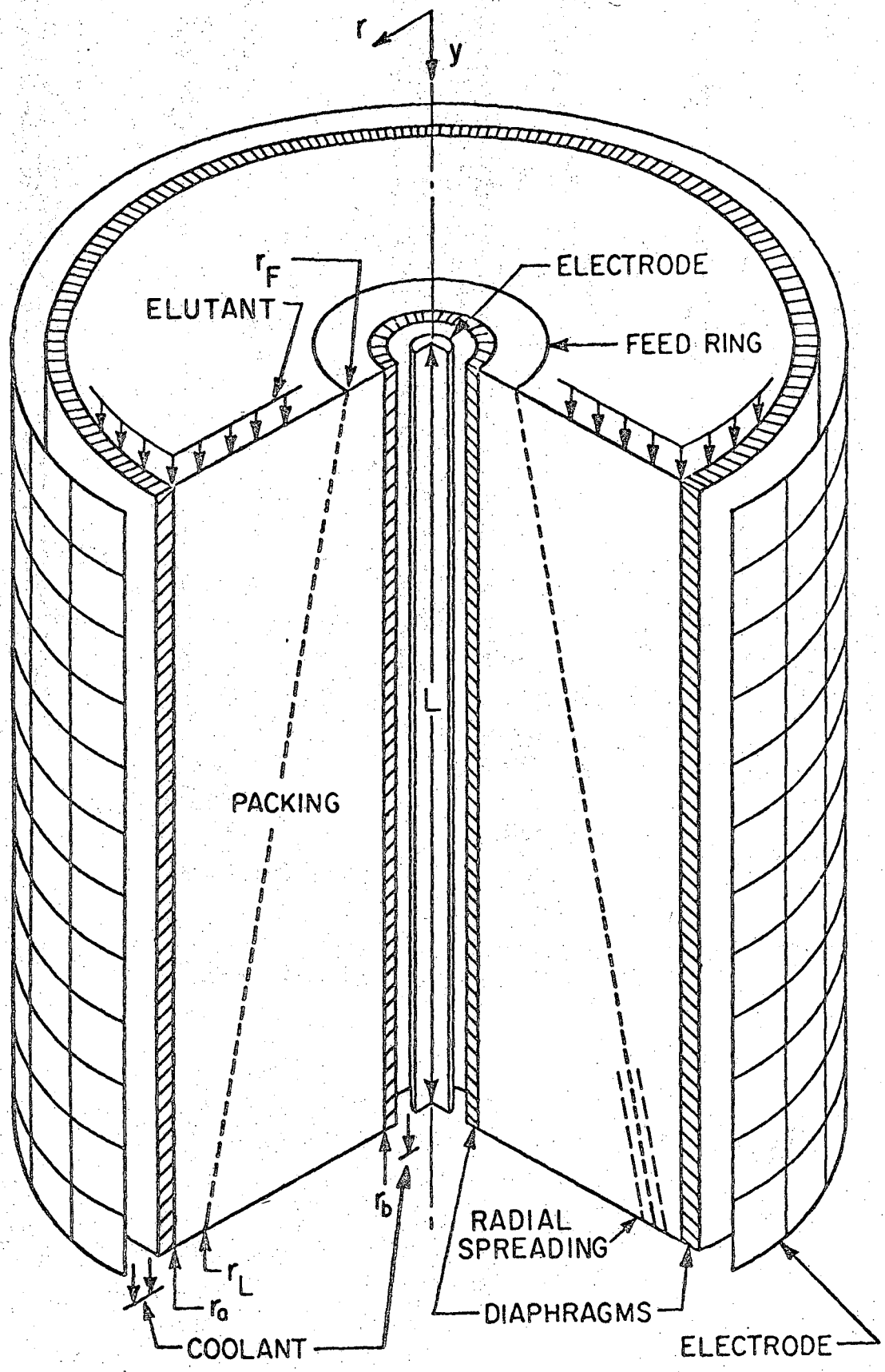

Figure 8. Sectional diagram of cylindrical column for continuous electrophoretic separation.

the bottom through eight circular offtake grooves. Background electrolyte or "elutant" is fed downwards continuously and uniformly across the entire bed cross-section. Cooling of the unit is achieved by a rapid circulation of a cooled electrolyte between the ceramic diaphragms and the electrodes. Operating voltages lie in the 25-100 volt range, with approximately half of the voltage drop dissipated across the porous diaphragms.

Electrophoresis-Convection Unit

The apparatus developed by Bier,[37] Fig. 9, is based on the principle of electrodecantation of Pauli,[26] and can be used for separating amphoteric colloidal mixtures. A component which has its isoelectric point at the operating pH can be separated from the mixture. The apparatus consists of two parallel semipermeable membranes (3-4 mm apart) with a porous filter between them. The solution is fed continuously at the top of the left-hand compartment. The polarity is adjusted so that all the negative ions or negatively charged colloids migrate to the left membrane. The ions pass through, while the colloids flow out at the top of the right-hand compartment; these in turn can be removed, either by changing the solution pH, or by feeding this stream to another similar unit with reversed polarities.

Membrane Electrophoresis

Separation of charged species is possible if differences in mobility exist between the ions for migration within ion-exchange membranes. Glueckauf and Kitt[29] found that the partial exclusion of co-ions by membranes resulted in large differences in the various co-ion

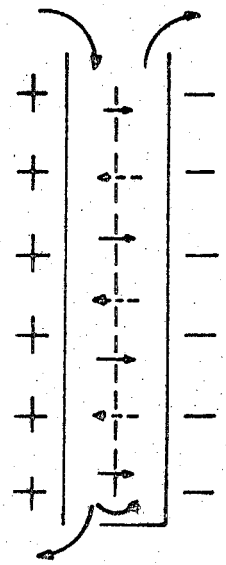

Fig. 9. Schematic side view of a forced-flow electrophoresis cell, showing semi-permeable membranes and central filter.

mobilities through such a membrane, especially for co-ions of different valences. Unfortunately the transport number for co-ions is close to zero. By placing a cation and an anion membrane next to each other, the transport numbers for cations and for anions each becomes approximately 0.5. The effect of these double membranes can then be harnessed to give a separation by an arrangement such as in Fig. 10. Unfortunately such double membranes produce large resistances to current flow and require large voltages even for small currents.

Electrodialysis

This is, in effect, a process for separating oppositely charged species. The basic unit, shown in Fig. 11, consists of a compartment formed by narrowly spaced cation and anion exchange resin membranes, with a d-c voltage gradient applied perpendicularly to the membrane surfaces. Since the transference number for the counter ions in an ion-exchange membrane is close to one, the cations and the anions can migrate out of the cell through the respective membranes, but the corresponding co-ions are prevented from entering the central compartment. Ions with the same sign can be separated in such a unit by using selective oppositely-charged multivalent complexing agents to change completely or preferentially the sign of one of the charged species through complex formation. Hershey, Mitchell, and Webb[27] separated Cs and Sr through the selective complex formation of Sr with EDTA and DPTA to give anion complexes, while Cs remained an uncomplexed cation. Bril, Bril, and Krumholz[28] have partially separated mixtures of rare earth ions using EDTA.

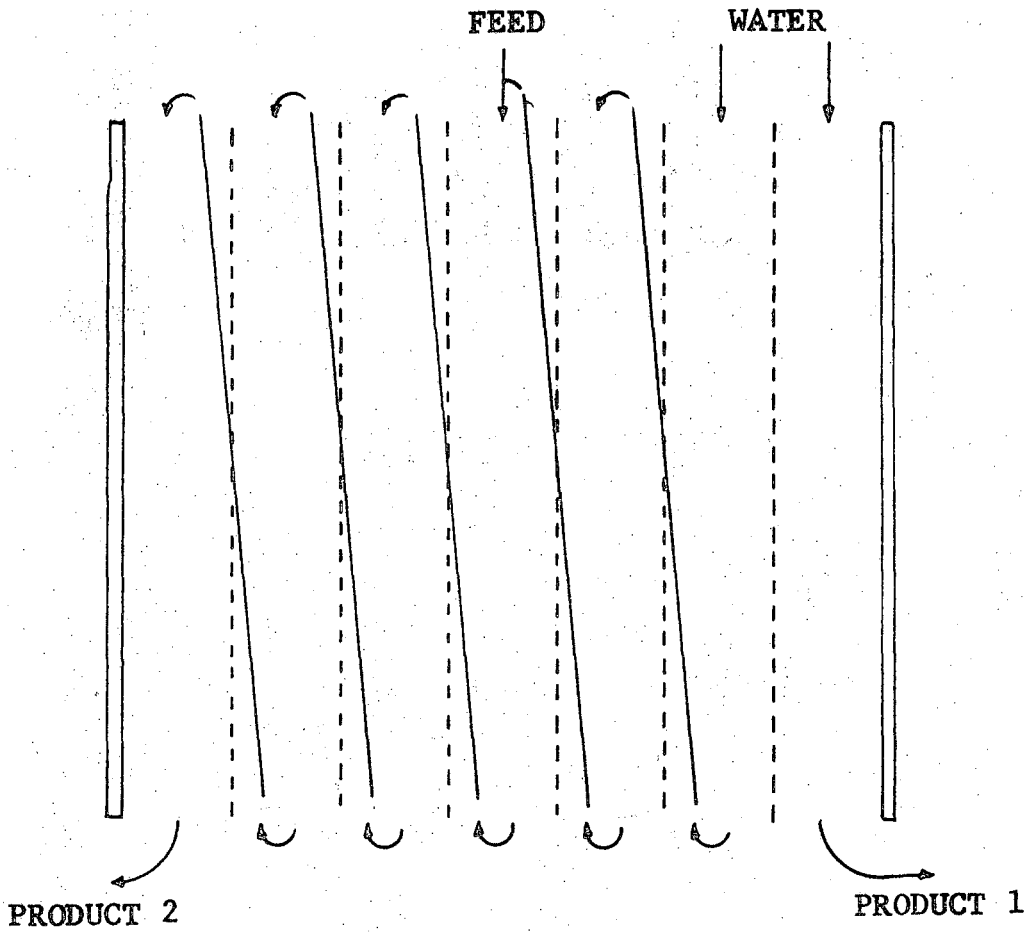

Fig. 10. Schematic flow diagram for multi-compartment cell (Glueckaut and Kitt).

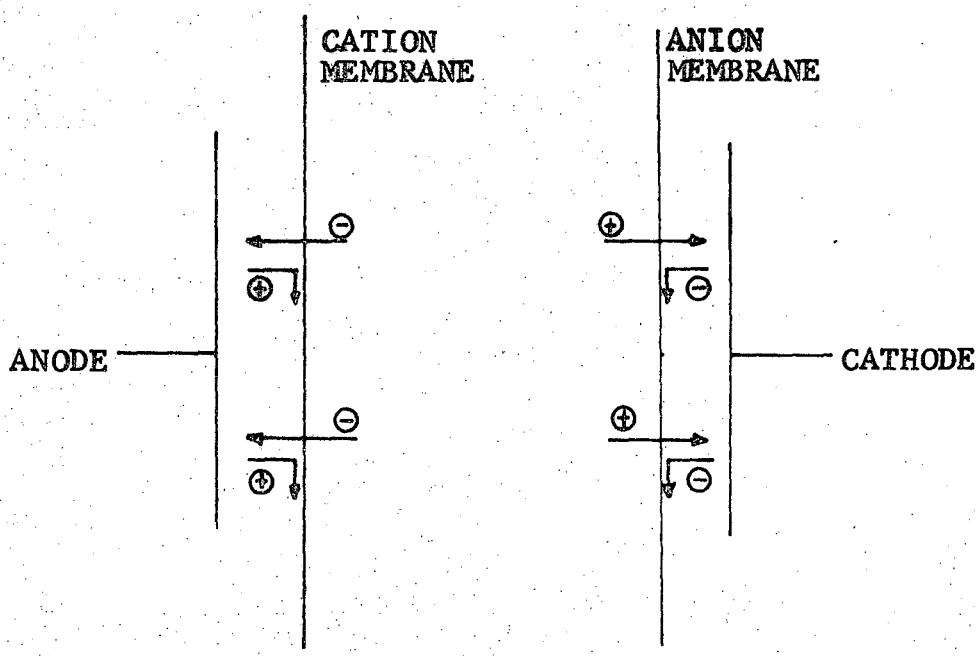

Fig. 11. Electrodialysis compartment.

Concentration-Polarization Separations

When a highly selective ion-exchange membrane is placed in an electrolyte solution and a dc voltage is applied across the membrane, differences in the transference numbers for counter ions and co-ions in the membrane relative to those in the solution result in a concentration gradient adjacent to each membrane surface. Co-ion builds up on one side of the membrane, and is depleted on the other. At steady state, electrophoretic migration of co-ion in one direction is offset by diffusion in the other. Due to electroneutrality, the counter-ion and co-ion concentrations are always equal. For counter-ions, transport near the membrane surface is the sum of electrophoretic migration and diffusional migration. Electrolyte depletion at the membrane surface causes the electrical resistance to increase and the mass transfer rate to become diffusion-controlled. (It is often desirable to eliminate the diffusion layer by stirring or otherwise promoting convection.)

In Electrogravitation, feed solution is introduced between two closely-spaced vertical membranes; for separating cations, anion membranes are used, and vice versa. A density gradient caused by the concentration gradients induces natural convection; the lighter liquid at the depleted membrane surface rises, while the concentrated electrolyte sinks. The concentrated layer tends to have a higher concentration of the faster-moving species; hence ions of low mobility predominate in the dilute solution at the top, while ions of higher mobility accumulate in the more concentrated solution at the bottom. This type of unit was first demonstrated by Murphy,[31] who used two silver-silver chloride electrodes in

place of the membranes. Frilette,[32] using anion membranes in the unit shown in Fig. 12, partially separated H^+ and Na^+, K^+ and Li^+, and K^+ and Na^+.

As a possible new separation device, proposed here for the first time, a stable broad-band concentration gradient can be developed in a packed bed of ion-exchange resin confined by two similar membranes, through application of a d-c voltage. The resulting separation will depend on solution-phase and resin-phase mobilities of the ions and on the resin selectivity for the ions.

As an example, cations are separated on cation resin between two anion membranes. Electrolyte solution containing two cations is introduced at one end of the unit, as shown in Fig. 13, and voltage is applied across the unit. Since anion membranes are used, through which only anions migrate, the cations remain trapped between the membranes.

Concentration gradients starting at each membrane surface will gradually spread across the bed until a steady-state gradient is developed. At this steady-state, for the two cations, the combined electrophoretic migration in solution and on the resin in one direction is offset by diffusion in solution in the other direction due to the concentration gradient. Ion transport is governed by solution-phase mobilities at the concentrated end and by resin-phase mobilities at the dilute end. Separation requires that differences in resin-phase mobilities, solution-phase mobilities, or resin selectivity exist for the ions to be separated. The net transport of current is equal exactly to anion electrophoretic and diffusional migration. The equation for migration of ions under such

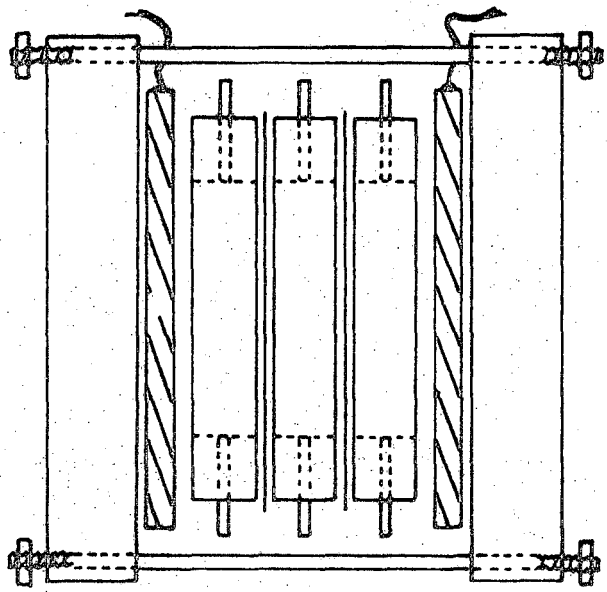

Fig. 12. Frillette electrogravitation cell.

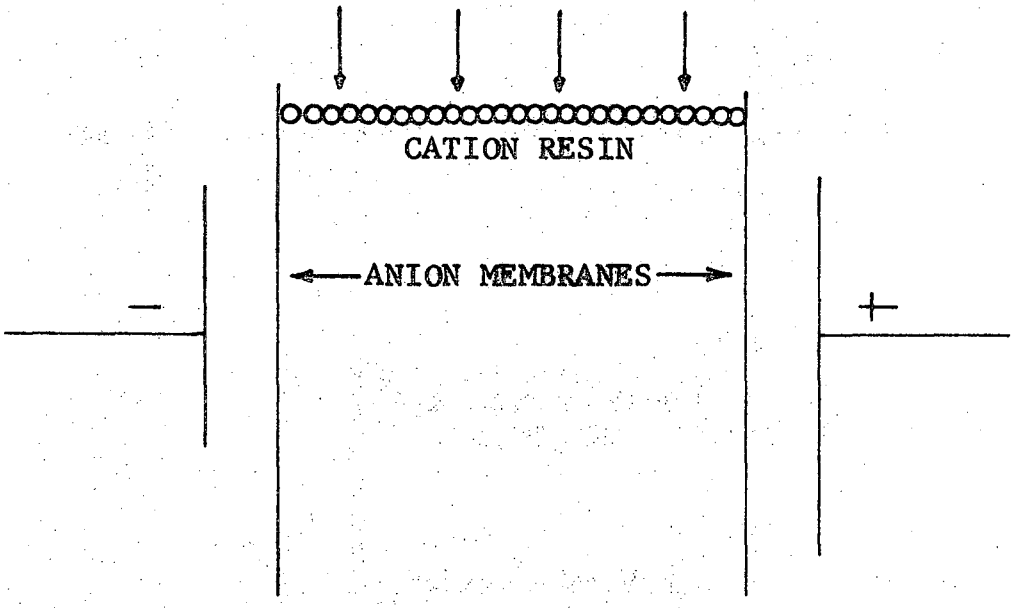

Fig. 13. Concentration polarization separation unit.

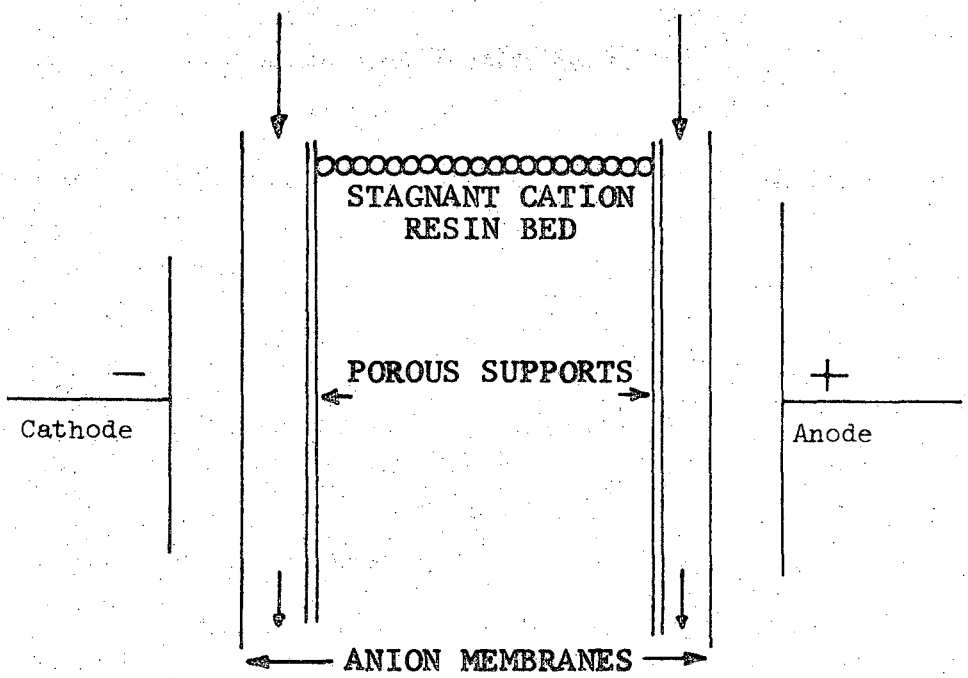

Fig. 14. Refined concentration polarization separation unit.

conditions is:

$$i \frac{t_i}{F} = -D_i \left(\frac{\partial C_i}{\partial Z_e} + Z_i C_i \frac{F}{RT} \frac{\partial E}{\partial Z_e}\right) - \overline{D}_i \left(\frac{\partial \overline{C}_i}{\partial Z_e} + Z_i \overline{C}_i \frac{F}{RT} \frac{\partial E}{\partial Z_e}\right) \quad , \quad (1)$$

where i = current; t_i = effective transference number ($t_i > 0$ for ions passing through membrane, anions in this case; $t_i = 0$ for ions not passing through the membrane, cations in this case); E = voltage; Z_i = valence; D_i and $\overline{D}_i$ are the ion diffusivities in the solution and resin phases respectively; C_i and $\overline{C}_i$ are the corresponding equivalent concentrations.

In the above equation the applicability of the Nernst-Einstein relation for both phases has been assumed.

$$D = \frac{RT}{F} U \quad . \quad (2)$$

Defining a new parameter

$$\Psi_i = C_i D_i + \overline{C}_i \overline{D}_i \quad , \quad (3)$$

and substituting it into Eq. (1) yields

$$i \frac{t_i}{F} = -\left(\frac{\partial \Psi_i}{\partial Z_e} + Z_i \frac{F}{RT} \Psi_i \frac{\partial E}{\partial Z_e}\right) \quad . \quad (4)$$

If the system contains two cation species (1 and 2) and a single anion (3), the equations for the separate species becomes:

$$t_1 = 0 \qquad 0 = \frac{\partial \Psi_1}{\partial Z_e} + Z_1 \frac{F}{RT} \Psi_1 \frac{\partial E}{\partial Z_e} \tag{5}$$

$$t_2 = 0 \qquad 0 = \frac{\partial \Psi_2}{\partial Z_e} + Z_2 \frac{F}{RT} \Psi_2 \frac{\partial E}{\partial Z_e} \tag{6}$$

$$t_3 = 1 \qquad -i/F = \left| \frac{\partial \Psi_3}{\partial Z_e} + Z_3 \frac{F}{RT} \Psi_3 \frac{\partial E}{\partial Z_e} \right| . \tag{7}$$

To get the steady-state concentration profile for the cations, Eqs. (5) and (6) can be combined, resulting in;

$$\frac{1}{\psi_1} \frac{\partial \psi_1}{\partial Z_e} = \frac{Z_1}{Z_2} \frac{1}{\psi_2} \frac{\partial \psi_2}{\partial Z_e} . \tag{8}$$

Integration yields

$$\ln \frac{\psi_1}{\psi_{10}} = \frac{Z_1}{Z_2} \ln \frac{\psi_2}{\psi_{20}} , \tag{9}$$

or

$$\frac{\psi_1}{\psi_{10}} = \left(\frac{\psi_2}{\psi_{20}}\right)^{Z_1/Z_2} , \tag{10}$$

where ψ_{10} and ψ_{20} refer to the conditions at one side of bed, and ψ_1 and ψ_2 the conditions at any other point.

Either Eqs. (5) or (6) can be integrated to give the relation between the concentration levels at each side of the bed and the applied voltage.

The selectivity coefficient α_2^1 for the resin gives the relation between the solution and resin phase cation concentrations;

$$\alpha_2^1 = \frac{C_2 \quad \overline{C}_1}{C_1 \quad \overline{C}_2} \quad . \tag{11}$$

The expression for the resin capacity $\overline{Q}$ is

$$\overline{Q} = \overline{C}_1 + \overline{C}_2 \quad . \tag{12}$$

These two expressions can be combined and the resin-phase concentration of each ion can be solved for in terms of solution phase concentrations.

$$\overline{C}_1 = \frac{C_1\overline{Q}}{\alpha_1^2 C_2 + C_1} \tag{13}$$

$$\overline{C}_2 = \frac{\alpha_1^2 \overline{Q} C_2}{\alpha_1^2 C_2 + C_1} \quad . \tag{14}$$

Plugging Eqs. (3) and (13) into Eq. (10) results in:

$$\frac{C_1 D_1 + \dfrac{\overline{D}_1 C_1 \overline{Q}}{\alpha_1^2 C_2 + C_1}}{C_{10} D_1 + \dfrac{\overline{D}_1 C_{10} \overline{Q}}{\alpha_1^2 C_{20} + C_{10}}} = \left(\frac{C_2 D_2 + \dfrac{\alpha_1^2 \overline{D}_2 C_2 \overline{Q}}{\alpha_1^2 C_2 + C_1}}{C_{20} D_2 + \dfrac{\alpha_1^2 \overline{D}_2 C_{20} \overline{Q}}{\alpha_1^2 C_{20} + C_{10}}} \right)^{Z_1/Z_2} \quad . \tag{15}$$

For the separation of ions of the same valence Z_1/Z_2 is 1. Maximum separation is achieved when the ion migration on one side of the bed occurs

primarily on the resin (dilute solution end) and in the solution phase at the other (concentrated end). This corresponds to the conditions:

$$\text{dilute end:} \quad \begin{aligned} \overline{Q}\,\overline{D}_1 &\gg D_1(\alpha_1^2 C_2 + C_1) \\ \alpha_1^2\overline{Q}\,\overline{D}_2 &\gg D_2(\alpha_1^2 C_2 + C_1) \end{aligned}$$

$$\text{concentrated end:} \quad \begin{aligned} D_1(\alpha_1^2 C_{20} + C_{10}) &\gg \overline{Q}\,\overline{D}_1 \\ D_2(\alpha_1^2 C_{20} + C_{10}) &\gg \alpha_1^2\overline{Q}\,\overline{D}_2 \end{aligned} \quad . \tag{16}$$

With these conditions, Eq. (15) reduces to the form:

$$\frac{C_1}{C_2} = \frac{C_{10}\overline{D}_2}{C_{20}\overline{D}_1}\,\alpha_1^2 \quad . \tag{17}$$

In solution, the mobilities or diffusivities of most ions are quite similar; hence separation is usually caused by the mobility or diffusivity ratio $\overline{D}_2/\overline{D}_1$ for the ions on the resin together with the resin selectivity coefficient K.

Since only the solution at the sides, which give maximum separation, are desired, the unit shown in Fig. 14 is proposed. In such a unit the feed is introduced on each side between a porous support (such as ceramic diaphragms) and the membrane. The presence of the membranes and the stagnant resin bed brings about the steady-state solution-phase concentration distribution given in Eq. (15). Having the central bed stagnant eliminates the need for continuous flows in this section, which would have to be recycled.

Such a unit achieves its maximum separation at the dilute end. It can readily be seen, from a mass balance over the entire system, that the concentration ratio of the two components at the outlet for the concentrated stream cannot change very markedly from the input ratio. A possible mode of operation would involve continual recycling of the concentrated solution and collection of the separated, but more dilute, solution. A cascading of several such units, or a reprocessing of previously collected streams, is sometimes necessary for difficult separations.

Such units require a horizontal operating position to keep the density gradients from producing undesired convection. Very low voltages should be used; higher voltages only cause excessive electrical resistance (and heating) at the depleted membrane surface without any increase in separation rate or extent. No extraneous ions are needed to operate this unit, nor are any introduced. The limitation of such a system is its low throughput, a consequence of the low voltages applied and the low mobilities of ions on the resin.

Continuous Ligand Electrochromatography

A block unit operating in the bulk mode and using aqueous-phase ligands has been developed in this study as a new high-capacity preparative-scale separation apparatus. The proposed designation for the separation which occurs in this type of unit is "ligand electrochromatography." Complexing agent flows through the main separation section of the apparatus, and is retained in it mainly by the low mobility of the

complexes it forms. Separation is achieved by the selective electrophoretic migration across the "bed" of complexing agent by an ion mixture supplied in stoichiometric excess. This process circumvents many difficulties and limitations found in other applications of electrophoresis.

A schematic drawing of the ligand electrochromatograph is shown in Fig. 15. The central separating section is a rectangular bed packed with inert polystyrene beads as "anticonvectant" with fluid flow lengthwise through the bed and electrophoretic flow of ions in a transverse direction. Complexing agent is introduced into the unit partly or totally with an excess of "retainer-species" ions R (which provide complex formation by nearly all of the complexing agent, but in a weaker complex than those formed by the species to be separated) and optionally partly with the feed mixture. The complexes formed will be neutral and have zero electrophoretic mobility, if the uncomplexed ligand and the ion mixture to be separated have equal but opposite valences. Otherwise, if the complexed species have a net charge, their electrophoretic migration must be accounted for in planning the block-unit operation. "Chaser-species" ions C (having stronger affinity for the complexing agent than do the feed-mixture ions) are introduced along the side of the unit by electrophoretic migration through a porous diaphragm.

Two feed arrangements are possible. The process feed (A+B) may be introduced at the entrance end of the bed together with complexing agent, as shown in Fig. 15; this arrangement is generally preferred if feed is rich in the more highly complexed species. Alternatively, the feed may be introduced without complexing agent along an upstream part of

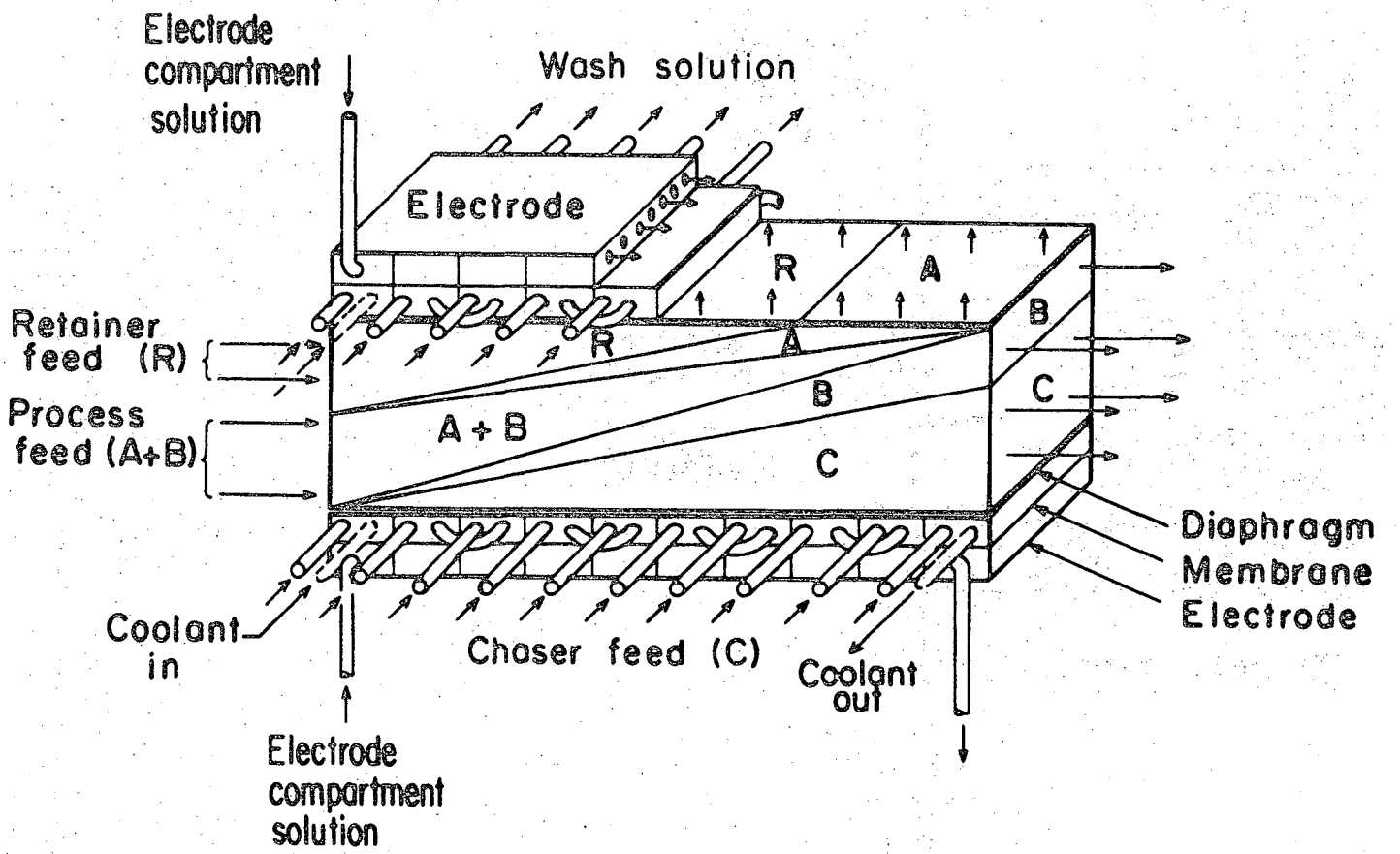

Fig. 15. Schematic diagram of continuous ligand-electrochromatograph.

the entrance side of the unit, this arrangement being preferred if the feed is rich in the less strongly complexed ion. For the latter case, the retainer-ion complexing-agent mixture is fed over the entire entrance end, and the chaser ion is introduced only along the downstream part of the entrance side.

The separated components A and B can be collected both along the exit side of the unit, both at the exit end of the unit, or one each along the side (B) and at the end (A). The last method (depicted in Fig. 15) is generally preferred, since it allows the highest ion throughput for any given power consumption.

The net electrophoretic migration of a cationic species i is given by the mobility of free ions of i (roughly the same for all ions having the same valence), multiplied by the molar concentration of free ions of i. Thus mixtures of ions having the same mobilities, but different concentrations of free ions due to selective complexing, will have different net electrophoretic migration rates and hence will separate into pure zones. Once the components are separated the concentration of free ions becomes the same for each species, and the migration rates become equal. The zones of separated components then continue to migrate adjacent to each other. In this separation process the ions preferred in complexing displace the less preferred ions (analogously to displacement development in ion exchange). Self-sharpening boundaries result, which attain a steady-state balance between migration (tending toward ideally sharp boundaries) and the disruptive effects of eddy dispersion.

The block unit, constructed to carry out this type of chromatography, consists of a packed bed 10cm × 4cm × 40cm supported between two ceramic diaphragms. Outside each diaphragm, the adjoining liquid is isolated into 10 compartments, each with a coolant line and input-output connections allowing discontinuous (or continuous) replacement of the liquid in each compartment. The compartments are separated from the electrode region by ion-exchange membranes, which exclude the feed or product ions from the electrode regions. Anion membranes are used for cation separation, and vice-versa. Graphite electrodes are placed on each side of this sandwich construction. Electrolyte flows lengthwise between the respective graphite electrode and each membrane. The main components housing the separation chamber, side compartments, and the electrode compartments are made of Lucite. This allows visual inspection of the flows in the unit.

The electrolyte from each electrode chamber is de-gasified, recombined, cooled, and recycled. The unit is cooled partially by the recirculated electrolyte and partially by coolant water circulated through polyethylene tubing that winds through all 20 side compartments.

Operating voltages are 10-60 volts, with residence times of 0.5 to 2 hours. Typically about half the voltage is dissipated across the membranes and the diaphragms, the remaining half serving directly to produce the separation.

References

1. S. R. Caplan, J. Electrochem. Soc. 108, 577 (1961).
2. E. Ravoo, P. J. Gellings, and T. Vermeulen, Anal. Chim. Acta. 38, 219 (1967).
3. G. E. Boyd and B. A. Soldano, J. Am. Chem. Soc. 75, 6091 (1953).
4. B. A. Soldano and G. E. Boyd, J. Am. Chem. Soc. 75, 6099 (1953).
5. G. E. Boyd and B. A. Soldano, J. Am. Chem. Soc. 75, 6105 (1953).
6. M. Tetenbaum and H. P. Gregor, J. Phys. Chem. 58, 1156 (1954).
7. C. R. Morig and M. G. Rao, Chem. Eng. Sci. 20, 889 (1965).
8. B. Hering and H. Bliss, A.I.Ch.E.J. 9, 495 (1963).
9. A. E. Lagos and J. A. Kitchener, Trans. Faraday Soc. 56, 1245 (1960).
10. A. Schwarz, J. A. Marinsky, and K. S. Spiegler, J. Phys. Chem. 68, 918 (1964).
11. J. deLopez-Gonzales, and H. Jenny, J. of Colloid Sci. 14, 533 (1959).
12. J. C. R. Turner, M. R. Church, A. S. W. Johnson, and C. B. Snowdon, Chem. Eng. Sci. 21, 317 (1966).
13. W. T. Grubb, J. Phys. Chem. 63, 55 (1959).
14. N. W. Rosenberg, J. H. B. George, and W. D. Potter, J. Electro. Chem. Soc. 104, 111 (1957).
15. R. Arnold and D. F. A. Koch, Aust. J. Chem. 19, 1299 (1966).
16. K. S. Spiegler and C. D. Coryell, J. Phys. Chem. 57, 687 (1953).
17. K. S. Spiegler and C. D. Coryell, J. Phys. Chem. 56, 106 (1952).
18. D. G. Howery and S. Tada, J. Macromol. Sci. A3, 297 (1969).
19. B. A. Soldano and G. E. Boyd, J. Am. Chem. Soc. 75, 6107 (1953).
20. L. Nady and T. Vermeulen, (next chapter).

21. Z. Pucar, in M. Lederer (ed), Chromatographic Reviews, Vol. 3, Elsevier, Amsterdam, 1961, pg. 38.

22. J. Barrollies, E. Watzke, and H. Gibian, Z. Naturforsch. 13b, 754 (1958).

23. N. Blakebrough and R. Brookes, Biotech. Bioeng. 6, 223 (1964).

24. J. St. L. Philpot, Trous. Faraday Soc. 36, 38 (1940).

25. H. C. Mel, J. Phys. Chem. 31, 559 (1959).

26. M. Adolf and W. Pauli, Biochem. Z. 152, 360 (1924).

27. H. C. Hershey, R. D. Mitchell, and W. H. Webb, J. Inorg. Nucl. Chem. 28, 645 (1966).

28. K. Bril, S. Bril, and P. Krumholz, J. Phys. Chem. 63, 256 (1959).

29. E. Glueckauf and G. P. Kitt, J. Appl. Chem. 6, 511 (1956).

30. R. Dobry and R. K. Finn, Chem. Eng. Progress 54, No. 4, 59 (1958).

31. G. W. Murphy, J. Electro. Chem. Soc. 97, No. 11, 405 (1950).

32. V. J. Frilette, J. Phys. Chem. 61, 168 (1957).

33. R. M. Hybarger, C. W. Tobias, and T. Vermeulen, Ind. Eng. Chem. Fundamentals 2, No. 1, 1963, pg. 65.

34. E. Ravoo, C. W. Tobias, and T. Vermeulen, Annular. Bed Electrochromatography, Report No. 2, University of California, Berkeley, California, 1963.

35. L. Nady, V. N. Gupta, and D. G. Howery, "Experimental Studies in Continuous Electrophoresis," Report 4, Part 1, 1965, University of California, Department of Chemical Engineering, Berkeley, California.

36. J. Krochta, M.S. Thesis in Chemical Engineering, University of California, Berkeley, California, 1967.

37. Bier, Electrophoresis, Vol. 11, Academic Press, New York, 1967.

38. J. E. Powell and F. H. Spedding, Chemical Engineering Progress Symposium series No. 24, Vol. 55, pg. 101(1959).

II. MOBILITY OF TRIVALENT-MONOVALENT CATION MIXTURES ON ION EXCHANGERS

Introduction

Both ion-exchange chromatography and continuous electrophoresis across a packed bed of inert particles are well-known separation methods for ionic solutes. When resin selectivities and resin-phase electrochemical mobilities, for the solutes to be separated, both reinforce the selective aqueous-phase mobility, it is advantageous to combine the elements of these two methods by using continuous electrochromatography; that is, by packing an electrophoresis unit with the appropriate ion-exchange resin.

To evaluate or predict the separations obtainable by electrochromatography, the mobilities of the solutes both in the bulk solution and on the resin must be known.[1] Mobility data in the resin phase are also valuable for the information they may provide on the internal diffusion behavior of pure and mixed ionic components.

Resin-phase mobilities of ions can be determined readily from conductivity measurements of the resins in contact with solutions of various concentrations. By applying a theory that involves the measured solution conductivity and bed conductivity, the particle conductivity can be obtained. For each ionic species, the electrochemical mobility may vary with the total ionic composition of the resin, but the particle conductivity for a resin containing only this counter-ion species will be the main parameter needed to describe the electrochemical mobility of this ion on that resin. When a resin contains more than one mobile species (counter ions, co-ions, or complex ions), the contribution of each to the total particle conductivity must be deduced in order to calculate the mobility of any individual ion on the resin.

Particle Conductivities vs. Bed Conductivities

The theories for conductivity of ion-exchange resin beds fall into two categories, as mentioned by Helfferich.[2] The potential-flow approach treats the bed as being composed of a continuous solution phase in which resin particles are suspended. The theoretical studies on the conductivity of heterogeneous systems by Maxwell,[3] Bruggeman,[4] Meredith and Tobias,[5] and Brown[6] can be applied for this approach. Because the beads of resin in a bed are not completely isolated, these theories have rarely been tried. The other category is based on an analogy with an electrical network. Sauer, Southwick, and Spiegler,[7] and Spiegler, Yoest, and Wyllie[8] have interpreted their own experimental data by an equation based on a network model. Suitable empirical adjustment of the four parameters in this equation enables it to fit all experimental results, including the Donnan-uptake region corresponding to high concentration levels in the external solution.

Because too little is known of the behavior of the network parameters, the potential-flow approach has been adopted in the present study. Among the theoretical developments using this approach, the relatively simple equation of Bruggeman has been found to give acceptable results. Application of this equation to ion-exchange resins has been demonstrated by Howery and Tada.[9] In Bruggeman's treatment, a mixture of two phases is considered quasi-homogeneous with respect to any one dispersed-phase particle, thus fitting Maxwell's potential theory for a single particle in a continuum. Therefore the differential change in conductivity of the mixture, with changing volume-fraction of the dispersed phase, is

$$-\frac{dK'_m}{d\epsilon} = \frac{3K'_m(K'_m - K_p)}{(\epsilon)(2K'_m + K_p)} \quad , \tag{1}$$

where $K_m = \frac{k_b}{k_s}$ = the ratio of bed conductivity to solution conductivity; $K_p = \frac{k_p}{k_s}$ = the ratio of particle conductivity to solution conductivity; and ϵ is the volume-fraction not occupied by the particles.

Integrating with the lower limit $K'_m = 1$ as $\epsilon = 1$, and the upper limit $K'_m = K_m$, one then obtains the Bruggeman equation

$$\epsilon = \frac{K_m - K_p}{K_m^{1/3}(1 - K_p)} \quad . \tag{2}$$

Ion Mobility from Particle Conductivity

When only one type of counter ion is present on the resin and the surrounding solution is so dilute that there is no uptake of external electrolyte into the resin matrix, the particle conductivity can be considered as the sum of all the mobilities of the counter ions on the resin. Since the counter ions are all identical, their contributions to the particle conductivity will be equal. The ionic-species mobility (cm^2 $volt^{-1}$ sec^{-1}) on the resin is then given by[15]

$$\overline{U}_i = \frac{1000\, k_p\, t_i}{\overline{C}_R\, F} \quad , \tag{3}$$

where t_i = transference number (=1 for resin in one ionic form); k_p = specific particle conductivity (mho cm^{-1}); $\overline{C}_R$ = resin volume capacity (meq. ml^{-1}); F = Faraday constant (Coul. eq^{-1}).

The above relation applies only when there is no sorption of external electrolyte. Even at low to moderate solution concentrations (0.05 to 0.5 molar), some sorption occurs; this can be in the form of ionized ions, neutral ion pairs, or complex ions. The form of the sorbed electrolyte must be identified so that its contribution to the particle conductivity can be properly accounted for.

Apparatus

The A. C. conductivity bridge that was used for this research is depicted schematically in Fig. 1. The components shown are as follows:

1. A Jones conductivity bridge (Leeds & Northup Co.) that can measure resistances up to 60,000 ohms and has variable built-in capacitors totaling 0.0010 μfd. for compensation of the capacitance.

2. An audio-frequency oscillator (Hewlett-Packard Co., model 2001).

3. An oscilloscope (Tektronix Inc., type 512).

4. Two isolation transformers (step-up ratio 1:3.) which greatly improved the stability and sensitivity of detection by eliminating noise from the oscillator.

5. A glass conductivity cell (Industrial Instruments Co.), with its cell constant 1.099 cm^{-1}.

6. A glass conductivity column, shown in Fig. 2. This glass cell was first filled with distilled water, then the resin particles were packed in it replacing the water. In the cell, the ground-glass-joint plugs each have a platinum electrode fused to their inside surface. Inlet and outlet

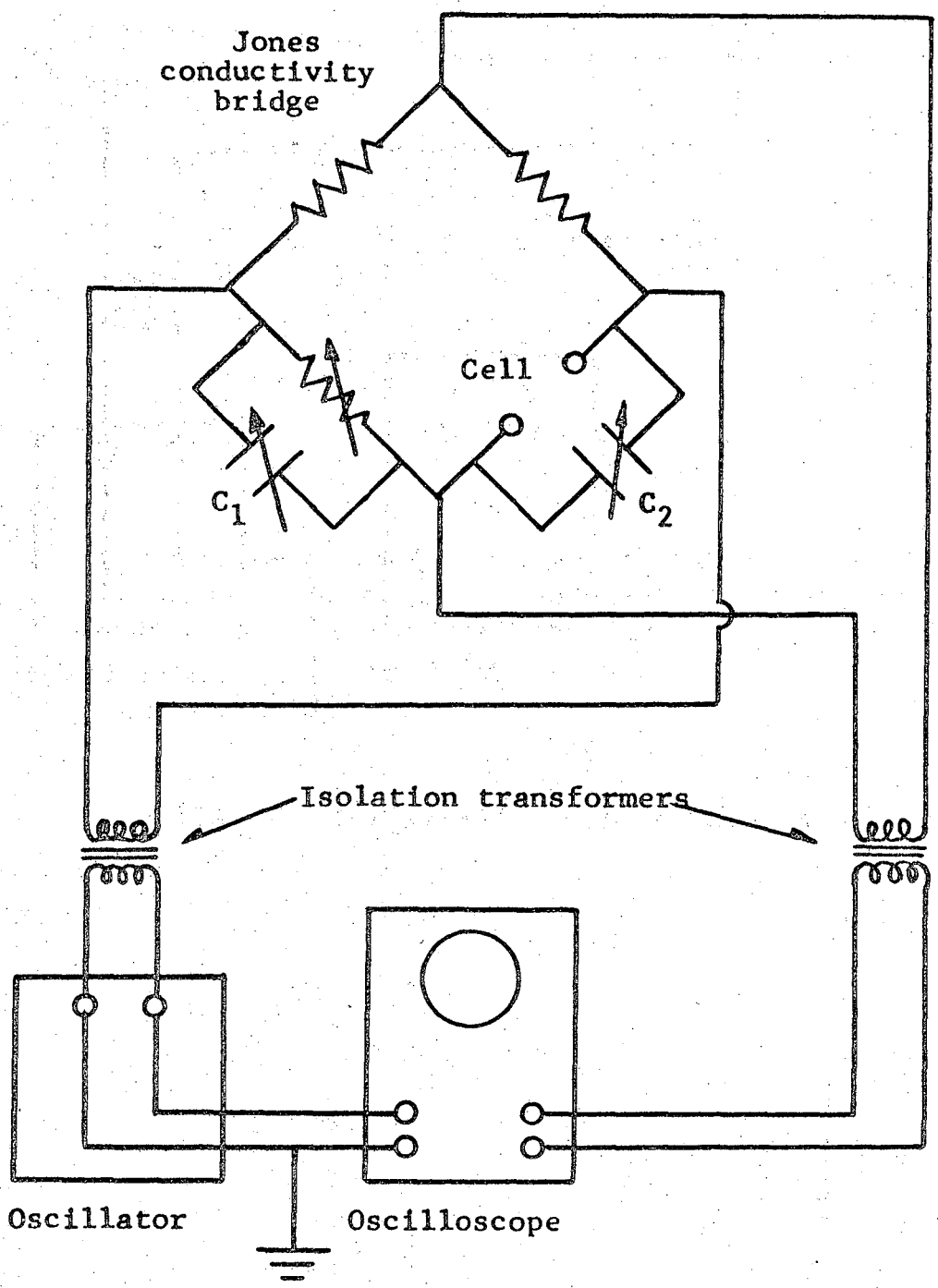

Fig. 1. Conductivity bridge circuit.

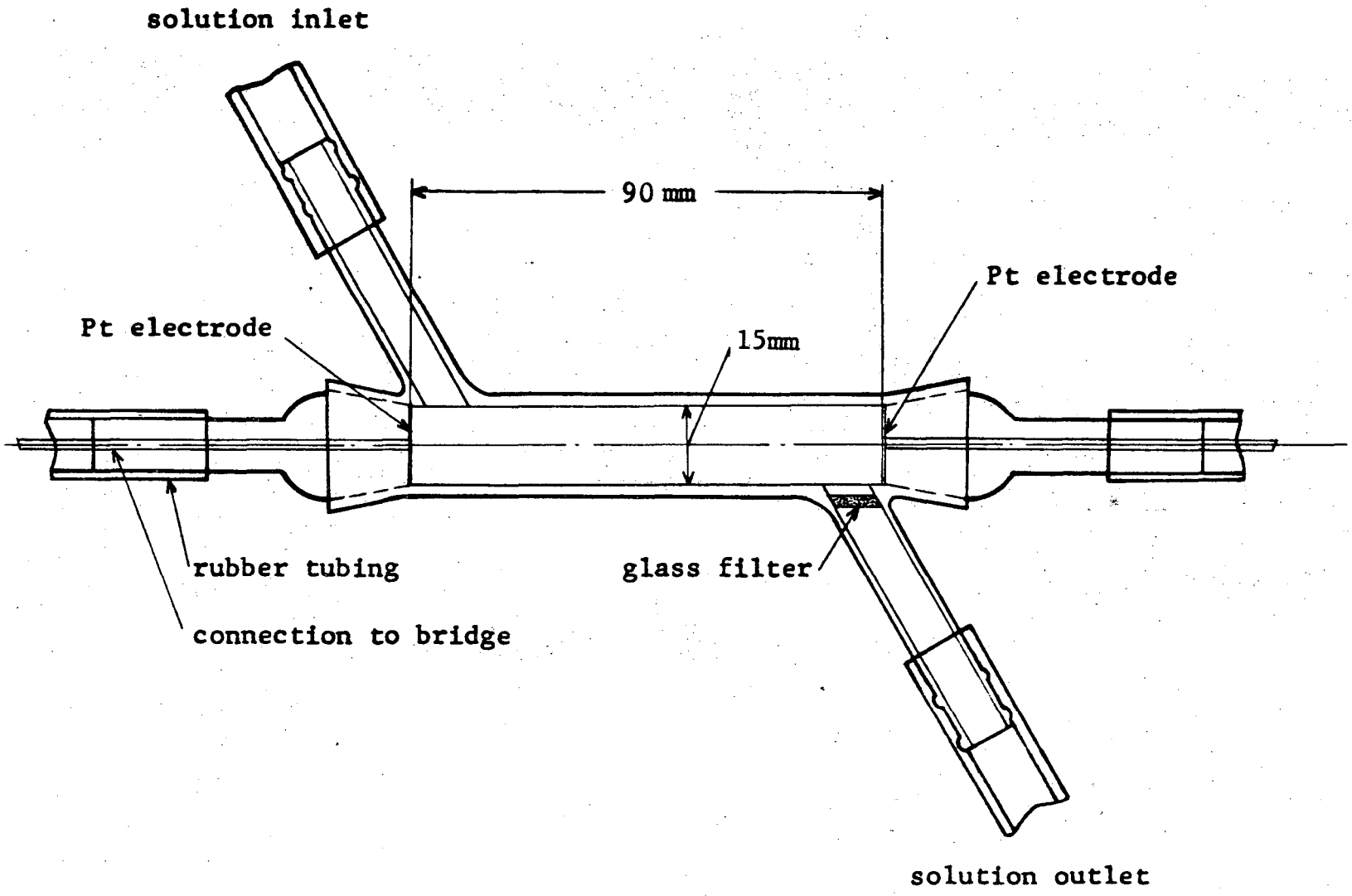

Fig. 2. Conductivity column.

side tubes are provided for solution flow; a small glass filter has been fused to the outlet tube to retain the resin inside. Filling with resin particles was continued up to the tip of the inlet tube. The height of resin in this tube had been shown not to affect the measurement, but it still was kept as constant as possible. The cell constant of the glass conductivity column, 4.71 cm^{-1}, was determined using 0.01N KCl standard solution.

In making the measurements, the oscilloscope was used as a null detector. Two signals of 1kc frequency were fed to the oscilloscope, one directly from the oscillator to the horizontal plate and the other through the conductivity bridge to the vertical plate. A horizontal line was observed on the oscilloscope when the bridge was in balance. All connecting wires were shielded. Solution was contained in a 100 ml test tube and the conductivity cell was dipped into the solutions. The test tube and the glass conductivity column were immersed in a constant-temperature bath held within 30 ± 0.5°C; a one-hour wait sufficed to give steady conductivity readings.

Conductivity Measurements for Monovalent Ions:

Conductivities were measured for NaCl solution with Na-form Dowex 50W for cross-linking of 2% (50-100 mesh), 4% (20-50 mesh), and 8% (20-50 mesh); the resins for these runs were each prepared in three cycles of the following operations.

1. Eluting with about two bed volume of 2N HCl.

2. Rinsing with distilled water at the rate of 10 bed volumes per hour, for about half an hour.

3. Feeding about two bed volumes of 1N NaOH.

4. Rinsing with distilled water at the rate of 10 bed volumes per hour, for about half an hour.

For NaCl solution with Na-resin, the solution concentration varied from 0.005N to 0.5N, and the conductivities were measured at 30°C. At each concentration the solution was run through the column until the bed conductivity remained steady. The conductivity of the solution alone was measured separately in the solution conductivity cell.

Conductivities of Rare Earths Alone and in Mixtures:

Dowex 50W-X4 was used for the investigation of rare earth conductivities on resins. The 4% crosslinked resin was chosen as the best compromise between the need for a large isoconductance value (low crosslinking) and for good selectivity (high crosslinking).

The rare earth ions investigated were cerium (Ce^{+++}), lanthanum (La^{+++}), holmium (Ho^{+++}), and neodymium (Nd^{+++}).

In addition to investigating particle conductivities of Dowex 50W-X4 resin in the pure rare-earth-ion form, the conductivities for the Ce^{+++} - Ag^{+} and La^{+++} - Ag^{+} pair were studied as a function of their equivalent ratios on the resin. Ag^{+} was chosen for east of analysis in checking the resin composition.

Preparation of Resin in Pure Rare Earth Form

The resin was treated as described previously, ending up in the Na form. It was then converted to the rare earth form by feeding a solution 0.1M in the appropriate rare earth nitrate. To insure complete

conversion to the rare earth form, a minimum volume of solution equivalent to twice the capacity of the column was fed to the column. Subsequent to charging with the rare earth ion, the bed was washed with 10 bed volumes of distilled water. It was then contacted with various solutions of the same rare earth nitrate, with concentrations ranging from 0.005 to 0.1 molar. Each such solution was flowed through the bed until the conductivity reading remained steady.

Preparation of Resin in Partial Rare Earth--Silver Form

The resin treatment described previously was again followed, with the omission of the last NaOH charging step. A 1M $AgNO_3$ solution was passed through the bed, converting the resin to the Ag^+ form. Upon completion of this charging step, the bed was washed with distilled water.

From the data of Bonner and Jumper[11] on the equilibrium quotient for the Ce^{+++} - Ag^+ system on Dowex 50W-X4, the solution concentrations necessary to give the desired equivalent ratio on the resin phase were calculated. Due to the large selectivity of the resin for trivalent rare earth ions as opposed to monovalent silver, it was necessary to use a relatively concentrated initial solution of Ag^+ and Ce^{+++} to convert the resin from pure silver to the desired Ce^{+++} - Ag^+ resin composition. Once this step was accomplished, a more dilute solution (but resulting in the ame Ce^{+++} - Ag^+ resin composition), with a solution conductivity near the estimated isoconductance point for this resin composition, was passed through the resin bed until the bed conductivity became steady. The bed conductivity was then compared with the measured solution conductivity; from this comparison it was then possible to estimate the solution concentration needed to give a solution conductivity that was within 10% of

the new bed conductivity. From these points the isoconductance values could be extrapolated very readily.

Following measurement of the isoconductance point, the resin was washed with distilled water and then contacted with 6N HNO_3 to elute the silver and rare earth ions. The silver concentration was determined by titrating a small sample of the eluted solution with SCN^-.

Conductivity measurements for the Ce^{+++} - Ag^+ system were made over a 6 deg C range, to determine activation energies for electromigration.

RESULTS AND DISCUSSION

Results on Single-Counter-Ion Systems

Conductivity data for Na-form Dowex 50W-X4 in NaCl solution are shown in Fig. 3. The isoconductance point occurs at the concentration for which the conductivity of the solution, the bed, and the resin matrix are all equal; thus it lies at the intersection of a line equating bed and solution conductivities with the experimental curve, as shown in Fig. 3.

Tables I and II give measured solution and bed conductivities and calculated particle conductivities, as determined by Eq. (1), for Dowex 50W-X2, X4, and X8 in Na-form, and Dowex 50W-X4 in Ag-form. Na-form particle conductivities are compared to the isoconductance values in Fig. 4. Adoption of $\epsilon = 0.40$, the experimental value for void volume-fraction in these beds, has led to particle conductivities that are independent of the solution concentration and conductivity and are thus equal to the isoconductance values over the investigated concentration range.

The sorption (or Donnan uptake) of excess NaCl by the resin is measurable but small for the concentrations investigated.[16] Also, no increase occurred in particle conductivity as the solution concentration (and sorption) increased. For the 4% resin the expected increase in the particle conductivity (due to sorption) amounts to only 6% at 0.5M solution concentration, and is less at lower concentrations. This is of the same order as the average deviation of the calculated particle conductivities from the measured isoconductance value.

For Ag-form resin, the particle conductivity of Dowex 50W-X4 is shown as a function of $AgNO_3$ solution conductivity in Fig. 5. The calculated particle conductivities are independent of solution concentration (0.01 to 0.5 molar) and agree well with the isoconductance point. Again, particle conductivities do not increase at the higher solution concentration, even though the present authors have found significant sorption (7% increase in counter-ion resin concentration at 0.5M solution concentration).[16] In that study the authors have proposed that for a given resin the sorption of free ions at a given solution-phase electrolyte activity is the same for electrolytes of specified cation and anion valences. Differences in the sorption of electrolytes at a given solution activity is then attributed to complex formation, uncharged in the case of (+1)(-1) electrolytes. If this were not the case and most of the sorbed $AgNO_3$ at 0.5M were ionized, a 30% increase in particle conductivity should have occurred; the absence of such an increase supports the interpretation that most of the sorbed $AgNO_3$ in the resin is in a neutral ion-pair form.

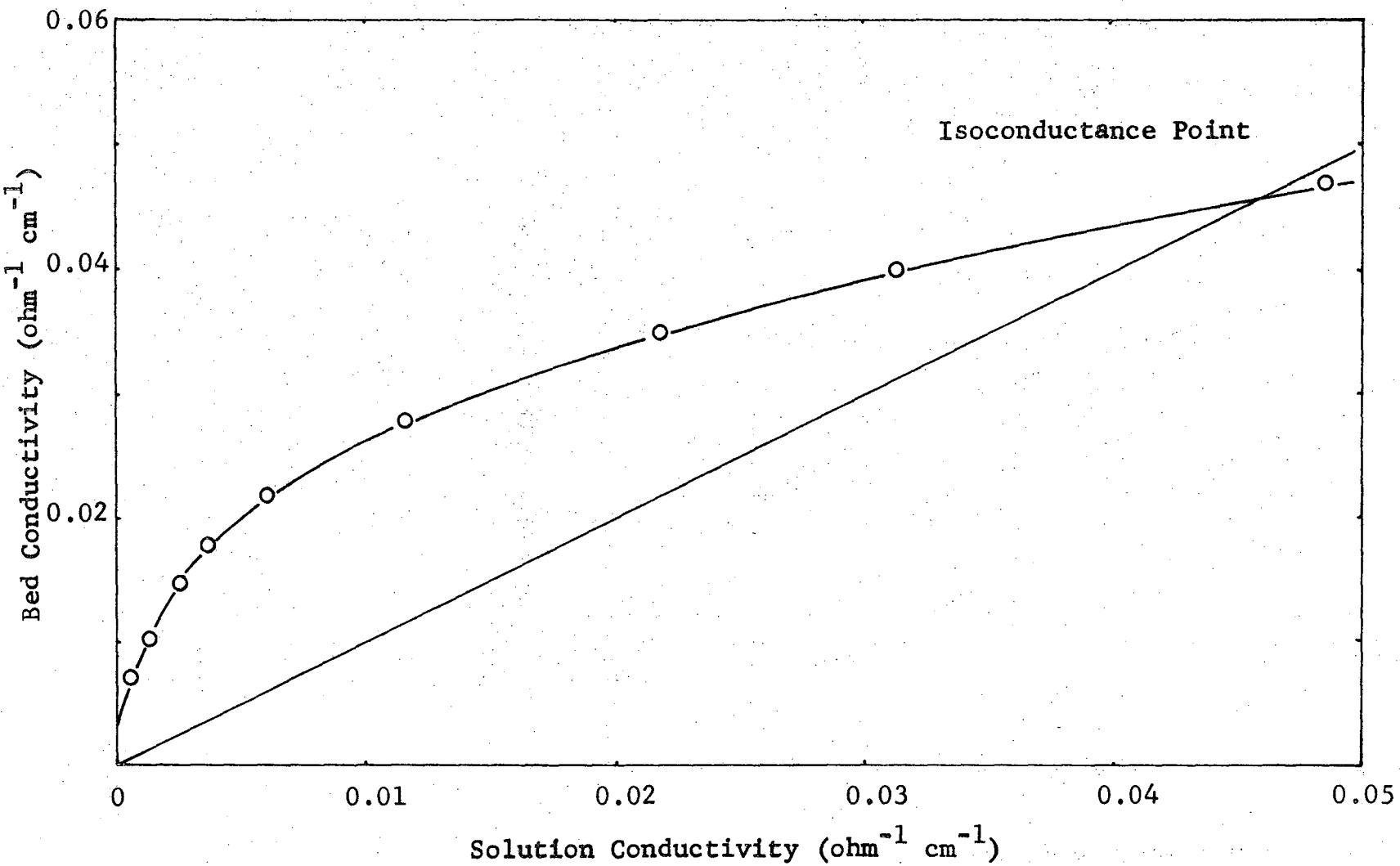

Fig. 3. Bed conductivity at 30°C of Dowex 50W-X4 resin (50-100 mesh) in sodium form, in NaCl solution.

Table I. Particle Conductivities for Sodium-Form Dowex 50W; $\in = 0.40$, 30°C

Conc. (M/L)	2% DVB			4% DVB			8% DVB		
	k_s	k_b	k_p	k_s	k_b	k_p	k_s	k_b	k_p
0.00500	0.000677	0.0069	0.0478	0.0006759	0.006927	0.0482	0.000688	0.00577	0.0290
0.0100	0.001312	0.01003	0.0425	0.001312	0.01016	0.0439	0.001312	0.00869	0.0311
0.0200	0.00256	0.0143	0.0429	0.002562	0.01457	0.0444	0.00255	0.01233	0.0327
0.0300	0.00376	0.0173	0.0442	0.00376	0.01764	0.0457	0.00376	0.01473	0.0334
0.0500	0.00612	0.0215	0.0452	0.00611	0.02176	0.0464	0.00611	0.01791	0.0337
0.100	0.01162	0.0278	0.0466	0.0116	0.02789	0.0467	0.01162	0.02254	0.0361
0.200	0.0219	0.0352	0.0471	0.02185	0.03489	0.0463	0.02189	0.02771	0.0321
0.300	0.0311	0.0406	0.0482	0.03122	0.03992	0.0466	0.03053	0.03148	0.0321
0.500	0.04863	0.0486	0.0486	0.0484	0.04705	0.0462	0.04863	0.03709	0.0304

Table II. Particle Conductivities for Silver-Form Dowex 50W-X4; $\in$ = 0.40, 30°C

Concentration M/L	k_s	k_b	k_p
0.0100	0.001372	0.01121	0.0522
0.0250	0.00329	0.01664	0.0459
0.0500	0.006316	0.02211	0.0470
0.100	0.01204	0.02804	0.0461
0.200	0.02229	0.03438	0.0447
0.300	0.03167	0.03909	0.0447
0.500	0.04841	0.04613	0.0447

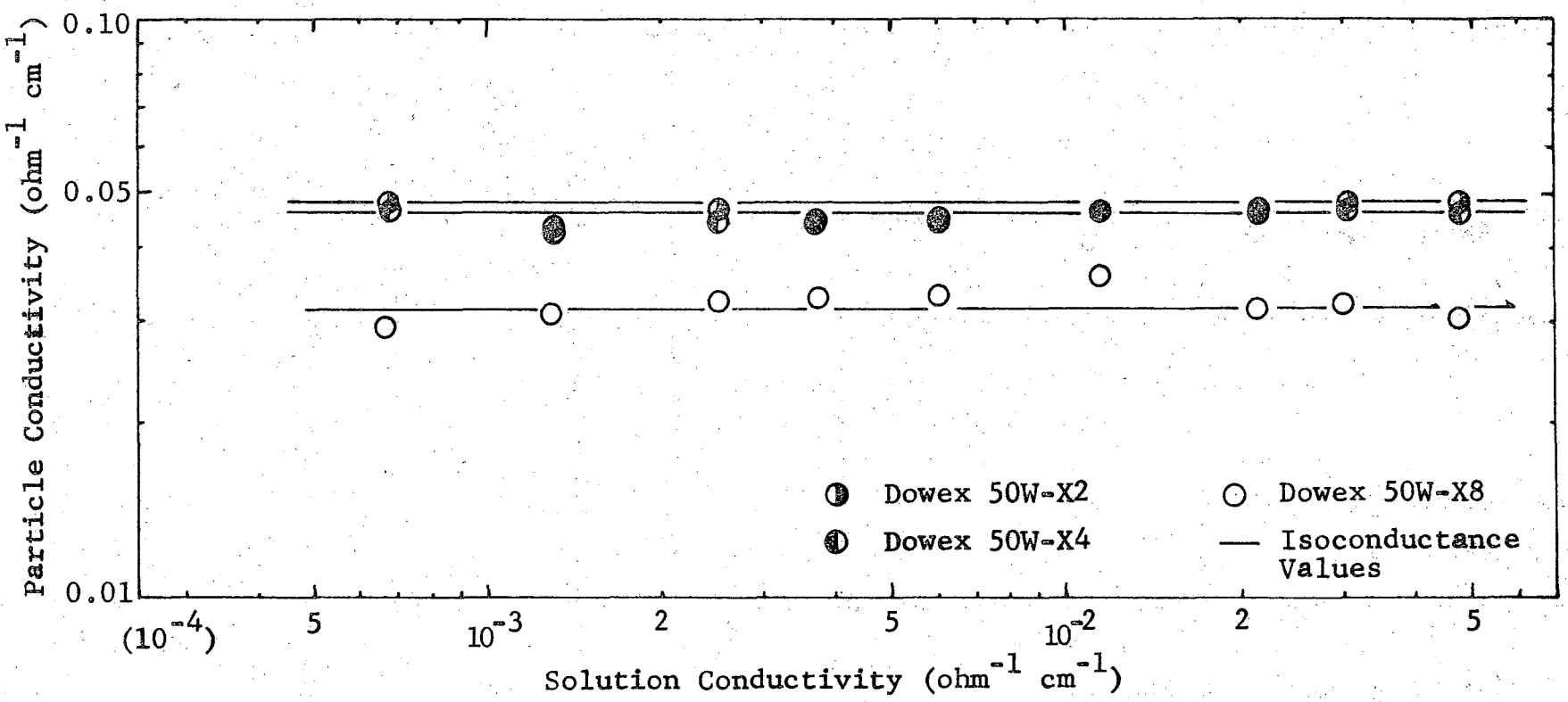

Fig. 4. Resin-particle conductivities for Dowex 50W-X4 at 30°C in sodium form, calculated with $\epsilon = 0.40$.

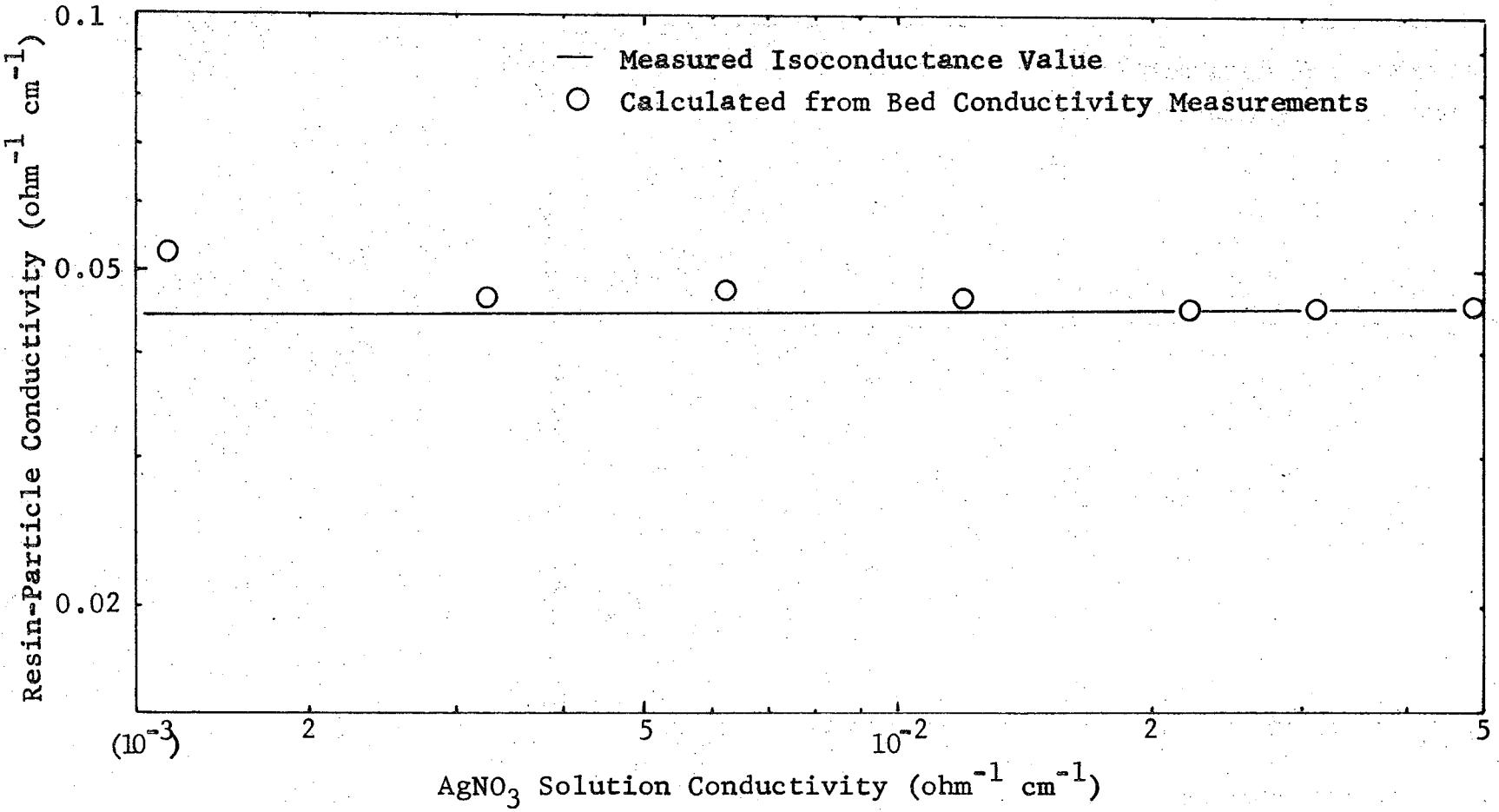

Fig. 5. Resin-particle conductivity for Dowex 50W-X4 at 30°C in Ag^+ form, $\epsilon = 0.40$.

For four rare earth nitrates (cerium, lanthanum, neodymium, and holmium), Table III gives measured solution and bed conductivities and calculated particle conductivities for Dowex 50W-X4 (again for a void fraction of 0.40). Figure 6 gives the relation between particle conductivity and solution conductivity, and shows that particle conductivities increase appreciable with increasing solution conductivity or concentration. This increase in conductivity can only be attributed to sorbed excess ions which are known to be present;[16] and, in particular, to the much higher mobility of the sorbed co-ions ($\bar{m}_{NO_3^-}$). Figure 7 plots these particle conductivities as a function of the concentration of sorbed co-ions, $\bar{m}_{NO_3^-}$. The concentration of free nitrate ions in the resin phase is taken to be the same as for $La(ClO_4)_3$, which is not known to form complexes at the same solution activity. The measured total uptake, $\bar{\sigma}_{NO_3^-}$, includes the nitrate complexed with rare earth ions as a divalent complex counter ion as well as the free NO_3^- ions, and will vary from one rare earth to another.

Figure 7 shows that the increase in particle conductivity is due primarily to the sorbed free nitrate ions (as estimated from $La(ClO_4)_3$ behavior). This is true because the four rare earth nitrates have the same slope; that is, the same dependence of particle conductivity of free co-ion concentration; a plot of particle conductivity against total co-ion uptake $\bar{\sigma}_{NO_3^-}$ would give a different slope for each rare earth. The total uptake of electrolytes $\bar{\sigma}_{NO_3^-}$ varies for the different rare earths in the following order:[19]

$$\bar{\sigma}_{NO_3^-}\ (Ho^{+++}) < \bar{\sigma}_{NO_3^-}\ (La^{+++}) < \bar{\sigma}_{NO_3^-}\ (Ce^{+++}) < \bar{\sigma}_{NO_3^-}\ (Nd^{+++}) \quad ,$$

Table III. Particle conductivities for Rare Earth-Form Dowex 50W-X4, $\epsilon = 0.40$; 30°C

Conc. M/L	Cerium			Lanthanum		
	k_s	k_b	k_p	k_s	k_b	k_p
0.00500	0.001853	0.003191	0.00442	0.001945	0.002825	0.00355
0.0100	0.003478	0.00411	0.00457	0.003627	0.003674	0.00371
0.0200				0.006718	0.004917	0.0039
0.0250	0.00782	0.00588	0.00477			
0.0300				0.009557	0.005947	0.00407
0.0500	0.01427	0.008135	0.0051	0.01477	0.007747	0.00442
0.100	0.02562	0.01178	0.00561	0.02617	0.01156	0.00517

Conc. M/L	Neodymium			Holmium		
	k_s	k_b	k_p	k_s	k_b	k_p
0.00500	0.001911	0.003528	0.00509	0.002109	0.004305	0.00656
0.0100	0.003557	0.004551	0.00531	0.003968	0.005427	0.00660
0.0200	0.006553	0.005962	0.00559	0.007045	0.006988	0.00695
0.0300	0.009314	0.007104	0.00583			
0.0500	0.01422	0.008937	0.00620	0.01506	0.01026	0.00765
0.100	0.02556	0.01253	0.00653	0.02568	0.01436	0.00880

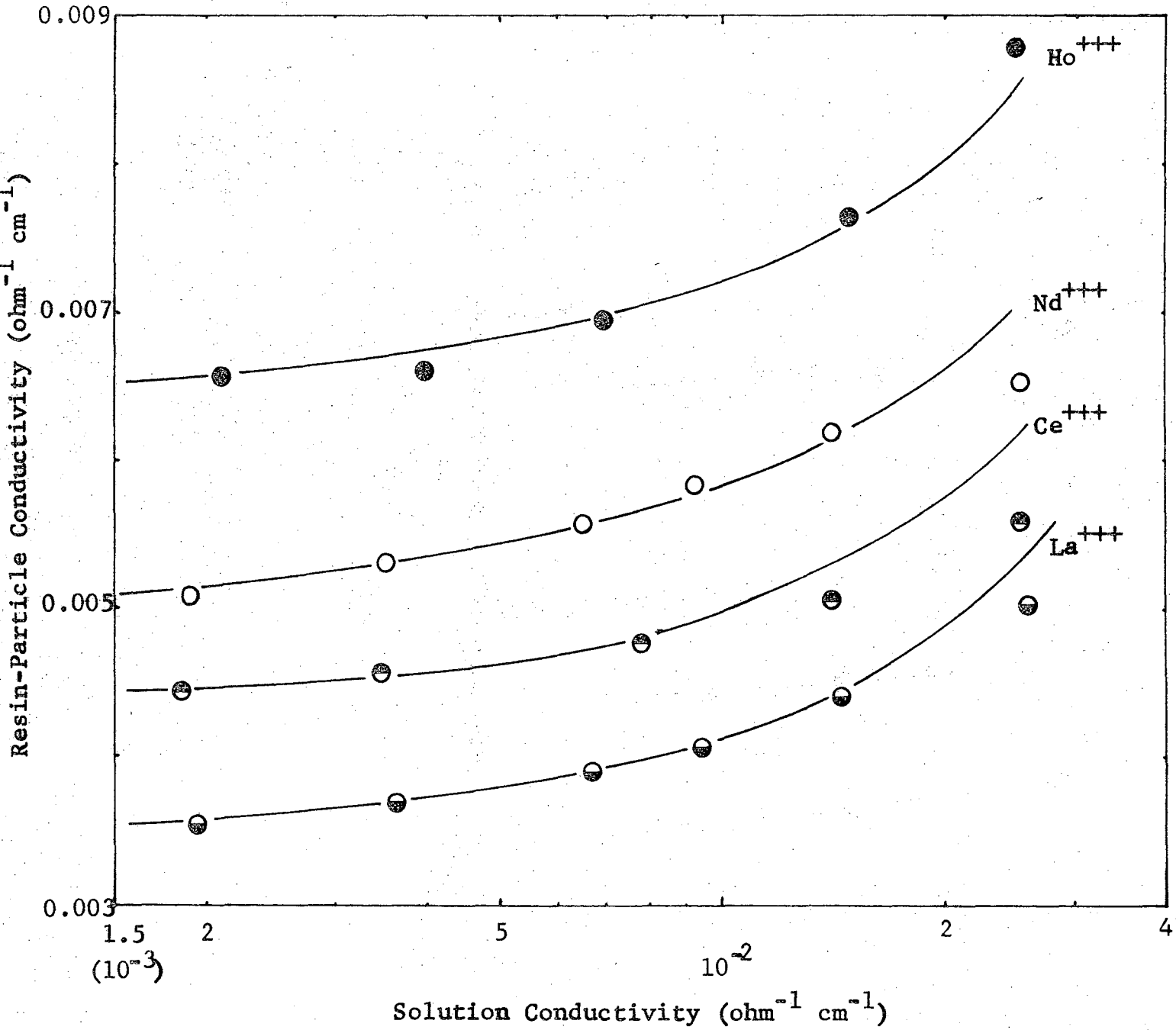

Fig. 6. Resin-particle conductivities for Dowex 50W-X4 in equilibrium with rare earth nitrate solutions; $\in$ = 0.40, 30°C.

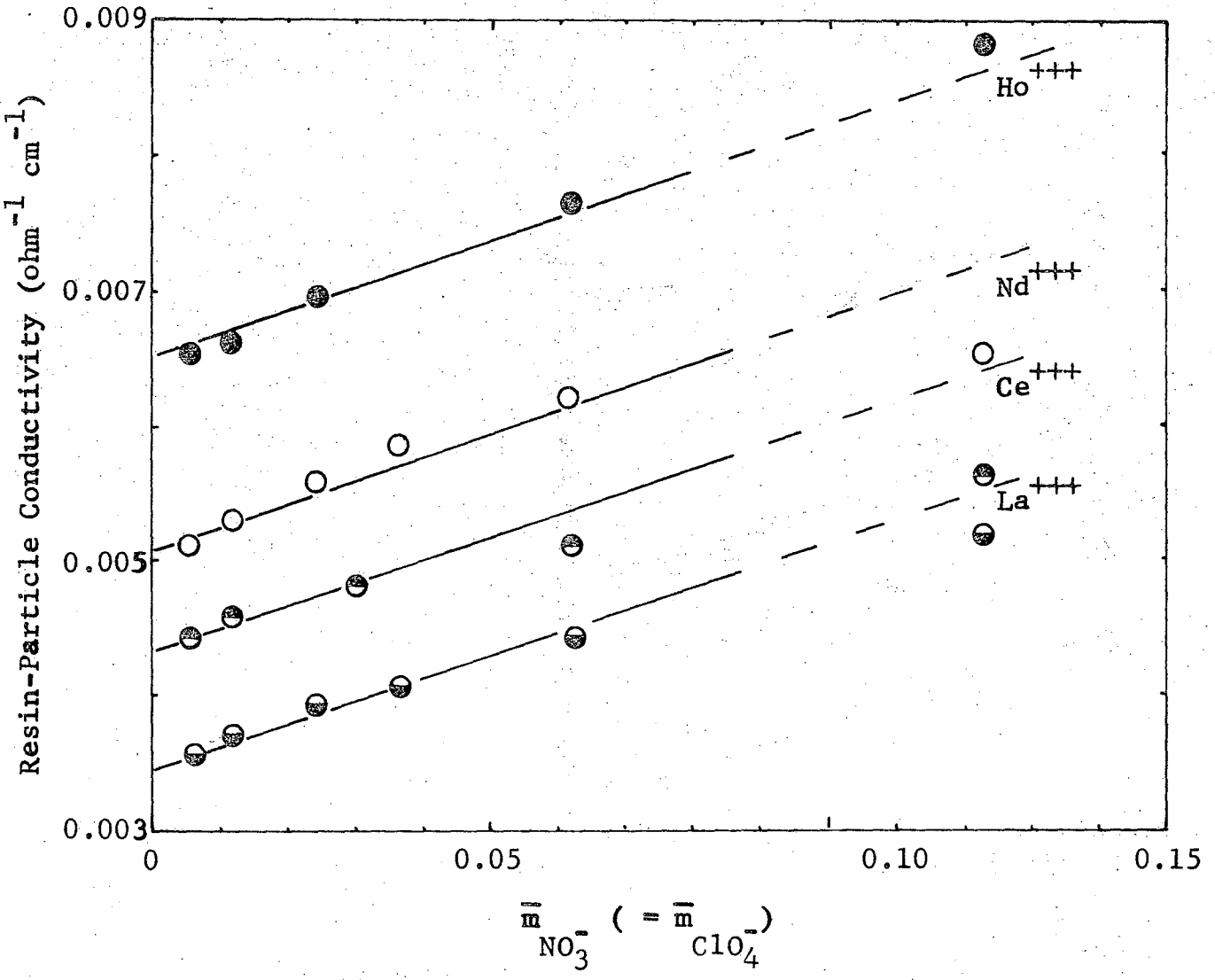

Fig. 7. Increase in resin-particle conductivities as a function of the sorbed co-ion concentration for Dowex 50W-X4 equilibrated with rare earth nitrate solutions.

with the total sorbed nitrate for $Nd(NO_3)_3$ 50% greater than for $Ho(NO_3)_3$. Deviations observed at the higher solution conductivity values are probably due to the increasing sensitivity of the Bruggeman relation to the void volume for conditions far from the isoconductance point.

The particle conductivity for $\bar{m}_{NO_3^-} = 0$ corresponds to the particle conductivity due to the migration of the counter ions only, and can be used in conjunction with Eq. (3) to calculate the ionic mobility of the rare earth cations on the resin.

Mobilities and Diffusivities

Resin conductivity data can be used to calculate self-diffusion coefficients for ions on the resin. The relation between the ionic mobility and the self-diffusion coefficient is given by the Nernst-Einstein equation

$$D_i = \frac{RT}{Z_i F} U_i \quad , \tag{4}$$

where D_i is the self-diffusion coefficient ($cm^2\ sec^{-1}$), R is the gas constant (watt sec deg^{-1} $mole^{-1}$), T the absolute temperature, F the Faraday constant (coul $equ.^{-1}$), u_i the ionic mobility (cm^2 $volt^{-1}$ sec^{-1}), and z_i is the valence of the ion.

The ionic mobilities and self-diffusion coefficients are given in Table IV.

The self-diffusion coefficients for sodium are about 3 times larger than those measured by Boyd and Soldano.[12] They are however remarkably similar to those reported by Hering and Bliss[13] for exchange experiments

Table IV. Ionic Mobilities and Self-Diffusion Coefficients of Ions on Dowex 50 at 30°C

DVB	Ionic Form	k_p [a]	C_R ($\frac{meq}{ml\ resin}$)	U	D(cm/sec)
4	Ag^+	0.0446	2.78	1.66×10^{-4}	4.3×10^{-6}
	La^{+++}	0.00345	2.9	1.19×10^{-5}	1.04×10^{-7}
	Ce^{+++}	0.00433	2.9	1.55×10^{-5}	1.35×10^{-7}
	Nd^{+++}	0.00508	2.9	1.82×10^{-5}	1.61×10^{-7}
	Ho^{+++}	0.00657	2.9	2.35×10^{-5}	2.08×10^{-7}
2	Na^+	0.0485	1.25	4.02×10^{-4}	1.05×10^{-5}
4	Na^+	0.046	2.2	2.22×10^{-4}	5.7×10^{-6}
8	Na^+	0.0316	3.17	1.03×10^{-4}	2.7×10^{-6}
(Water)	Na^+			5.7×10^{-4}	

[a] Values are for the resin particles in the desired form and in equilibrium with distilled water.

interpreted with a Nernst-Planck model. The self-diffusivity for lanthanum is about 40% higher than the value reported by Soldano and Boyd.[12]

The rare earth mobilities and corresponding self-diffusivities are found to increase with increasing atomic weight (and decreasing ion radii). Significant differences in mobility on the resin exist for the rare earths. Holmium has a mobility about twice that of lanthanum.

Results for Mixtures of Ions

Table V gives the measured solution and bed conductivities and calculated particle conductivities for Dowex 50W-X4 in mixed Ce^{+++} - Ag^{+} and La^{+++} - Ag^{+} form. The calculated particle conductivities are presented as a function of the equivalent fraction of silver on the resin in Figs. 8 and 9. The solution concentration of Ag for these results varied from 0.1 to almost 0.4 molar (for values of E_{Ag^+} close to 1); the values for the rare earths were always less than 0.005 molar. At these concentrations, negligible sorption of excess rare earth is expected. The sorption of $AgNO_3$ (which is appreciable) is mostly in the form of neutral ion pairs and is not expected to significantly affect the results.

The straight lines represent the theoretical result assuming Kohlrausch's theory of the independent rate of migration of ions to hold for the resin phase. The experimental points lie on a separate curve below this line, demonstrating significant interaction between the two ions. In measuring self-diffusion coefficients of ions on a resin, for instance Zn^{++} and Na^{+},[17] the presence of the faster ion tends to increase the diffusivity of the slower ion, while the presence of the slower ion

Table V. Particle Conductivities for Mixed Rare-Earth and Silver Form Dowex 50W-X4; $\in$ = 0.40, 30°C

Cerium and Silver

Solution $Ce(NO_3)_3$ M/L	Concentration $AgNO_3$ M/L	$\bar{Y}_{Ag}$	k_s	k_b	k_p
0.00245	0.043	0.140	0.00628	0.006856	0.0727
0.00166	0.105	0.336	0.01301	0.01319	0.0133
0.00177	0.180	0.543	0.02074	0.02112	0.0214
0.00215	0.316	0.77	0.03434	0.03364	0.0332
0.00215	0.316	0.77	0.03424	0.03312	0.0324
0.00127	0.38	0.88	0.04055	0.03978	0.0393
0.000158	0.380	0.97	0.04116	0.0428	0.0439
--	0.460	1.00	0.04677	0.04532	0.0444

Lanthanum and Silver

Solution $La(NO_3)_3$ M/L	Concentration $AgNO_3$ M/L	$\bar{Y}_{Ag}$	k_s	k_b	k_p
0.00237	0.043	0.114	0.006316	0.00614	0.006024
0.00108	0.050	0.163	0.00670	0.007147	0.00746
0.00206	0.100	0.267	0.01263	0.01142	0.01066
0.00168	0.150	0.403	0.01773	0.01682	0.01623
0.00141	0.200	0.59	0.02261	0.02343	0.240
0.000477	0.300	0.867	0.0314	0.03413	0.03605
--	0.460	1.00	0.04677	0.	0.0444

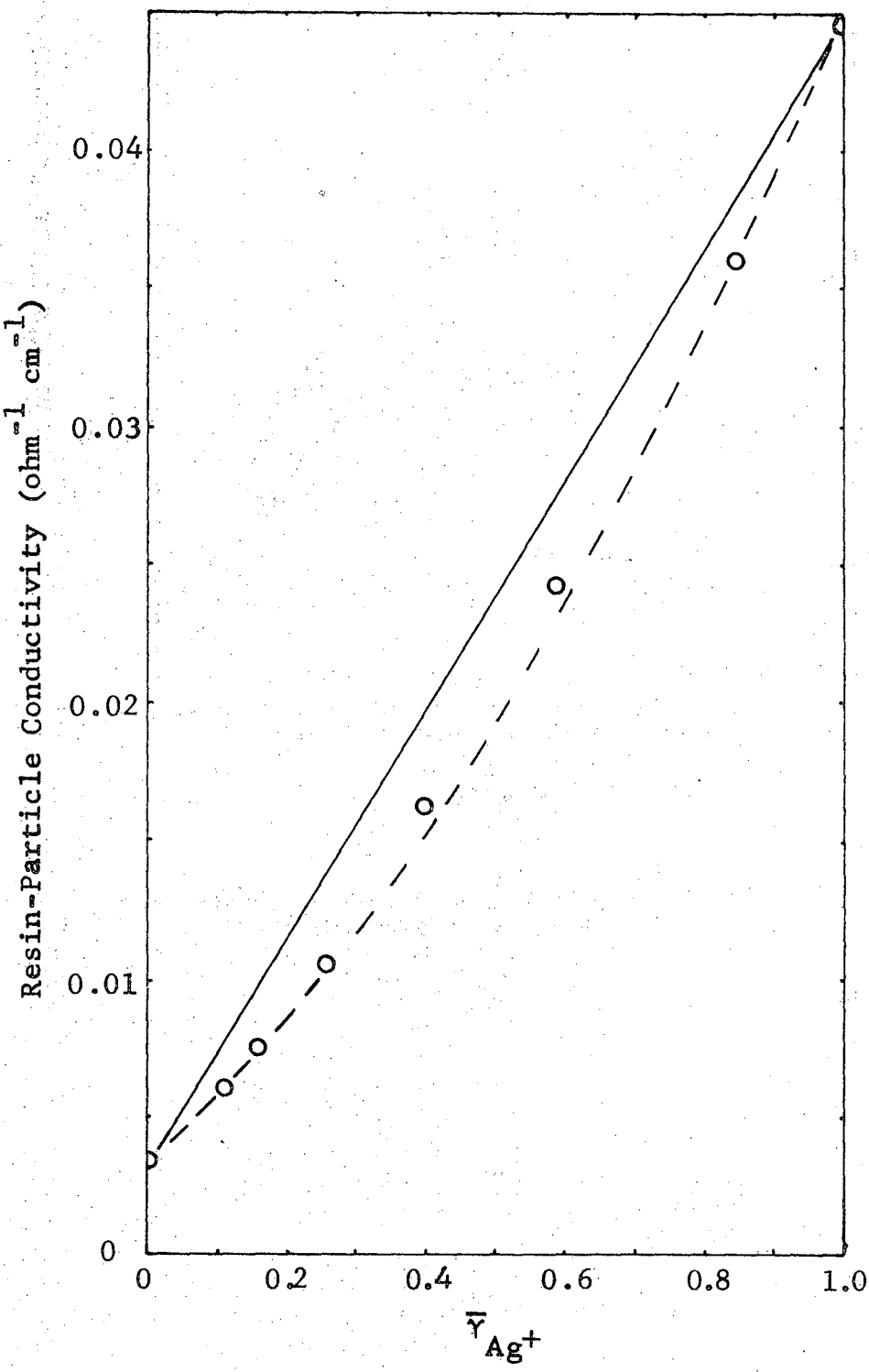

Fig. 8. Resin-particle conductivity for Dowex 50W-X4 at 30°C, in a La^{+++} - Ag^+ ion form, as a function of the equivalent fraction of silver on the resin; $\in$ = 0.40.

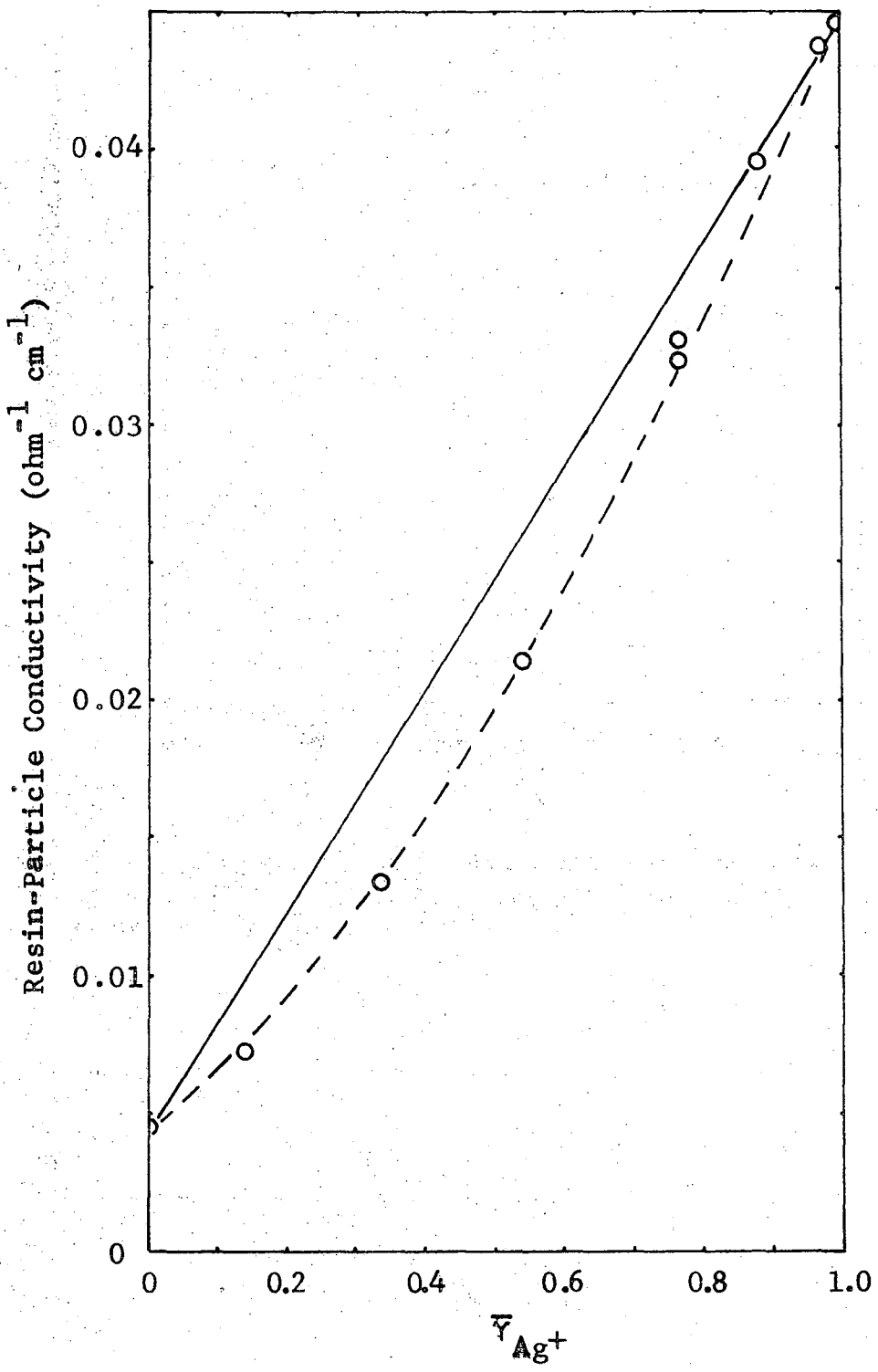

Fig. 9. Resin-particle conductivity for Dowex 50W-X4 at 30°C in a Ce^{+++} - Ag^+ ion form, as a function of the equivalent fraction of silver on the resin; ϵ = 0.40.

tends to decrease the diffusivity of the faster ion. The diffusivities can be expressed approximately as the equivalent fraction of the components on the resin. Then, for a mixture of two ions (A and B), the mobilities of A on pure-A resin, A on pure-B resin, B on pure-B resin, and B on pure-A resin must be known. The mobility of an ion on a resin in the same-ion form can be calculated from the measured conductivity. The mobility of an ion on a resin in the other-ion form can be deduced only empirically as the value that gives a reasonable fit for the particle conductivity as a function of equivalent fraction.

The resin-particle conductivity for a mixture is given by

$$\overline{\Lambda}_{MIX} = \overline{\Lambda}_{Ce^{+++}} (1-\overline{Y}_{Ag^+}) + \overline{\Lambda}_{Ag^+} \overline{Y}_{Ag^+} \quad , \tag{5}$$

where $\overline{Y}_{Ag^+}$ = the equivalent fraction of Ag^+ on the resin. If a linear variation is assumed for $\overline{\Lambda}_{Ce^{+++}}$ and $\overline{\Lambda}_{Ag^+}$ as a function of $\overline{Y}_{Ag}$, then the result becomes:

$$\overline{\Lambda}_{MIXTURE} = \overline{\Lambda}_{Ce^{+++}_{(E=0)}} (1 + f\overline{Y}_{Ag^+})(1 - \overline{Y}_{Ag^+}) + \overline{\Lambda}_{Ag^+_{(E=1)}} (g + \overline{Y}_{Ag^+} - g\overline{Y}_{Ag^+})\overline{Y}_{Ag^+}, \tag{6}$$

where f is the ratio of the mobility of Ce^{+++} on resin in Ag^+ form to the mobility of Ce^{+++} on resin in the Ce^{+++} form, and g the ratio of the mobility of Ag^+ on the resin in Ce^{+++} form to the mobility of Ag^+ on resin in Ag^+ form.

The deviation from the straight line predicted by this equation is determined by a weighed sum of f and g; thus the separate factors cannot be ascertained from these experiments. A possible interpretation for the dashed curves in Figs. 9a and 9b is that $f=2$ and $g=0.5$.

The percentage increase in conductivity with temperature was insensitive to composition; the average increase relative to 30°C was 7.5% at 33°C and 15% at 36°C. This corresponds to an average activation energy of 4.3 kcal/gmole.

References

1. S. R. Caplon, J. of Electrochem. Soc. 108, 577 (1961).
2. F. Helfferich, Ion Exchange, McGraw-Hill, New York, 1962.
3. J. C. Maxwell, A Treatise on Electricity and Magnetism, 2nd ed., Vol. 1, p. 435, 1881.
4. D. A. G. Bruggeman, Ann. Physik. 24, 636 (1935).
5. R. E. Meredith and C. W. Tobias, J. Electrochem. Soc. 108, 286 (1961).
6. J. F. Brown, J. Chem. Phys. 23, 1514 (1955).
7. M. C. Sauer, P. F. Southwick, K. S. Spiegler, and M. R. J. Wyllie, Ind. Eng. Chem. 47, 2187 (1955).
8. K. S. Spiegler, R. L. Yoest, and M. R. J. Wyllie, Discuss. Faraday Soc. 21, 174 (1956).
9. D. G. Howery and S. Tada, J. Macromol. Sci. A3, 297 (1969).
10. A. Günter-Shulze, Z. Electrochem. 28, 89, 387 (1922).
11. O. D. Bonner, C. F. Jumper, and O. C. Rogers, J. Phys. Chem. 62, 250 (1958).
12. G. E. Boyd and B. A. Soldano, J. Am. Chem. Soc. 75, 6091 (1954).
13. B. Hering and H. Bliss, A.I.Ch.E.J. 9, 495 (1963).
14. S. Glastone, Introduction to Electro-Chemistry, D. Van Nostrand Co., New Jersey, 1960.
15. K. S. Spiegler and C. O. Coryell, J. Phys. Chem. 57, 687 (1953).
16. L. Nady and T. Vermeulen, next chapter of this thesis.
17. B. A. Soldano and G. E. Boyd, J. Am. Chem. Soc. 75, 6107 (1953).

III. SORPTION OF SIMPLE AND COMPLEXED IONS BY ION EXCHANGERS

Introduction

Ion-exchange resins are solid organic polymers with ionic groups permanently attached to the organic network. Such fixed ionic groups have negative charges for the case of a cation resin, and positive charges for an anion resin. Equivalent number of counter ions (ions of opposite charge relative to the fixed ions) must be present near the fixed ions to maintain electroneutrality. Counter ions are mobile and may exchange with other ions of like charge from the solution. Ions having the same type of charge as the fixed groups attached to the resin are called co-ions.

Due to the presence of the fixed ions, a tendency exists to exclude co-ions from the resin. However, this exclusion is not complete. The concentration of sorbed electrolyte (co-ions, plus an equivalent amount of excess counter-ions) generally increases with increasing solution-concentration of electrolyte and with decreasing resin crosslinking. The presence of such excess electrolyte affects ionic transport properties in the resin, and must be taken into account in any measurement of ionic diffusivities or mobilities for the resin phase.

To assess properly the effect of the sorbed electrolyte on ionic transport properties in the resin, the form of the sorbed species (whether present as uncomplexed ions, complexed ions, or neutral complexes) must be determined.

The Donnan treatment commonly adopted for the sorption of electrolytes by ion-exchange resins assumes equilibration of the electrochemical potentials of all species between resin and solution. Complete dissociation

of the electrolyte into charged ions in both phases is implicit in this treatment. Thus the possibility of ion-pair or complex-ion formation in either phase is not explicitly accounted for, except as possible corrections in activity coefficients for the ions, with such activity coefficients usually unavailable for the resin phase.

In the following sections a detailed analysis of electrolyte sorption is presented, including Donnan sorption. The effect of complex formation, both in solution and in the resin phase, is considered. Guidelines are given for determining the form of the sorbed species in any given case, and consequently for choosing the equations that describe the sorption.

Theory of Donnan Uptake and Complexing

The general thermodynamic formulation of the Donnan equilibrium, as reported by Helfferich,[1] consists of equating the solution- and resin-phase activities of the ionic species, with a correction term for the pressure difference between the two phases. For an electrolyte AY dissociating in solution to give ν_A moles of cation A and ν_Y moles of anion Y, the formulation becomes:

$$\left(\frac{\bar{a}_{\pm}}{a_{\pm}}\right)^{\nu} = \left(\frac{\bar{a}_w}{a_w}\right)^{\nu_{AY}/\nu_w} , \qquad (4)$$

where $a_{\pm}$ is the activity of the electrolyte in solution, $\bar{a}_{\pm}$ is the activity of the electrolyte in the resin phase, a_w and $\bar{a}_w$ are the activities of the water in the solution and the resin phases respectively,

$\nu = \nu_A + \nu_Y$ is the sum of the stoichiometric coefficients of the ions, v_{Ay} is the molar volume of the electrolyte, and v_w is the molar volume of water. The term on the right side of Eq. (4) remains essentially constant over order-of-magnitude changes in solution- and resin-phase activities and, for resin of low crosslinking, is approximately 1; that is, $\bar{a}_\pm$ is nearly equal to $a_\pm$.

The mean activities are related to ionic molalities through the activity coefficients.

$$a_\pm^{\nu} = m_A^{\nu_A} m_Y^{\nu_Y} \gamma_\pm^{\nu} \tag{5}$$

$$\bar{a}_\pm^{\nu} = \bar{m}_A^{\nu_A} \bar{m}_Y^{\nu_Y} \bar{\gamma}_\pm^{\nu} \quad . \tag{6}$$

The electroneutrality relations for the ion exchanger and the solution are

$$|z_A|\bar{m}_A = \bar{m}_r + |z_Y|\bar{m}_Y \tag{7}$$

$$|z_A|m_A = |z_Y|m_Y \quad , \tag{8}$$

where $\bar{m}_r$ is the molality of the univalent ionic groups fixed on the resin.

For a cation exchanger, substituting Eqs. (6) and (7) into Eq. (4) results in the general expression for the sorption of co-ion Y:

$$\bar{m}_Y^{\nu_Y} = \frac{(|z_A|)^{\nu_A}}{(|z_Y|\bar{m}_Y + \bar{m}_r)^{\nu_A} \bar{\gamma}_\pm^{\nu}} \; a_\pm^{\nu} \left(\frac{\bar{a}_w}{a_w}\right)^{\nu \, AY/v_w} \quad . \tag{9}$$

For a 1-1 electrolyte (ν=2), Eq. (9) becomes

$$\bar{m}_Y = \frac{1}{(\bar{m}_Y + \bar{m}_r)\,\bar{\gamma}_\pm^{\,2}}\; a_\pm^{\,2} \left(\frac{\bar{a}_w}{a_w}\right)^{V_{AY}/V_w} \qquad (10)$$

For a 3-1 electrolyte (such as the rare earth nitrates or perchlorates), the equation is

$$\bar{m}_Y = \frac{(3)^{1/3}}{(\bar{m}_Y + \bar{m}_r)^{1/3}\,\bar{\gamma}_\pm^{\,4/3}}\; a_\pm^{\,4/3} \left(\frac{\bar{a}_w}{a_w}\right)^{V_{AY}/3V_w} \qquad (11)$$

To get the familiar Donnan expression in terms of solution concentrations, Eqs. (5) and (8) may be used to substitute for the solution activity. For dilute solutions, the uptake of co-ions is small compared to the fixed sites ($\bar{m}_Y \ll \bar{m}_r$), and the expression ($\bar{m}_Y + \bar{m}_r$) may be replaced by $\bar{m}_r$.

However, quantitative predictions of sorption equilibria, as a test for the theory, cannot be made due to lack of adequate knowledge about the activity coefficients for the species in the resin phase.

Complex Formation

Though complex formation is not explicitly taken into account in the Donnan equilibrium treatment, it has long been recongnized that a large uptake of an electrolyte could occur by this means.

Due to the relatively invariant environment within the resin phase (that is, the constant concentration of fixed ionic sites and the nearly constant concentration of ions) it is postulated that, as a given solution-phase activity of electrolyte, the tolerance of the resin for excess

ionized species of given charge type is the same for all electrolytes. Thus the sorption of 1-1 electrolytes capable of forming neutral complexes will be enhanced over that of 1-1 electrolytes that are completely dissociated. Similarly, multivalent electrolytes capable of forming complexes (either charged or neutral) will also be able to sorb more total moles of electrolyte at the allowable constant concentration level of free cation in the resin.

A "strong" electrolyte dissociates upon dissolving to give ν_A moles of A^{z_a} and ν_Y moles of Y^{z_Y} per mole of $A_{\nu_A} Y_{\nu_Y}$:

$$A_{\nu_A} Y_{\nu_Y} (s) \rightleftharpoons \nu_A A + \nu_Y Y \quad . \tag{12}$$

Considering the case of a mononegative anion (z=1) and a multipositive cation (z=2, 3, etc.), the following complex-forming equilibria can occur:

$$A^{Z_a+} + Y^- \rightleftharpoons AY^{(Z_A-1)+} \quad \frac{m_{AY}}{m_A m_Y} = K_1 \tag{13}$$

$$A^{Z_a+} + 2Y^- \rightleftharpoons AY_2^{(Z_A-2)+} \quad \frac{m_{AY_2}}{m_A m_Y^2} = K_2 \tag{14}$$

$$A^{Z_a+} + 3Y^- \rightleftharpoons AY_3^{(Z_A-3)+} \quad \frac{m_{AY_3}}{m_A m_Y^3} = K_3 \quad , \text{ etc.} \tag{15}$$

The general equation can be written

$$A^{Z_a+} + nY^- \rightleftharpoons AY_n^{(Z_A-n)+} \quad \frac{m_{AY_n}}{m_A m_Y^n} = K_n \quad . \tag{16}$$

The quantities K_n are the (cumulative) Bjerrum stability constants for the various complexes.

Complex formation for multivalent ions in aqueous solution has been well documented, especially for the rare earth nitrates and chlorides.[3-7] Thus, for a rare earth salt and a cation resin, some uptake of the dipositive and monopositive complexes as counter ions is expected, in addition to Donnan uptake of excess tripositive ions.

Uptake from Dilute Solutions

Complex ions can be taken up as counter ions by the resin even from very dilute solutions, provided that the equilibrium for complex-ion formation is reasonably favorable. (It is noted that resins generally hold more highly charged ions more strongly, and hence will tend to prefer uncomplexed ions.) For a tripositive mononegative salt with a cation resin, the first two complexes (AY^{++} and AY_2^+ the first one predominating) can be taken up by the resin as counter ions. The third complex (AY_3) will be neutral and may be sorbed as a nonelectrolyte. Any further complex formation will result in anionic species; due to their charge these will be excluded from the resin except as part of the Donnan sorption which may occur.

The uptake of the first complex by the resin is determined from the pertinent (rational) resin-selectivity coefficient K_A^{AY} and from the aqueous-phase equilibrium given by Eq. (13). Selectivity is determined by the equilibrium

$$3AY^{++} + 2\overline{Y}\cdot Resin \rightleftharpoons 2A^{+++} + 3\overline{AY}\cdot Resin$$

$$\alpha_A^{AY} = \frac{\overline{m}_{AY}^{\,3}\, m_A^{\,2}}{\overline{m}_A^{\,2}\, m_{AY}^{\,3}} \quad . \tag{17}$$

Combining the above equations to eliminate m_{AY}, and solving for $\overline{m}_{AY}$, gives

$$\overline{m}_{AY} = K_1(\alpha_A^{AY})^{1/3}\, \overline{m}_A^{\,2/3} m_A^{\,1/3} m_Y \approx (\text{constant})\cdot m_A^{\,1/3} m_Y \quad . \tag{18}$$

The similar equations for the second complex are

$$3AY_2^{+} + \overline{A}\cdot Resin \rightleftharpoons A^{+++} + 3\overline{AY}_2\cdot Resin$$

$$\alpha_A^{AY_2} = \frac{\overline{m}_{AY_2}^{\,3}\, m_A}{\overline{m}_A\, m_{AY_2}^{\,3}} \quad . \tag{19}$$

This relation, combined with Eq. (14), yields

$$\overline{m}_{AY_2} = K_2(\alpha_A^{AY_2})^{1/3} \cdot \overline{m}_A^{\,1/3} m_A^{\,2/3} m_Y^{\,2} \quad . \tag{20}$$

Then the total uptake of the anion $\overline{\sigma}_Y$ by the resin as a result of the complex counter ions (with N=2) becomes

$$\overline{\sigma}_Y = \sum_{n=1}^{N} n\, \overline{m}_{AY_n} = \overline{m}_{AY} + 2\overline{m}_{AY_2}$$

$$= K_1(\alpha_A^{AY})^{1/3}\, \overline{m}_A^{\,2/3} m_A^{\,1/3} m_Y + K_2(\alpha_A^{AY_2})^{1/3}\, \overline{m}_A^{\,1/3} m_A^{\,2/3} m_Y^{\,2} \quad . \tag{21}$$

The general result for resin uptake of a z_A-z_Y electrolyte, using Eq. (16), is

$$|z_A|AY^{(z_A-nz_Y)+} + (|z_A|-n|z_Y|)\overline{A}\cdot\text{Resin} \rightleftharpoons (|z_A|-n|z_Y|)\,A^{z_A} + |z_A|\overline{AY}_n\cdot\text{Resin}$$

$$\alpha_A^{AY_n} = \frac{\overline{m}_{AY_n}^{|z_A|}\, m_A^{(|z_A|-n|z_Y|)}}{\overline{m}_A^{(|z_A|-n|z_Y|)}\, m_{AY_n}^{|z_A|}} \quad . \tag{22}$$

Thus

$$\overline{m}_{AY_n} = \overline{m}_A^{\left(\frac{|z_A|-n|z_Y|}{|z_A|}\right)} (\alpha_A^{AY_n})^{\left|\frac{1}{z_A}\right|} K_n^{\left|\frac{nz_Y}{z_A}\right|} m_Y^n \quad , \tag{23}$$

and N in the term for total anion uptake is now $|z_A|-|z_Y|$

$$\overline{\sigma}_Y = \sum_{n=1}^{N} n\overline{m}_{AY_n} \quad . \tag{24}$$

Complex Formation with Donnan Sorption

In many cases, from 5 to 95% of the observed sorption (that is, the excess resin concentration over its measured stoichiometric capacity) can be due to the presence of charged or neutral complexes, rather than to Donnan sorption of completely dissociated salts. Whatever the ratio of complex to the total of complex and Donnan uptake, this ratio will tend to be relatively constant over order-of-magnitude changes in total aqueous phase concentrations.

The ability of a resin to sorb excess ionic species is given as a function of the solution-phase activity by the Donnan expression, Eq. (9). This equation predicts the same sorption for all $|z_A|-|z_Y|$ electrolytes at a given solution phase activity, provided the activity coefficients of the sorbed $|z_A|-|z_Y|$ electrolytes are the same.

Strong electrolytes are salts that dissociate completely in solution, hence do not form complexes. For strong $|z_A|-|z_Y|$ electrolytes, the activity coefficients for the various electrolytes in dilute solution are quite similar, and are given by the same Debye-Huckel or Brønsted type expressions. The activity coefficients for such electrolytes in the resin phase, though possibly different from those in the solution phase, should nevertheless be similar for all $|z_A|-|z_Y|$ electrolytes. It is expected that in the resin phase strong electrolytes will not associate, nor form complexes. Thus, sorption by the resin should be nearly the same for all strong electrolytes of a given charge type and will be a direct measure of resin tolerance for excess free co-ions as a function of solution phase activity.

Electrolytes that do not behave strictly as strong electrolytes and thus form complexes in solution, are expected to form complexes in the resin phase also. Such complex formation in the resin phase will have the net result of increasing the total uptake of electrolyte without increasing the amount of free co-ions. The equations for complex formation in the resin phase are analogous to those for the solution phase (Eqs. (13) through (16)), except that all quantities refer to the resin phase.

Either of two situations is possible: the counter ion can be either the ion of higher valence (A^{z_A}) or the one of lower valence (Y^{z_Y}). For either case, the counter-ion concentration in the resin phase will be large, and will not vary from the resin capacity value. When the counter ion has the higher valence (A^{z_A}), complex formation in the resin phase can be characterized by a new resin-phase complex-formation constant.

$$\bar{m}_A \bar{K}_n = \text{constant} = \bar{M}_n \quad ,$$

thus

$$\bar{M}_n = \frac{\bar{m}_{AY_n}}{(\bar{m}_Y)^n} \quad , \tag{25}$$

where $\bar{M}_n$ is the equilibrium constant for complex formation, multiplied by the resin capacity.

The total uptake of co-ions ($\bar{\sigma}_Y$) is the sum of the uptake of the free co-ions plus the complexed co-ions.

$$\bar{\sigma}_Y = \bar{m}_Y + \sum_{n=1}^{N} n\bar{m}_{AY_n}$$

$$\bar{\sigma}_Y = \bar{m}_Y + \sum_{n=1}^{N} n\bar{M}_n(\bar{m}_Y)^n$$

$$\bar{\sigma}_Y = \bar{m}_Y(1 + \bar{M}_1 + \sum_{n=2}^{N} n\bar{M}_n(\bar{m}_Y)^{n-1}) \quad . \tag{26}$$

At low to moderate concentrations (up to around 0.1 molal), the contribution of the terms within the summation will be small compared with the first two terms, and thus the total uptake of co-ions will be proportional to the sorbed free co-ion concentrations $\bar{m}_Y$. Since $\bar{m}_Y$ is given by the Donnan treatment, and the total uptake of co-ions is a linear function of the sorbed free co-ions, the <u>total</u> co-ion uptake (the free co-ions and those in the complexed form) will follow the same power dependence on solution-phase activity as does the <u>free</u> co-ion uptake. At low solution concentrations, then, complex formation will increase the sorption of electrolyte by a factor of $(1 + \bar{M}_1)$. If $\bar{M}_1 (= K_1 \bar{m}_A) \geqslant 1$, this increase can become quite appreciable.

At higher solution concentrations, with counter ions of higher valence states (z_A of 2 or more), the terms for complexes containing more than one co-ion should begin to contribute. Even so, because $\bar{M}_1$ will predominate, the total uptake of co-ion will follow much the same power dependence on solution-phase electrolyte activity as in the Donnan treatment.

When the counter ion has the lower valence (Y^{z_Y}), the total uptake of co-ion (A^{z_A}) becomes:

$$\bar{\sigma}_A = \bar{m}_A \left(1 + \sum_{n=1}^{n_{max}} (\bar{m}_Y)^n \bar{K}_n\right) \quad . \tag{27}$$

Only multiple complexing of co-ions will convert them into easily sorbed counter ions. In Eq. (27), n_{max} is the maximum coordination number allowed by the electronic structure of the co-ion. Often the $\bar{K}_n$ value

for $n = n_{max}$, and occasionally other K_n values as well, will give terms in $\bar{K}_n(\bar{m}_Y)^n m_A$ that are much larger than the Donnan uptake $\bar{m}_A$. A good example of such multiple-ion complex formation can be found in the well-known separations of polyvalent cations in HCl solutions on anion-exchange resins.[8]

Identification of Mechanism

Two approaches to the treatment of electrolyte sorption by ion exchangeers are possible. One approach is to take the Donnan treatment combined with the measured sorption for a given electrolyte, and to calculate the corresponding activity coefficients for that electrolyte in the resin phase. This approach, unfortunately, does not shed much light on the nature of the sorbed electrolyte.

The second approach is to assume that at a given solution-phase activity of an electrolyte, the net sorption of the electrolyte as free ions by the resin is given by the sorption of a corresponding $|z_A|-|z_Y|$ strong electrolyte at the same solution-phase activity. Thus the increased sorption of any electrolyte over that of a strong electrolyte can be attributed to ion association (complex formation) in the resin phase. This approach allows one to identify the various species sorbed by the resin from solution. Such information will be required in order properly to assess the contribution of the sorbed electrolyte to the measured conductivity of the resin particles.

The choice of equation in a given case is determined from sorption measurements for a known strong electrolyte. For dilute solutions, such measurements will immediately resolve whether Donnan sorption is occurring. If there is no sorption of the strong electrolyte (or if this sorption is

small compared to the measured uptake of other similar polyvalent electrolytes), then sorption is due mainly to the distribution of complexed and uncomplexed ions on the resin as counter ions. Equations (17) through (24) can be used for this case.

For more concentrated solutions, or where there is significant sorption of known strong electrolytes, Eq. (25) through (27) should be used to treat the enhanced sorption of electrolytes.

For a 1-1 electrolyte forming only a neutral molecule, the enhanced sorption of such an electrolyte over that of a strong 1-1 electrolyte gives immediately the concentration of the neutral species on the resin.

$$\bar{m}_{AY} = \bar{\sigma}_{Y(\text{measured})} - \bar{m}_{Y(\text{strong electrolyte})} \quad . \tag{28}$$

With $\bar{m}_A, \bar{m}_Y$, and $\bar{m}_{AY}$ known, the equilibrium constant for complex formation in the resin phase can be calculated.

For a $|z_A|-|z_Y|$ electrolyte forming only one complex, the additional relations needed to solve for all sorbed species are: $\bar{m}_Y$ the same as for strong $|z_A|-|z_Y|$ electrolyte; the mass balance for Y

$$\bar{\sigma}_Y = \bar{m}_Y + \bar{m}_{AY} \quad , \tag{29}$$

electroneutrality in the resin phase

$$\bar{m}_R + |z_Y|\bar{m}_Y = |z_A|\bar{m}_A + |z_{AY}|\bar{m}_{AY} \quad . \tag{30}$$

Since $\bar{m}_Y$, $\bar{\sigma}_Y$, $\bar{m}_R$ are known, $\bar{m}_A$ and $\bar{m}_{AY}$ can be calculated. The equilibrium constant for complex formation in the resin phase can again be calculated readily.

For a $|z_A|-|z_Y|$ electrolyte forming several complex species, the relations (in addition to Eq. (28)) become:

$$\bar{\sigma}_Y = \bar{m}_Y + \sum_{n=1}^{N} n\bar{m}_{AY_n} \quad , \tag{31}$$

and

$$\bar{m}_R + |z_Y|\bar{m}_Y = |z_A|\bar{m}_A + \sum_{n=1}^{N} |z_{AY_n}|\bar{m}_{AY_n} \quad . \tag{32}$$

For N=2 or more, there are more unknowns than equations. The additional needed equations (N-1 of them) must be provided from some knowledge of the equilibrium constants (however, only N-1 such constants are needed, since the last one may then be calculated from the total observed uptake).

Experimental Program

The electrolyte sorption by Dowex 50W-X4 of a number of rare earth nitrate solutions (Ho^{+++}, Ce^{+++}, La^{+++}, and Nd^{+++}), a perchlorate solution (La^{+++}), and silver nitrate and sodium chloride solutions was measured. Solution concentrations investigated varied from 0.01 to 0.1 molar for the rare earths, from 0.01 to 0.5 molar for silver nitrate, and from 0.1 to 1.0 molar for sodium chloride. The sorption of lanthanum perchlorate on Dowex 50W-X2, X8, and X12 was measured for concentrations from 0.1 to 1.0 molar.

Two 25-ml burets were each filled with approximately 15 ml of the wet resin in the hydrogen form. Fritted-glass disks retained the resin

in the column. The resin was then pretreated by the procedure described for conductivity measurements. Once the resin was in the desired ionic form, it was equilibrated with solution of the desired concentration by passing about 100 ml of solution (or about 20 times the expected sorption) through the column over a period of 3 to 5 hours.

The liquid level was then allowed to drop to the bed level, whereupon elution with de-ionized distilled water was begun into a 250 cc columetric flask. The liquid holdup of the equilibrating solution was calculated by adding the void volume in the bed to the residual volume between the glass filter and the buret tip (0.6 cc). The electrolyte present in this holdup liquid was subsequently subtracted from the total electrolyte eluted off. The remainder represented the electrolyte uptake by the resin.

Upon completing the electrolyte-sorption measurements for a given counter ion, the counter ions were eluted with 6N HNO_3 into a 250 cc volumetric flask. This served to measure the resin capacity and, if the resin capacity for the various ions remained constant, to insure that all the sorbed electrolyte had previously been entirely eluted.

Silver nitrate solutions were analyzed by titrating for Ag^+ with SCN^-; rare earth nitrates by titrating with EDTA in the presence of EBT (Eriochrome Black T). The sodium chloride solutions were analyzed for Cl^- by the Volhard method.

The uptake of water by the resin was determined from the measured volumetric capacity of the resin by using the empirical expression of Pepper:[9]

$$(V_m)_H = (W_m)_H + (V_{md})_H \quad , \tag{34}$$

where $(V_m)_H$ is the swollen volume in the m-form for a quantity of resin that has a 1.0-gm H-form dry weight, $(W_m)_H$ is the volume of water sorbed on the same basis, and $(V_{md})_H$ is the corresponding volume of the dry resin in the m-form. Gregor[10] lists specific volumes for dry exchangers; the values for Na^+, Ag^+, and divalent ions such as Ba^{++}, Ca^{++}, and Mg^{++} are all similar and can be taken as 0.63. It can be assumed that the specific volume of dry exchanger for the rare earths is also approximately 0.63.

Results and Discussion

The sorption of a number of electrolytes from solution by Dowex 50W-X4 cation resin is given in Table I and shown in Figs. 1 and 2.

Figure 1 gives the sorption of two 1-1 electrolytes, NaCl and $AgNO_3$, as a function of the solution-phase activity of the respective electrolyte. NaCl behaves as a strong electrolyte in water, and does not associate or form complexes in either the solution of resin phases. In contrast, $AgNO_3$ is known to associate in solution and is expected to associate (that is, to form neutral ion-pairs) in the resin phase as well. This is reflected in the enhanced sorption of $AgNO_3$ in the resin phase, about ten times that for NaCl at any given solution-phase activity. Thus approximately 91% of the sorbed $AgNO_3$ is present in the resin phase as associated ion pairs, and only about 9% as free ions. Table I presents the resin-phase concentrations of Ag^+, $AgNO_3$, NO_3^- and the corresponding

Table I. Sorption of Electrolytes on Dowex 50W-X4

Molality m_A	Activity $(\nu_Y)\frac{\nu_Y}{\nu} m_A \gamma_\pm$	Bed Volume cc	Resin Volume, cc (smoothed)	Total Electrolyte moles $\times 10^5$	Sorbed Electrolyte moles $\times 10^5$	Total Excess $\bar{\sigma}_Y$	Uncomplexed	Complexed	Counter Ions	$\bar{K}_1$
							Resin-Phase Molalities			
							$\bar{m}_Y$	$\bar{m}_{AY}$	$\bar{m}_A$	
NaCl on 0.0236 equivalents of resin (C_m = 2.86 cc)										
0.304	0.216	16.35	9.84	226.4	12.4	0.0177	0.0177		3.38	
0.507	0.345	15.59	9.4	372.5	31.7	0.0485	0.0485		3.62	
1.03	0.677	14.95	8.98	772.0	116.0	0.189	0.189		3.86	
$AgNO_3$ on 0.0231 equivalents of resin (C_m = 2.80 cc)										
0.050	0.0395	12.96	8.22	31.5	2.58	0.00475	0.00045	0.00431	4.26	2.25
0.152	0.106	12.75	7.98	107.0	21.5	0.0415	0.0036	0.0379	4.46	2.36
0.304	0.182	12.43	7.64	234.5	67.3	0.139	0.0122	0.1268	4.69	2.22
0.512	0.273	12.28	7.24	422.5	146.9	0.331	0.029	0.302	5.23	1.99
average										2.2
$La(ClO_4)_3$ on 0.0236 equivalents of resin (C_m = 2.86 cc)										
0.010	0.0148	13.55	8.13	7.81	2.09	0.0117	0.0117		1.493	
0.050	0.0556	13.55	8.11	39.55	10.91	0.0624	0.0624		1.52	
0.102	0.104	13.50	8.04	78.5	21.3	0.1233	0.1233		1.557	
$La(NO_3)_3$ on 0.0236 equivalents of resin (C_m = 2.86 cc)										
0.0103	0.013	13.35	8.13	8.77	2.66	0.0152	0.010	0.0052	1.49	0.335
0.0206	0.0227	13.33	8.125	17.9	5.7	0.0325	0.020	0.0125	1.49	0.416
0.031	0.031	13.3	8.12	26.5	8.25	0.0480	0.030	0.018	1.49	0.402
0.052	0.0464	13.75	8.11	46.8	15.44	0.0882	0.050	0.0382	1.49	0.513
0.105	0.081	13.35	8.04	88.8	27.8	0.161	0.100	0.061	1.51	0.404

(continued)

Table I. Continued

Molality m_A	Activity $\frac{a_\pm}{(\nu_Y)^{\overline{\nu}} m_A \gamma_\pm}$	Bed Volume cc	Resin Volume, cc (smoothed)	Total Electrolyte moles $\times 10^5$	Sorbed Electrolyte moles $\times 10^5$	Total Excess $\overline{\sigma}_Y$	Uncomplexed	Complexed	Counter Ions	$\overline{K}_1$
							Resin-Phase Molalities			
							$\overline{m}_Y$	$\overline{m}_{AY}$	$\overline{m}_A$	
0.105	0.081	13.05	8.04	85.8	26.0	0.1505	0.100	0.0505	1.51	0.36
average										0.403
			$Ce(NO_3)_3$ on 0.0231 equivalents of resin (C_m = 2.80 cc)							
0.010	0.0128	13.53	7.95	8.94	2.928	0.01719	0.0096	0.00759	1.538	0.514
0.020	0.0208	13.38	7.95	17.75	5.95	0.03495	0.0178	0.01715	1.537	0.626
0.0301	0.0301	13.58	7.94	27.7	9.65	0.0567	0.029	0.0277	1.537	0.62
0.0505	0.0454	13.18	7.94	43.7	14.34	0.0746	0.048	0.0266	1.547	0.359
0.102	0.0794	12.75	7.87	83.2	26.2	0.1566	0.096	0.606	1.56	0.405
average										0.505
			$Ce(NO_3)_3$ on 0.0236 equivalents of resin (C_m = 2.86 cc)							
0.010	0.0128	13.55	8.13	9.84	2.93	0.01668	0.0096	0.00759	1.538	0.48
0.020	0.0208	13.55	8.125	18.1	6.08	0.03465	0.0178	0.01685	1.538	0.615
0.0301	0.0301	13.15	8.12	25.95	8.4	0.0577	0.029	0.0287	1.537	0.644
0.0505	0.0454	13.35	8.11	44.15	14.5	0.08289	0.048	0.03489	1.547	0.47
0.102	0.0794	13.1	8.045	84.0	25.7	0.1488	0.096	0.0528	1.577	0.349
average										0.51
			$Nd(NO_3)_3$ on 0.0231 equivalents of resin (C_m = 2.80 cc)							
0.010	0.0128	13.58	7.95	9.63	3.43	0.02013	0.0096	0.01053	1.50	0.732
0.0301	0.0301	13.78	7.94	29.55	10.72	0.06314	0.029	0.03418	1.50	0.785
0.102	0.0794	13.48	7.87	93.5	31.9	0.1908	0.096	0.0948	1.50	0.66
average										0.726
			$Ho(NO_3)_3$ on 0.0236 equivalents of resin (C_m = 2.86 cc)							
0.011	0.0138	14.65	8.13	9.92	2.82	0.01605	0.0105	0.00555	1.49	0.355
0.0333	0.0325	13.75	8.12	27.83	7.73	0.0441	0.0318	0.0133	1.50	0.279
0.112	0.0846	14.21	8.04	95.1	26.1	0.1509	0.107	0.0439	1.53	0.268
average										0.30

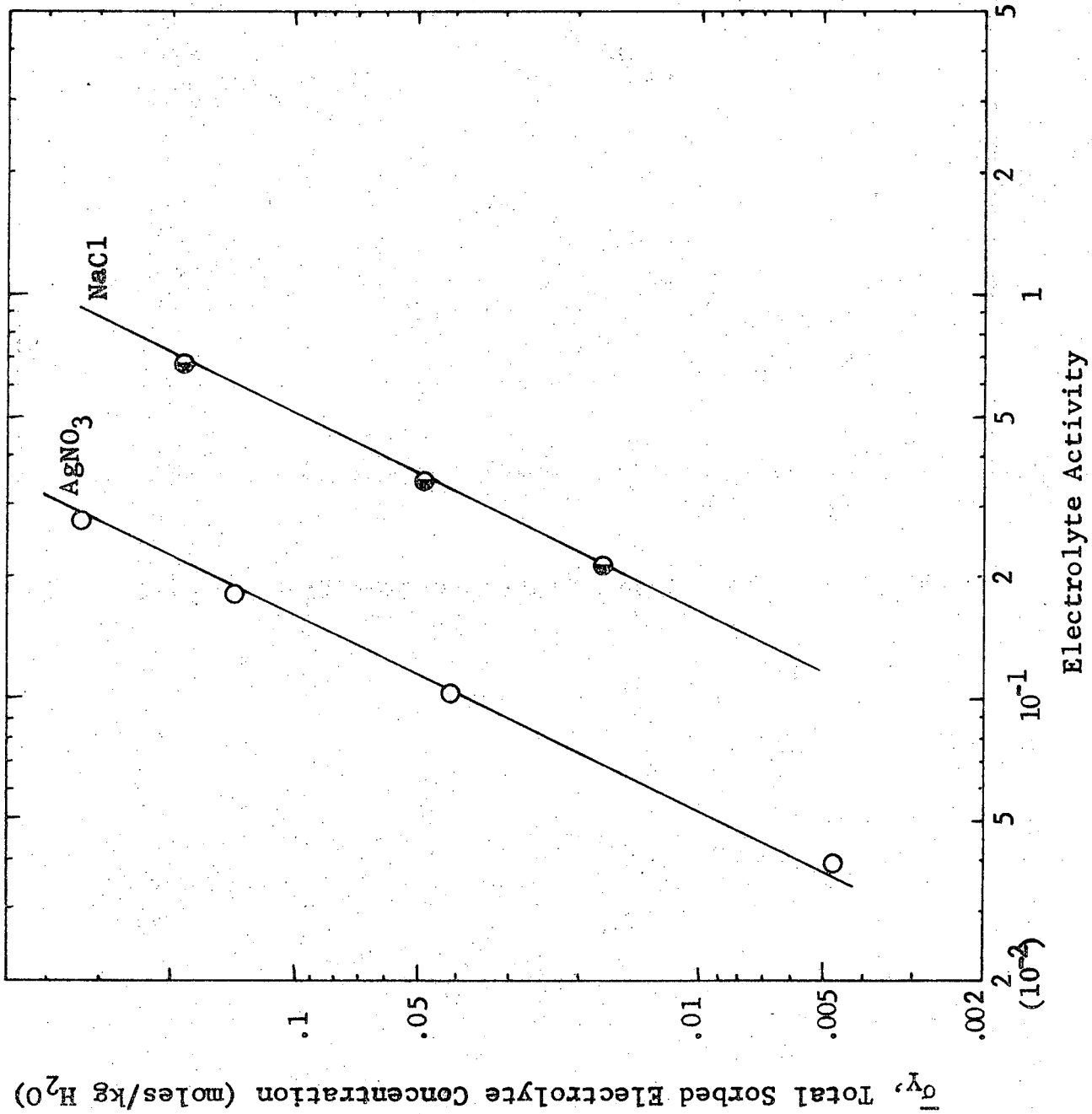

Fig. 1. Sorption of 1-1 electrolytes on Dowex 50W-X4.

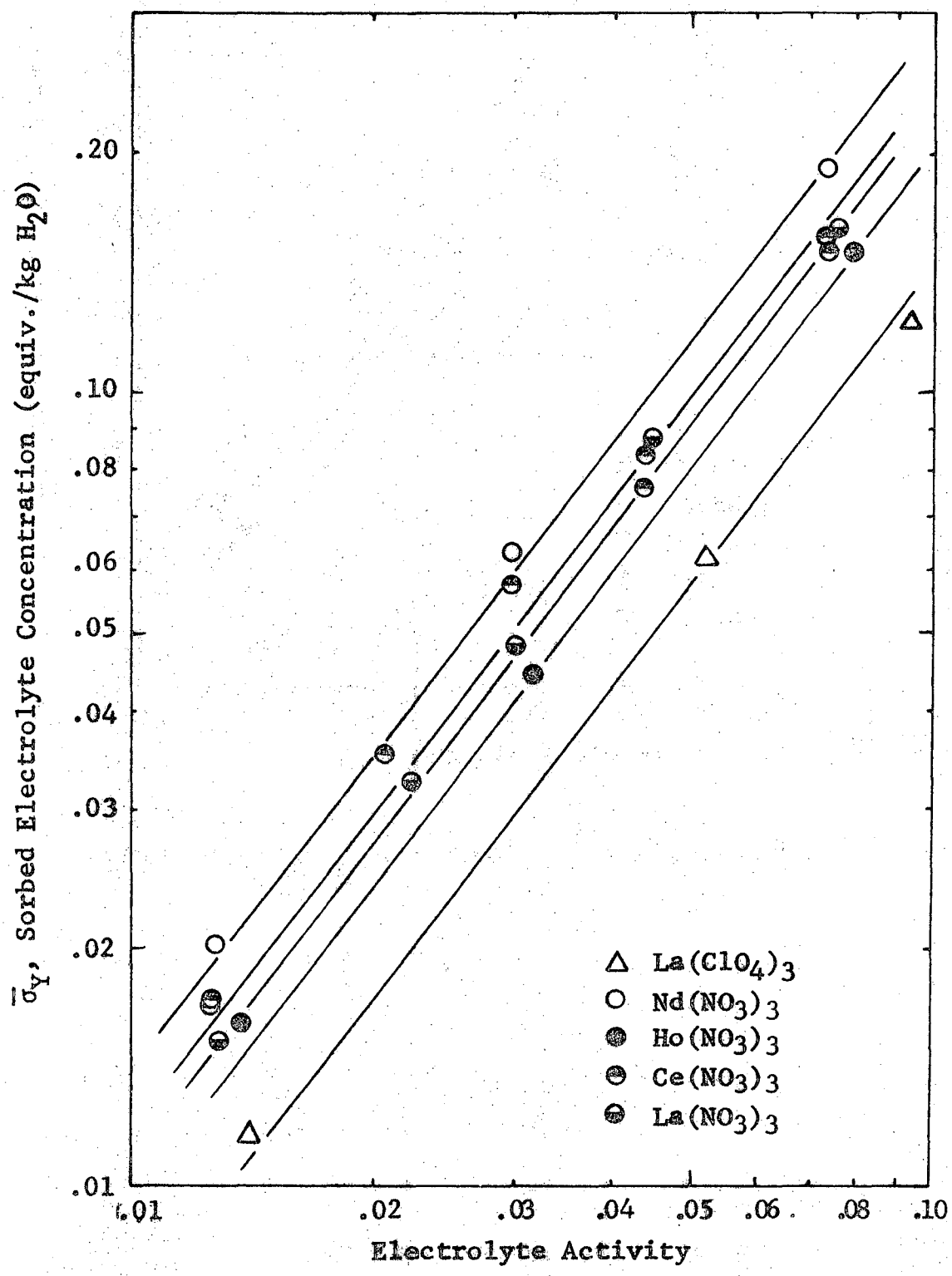

Fig. 2. Sorption of 3-1 electrolytes on Dowex 50W-X4.

association constant K_1 as functions of the solution-phase concentration of Ag^+. The association constant found for the resin phase (K=2.2) is somewhat larger than those reported for $AgNO_3$ in dilute solutions (K=0.7 for 0.05M $AgNO_3$).[11] Association constants for $AgNO_3$ in dilute solutions are reported to increase with increasing concentration. Thus the observed larger value for the resin phase (where the electrolyte concentration is high) appears reasonable.

Figure 2 shows the measured anion sorption for several rare earth nitrates and for $La(ClO_4)_3$, as a function of the solution-phase electrolyte activity. The activity coefficients for the rare earth nitrates are taken to be the same as for the rare earth chlorides;[11] and for $La(ClO_4)_3$, the same as for $Ga(ClO_4)_3$.[12] Data for the latter were readily available from the literature and were not expected to be significantly different. $La(ClO_4)_3$ behaves as a strong electrolyte, and was used to measure the co-ion concentration in the resin as a function of solution-phase electrolyte activity for a 3-1 electrolyte. The complex formation constants for the rare earth nitrates (K_n) in dilute solution decrease with each additional nitrate ($K_1 > K_2$, etc.).[4] Thus a significant complex formation of only divalent complex AY^{++} was assumed and the equilibrium constant for the formation of this complex (K_1) was calculated from the experimental data on this basis.

The effect of crosslinking on $La(ClO_4)_3$ sorption is given in Table II and shown in Fig. 3.

This model for dividing total uptake into uncomplexed and complexed sorption has been utilized in a concurrent study of resin-phase ionic mobilities.

Table II. Effect of Crosslinking on $La(ClO_4)_3$ Sorption

Molality m_A	Activity $\frac{a_\pm^{\nu_Y}}{(\nu_Y)^{\nu}\, m_A \gamma_\pm}$	Bed Volume cc	Resin Volume, cc (smoothed)	Total Electrolyte moles × 10^5	Sorbed Electrolyte moles × 10^5	Total Excess $\bar{\sigma}_Y$	Uncomplexed Resin-Phase Molalities $\bar{m}_Y$	Counter Ion Resin-Phase Molalities $\bar{m}_A$
		Dowex 50W-X2, 0.01675 equivalents of resin (C_m = 2.03 cc)						
0.102	0.104	13.5	8.1	90.3	29.6	0.1464	0.1464	0.97
0.536	0.67	12.95	7.77	435.0	142.5	0.7452	0.7452	1.22
1.15	4.8	11.75	7.05	817.5	277.5	1.662	1.662	1.67
		Dowex 50W-X4, 0.0236 equivalents of resin (C_m = 2.86 cc)						
0.010	0.0148	13.55	8.13	7.81	2.09	0.0117	0.0117	1.493
0.050	0.0556	13.55	8.11	39.55	10.91	0.0624	0.0624	1.52
0.102	0.104	13.50	8.04	78.5	21.3	0.1233	0.1233	1.557
		Dowex 50W-X8, 0.01845 equivalents of resin (C_m = 2.28 cc)						
0.102	0.104	9.25	5.55	55.6	12.1	0.111	0.111	1.92
0.536	0.67	9.25	5.55	286.5	69.0	0.633	0.633	2.09
1.15	4.8	8.9	5.34	578.0	154.0	1.512	1.512	2.51
		Dowex 50W-X12, 0.0168 dquivalents of resin (C_m = 2.11 cc)						
0.102	0.104	6.5	3.9	37.2	4.8	0.0804	0.0804	3.16
0.536	0.67	6.5	3.9	192.5	30.5	0.513	0.513	3.31
1.15	4.8	6.25	3.75	397.5	82.2	1.506	1.506	3.93

UCRL-19526

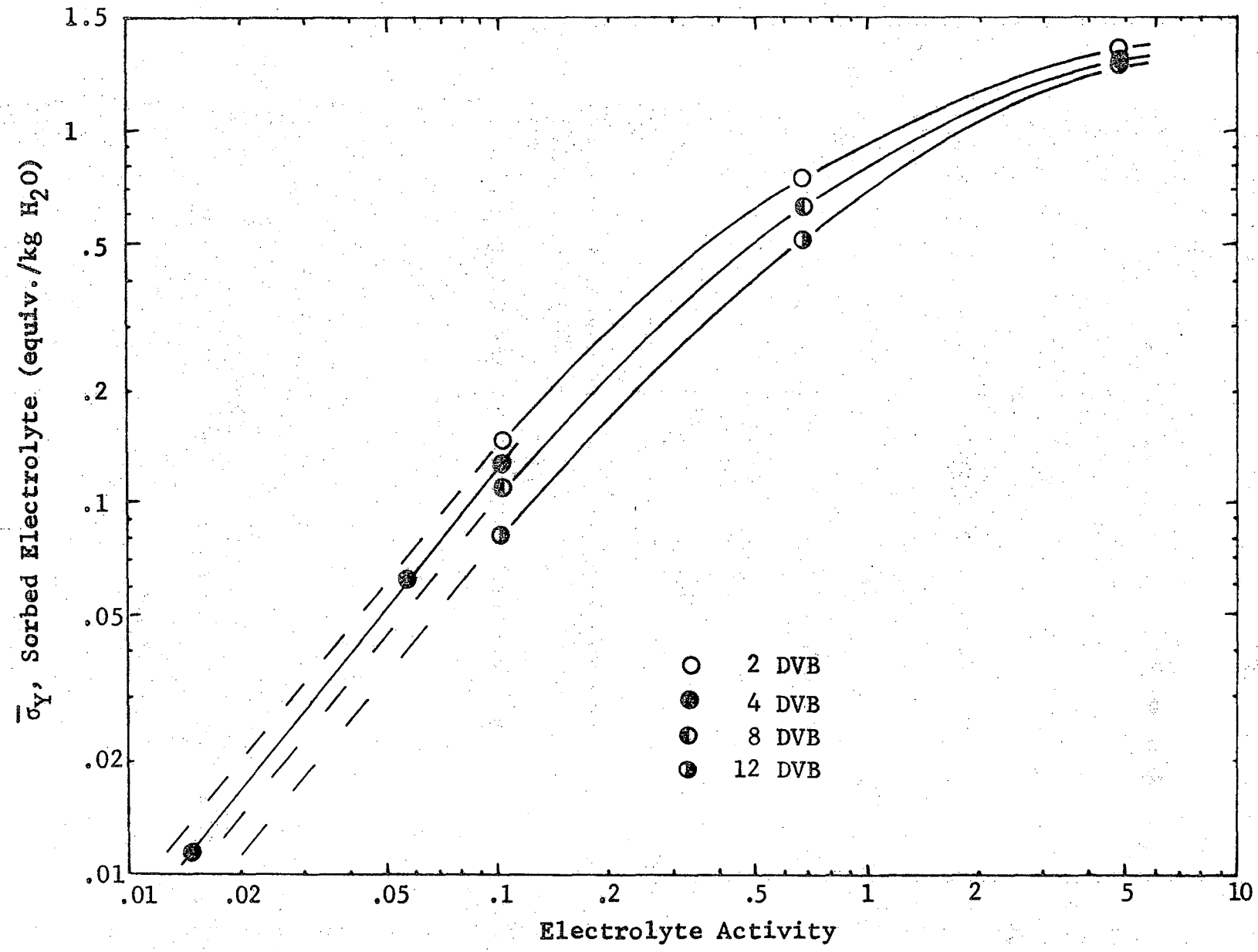

Fig. 3. Sorption of $La(ClO_4)_3$ on Dowex 50 for various crosslinkages.

References

1. F. Helfferich, Ion Exchange, McGraw-Hill, New York, 1962.
2. A., Günter-Schulze, Z. Electrochem. 28, 89, 387 (1922).
3. Y. Marcus and F. Nelson, J. Phys. Chem. 63, 77 (1959).
4. G. R. Choppin and W. F. Strazik, Inorg. Chem. 4, 1250 (1965).
5. D. F. Peppard, G. W. Mason, and I. Hucler, J. Inorg. Nucl. Chem. 24, 881 (1962).
6. M. L. Bansal, S. K. Patil, and H. D. Sharma, J. Inorg. Nucl. Chem. 26, 993 (1964).
7. V. V. Fomin, R. E. Kartushova, and T. I. Rudenko, Zh. Neorg. Khimi. 3, 2117 (1958).
8. V. Schindewolf, Z. Electrochem. 62, 335 (1958).
9. K. W. Pepper, D. Reichenberg, and D. K. Hale, J. Chem. Soc. , 3129 (1952).
10. H. P. Gregor, F. Gutoff, and J. I. Bregman, J. Colloid Sci. 6, 245 (1951).
11. W. J. Hamer, The Structure of Electrolytic Solutions, Wylie and Sons, New York, 1959.
12. C. S. Patterson, S. Y. Tyree Jr., and K. Knox, J. Am. Chem. Soc. 77, 2195 (1955).

IV. CONTINUOUS LIGAND ELECTROCHROMATOGRAPHY

Introduction

A new device, using the selective interaction of complexing agents for different ions, has been developed for the continuous preparative-scale "Ligand" electrochromatographic separations of charged species such as the rare earths.

Complexing agents have been used before to achieve electrophoretic separations of ions.[1-5] Lederer[3] found differences in the rate of migration of rare earth ions on paper strips when in the presence of 1% citric acid. EDTA has been used[1,2] to separate cationic mixtures by the selective complexing of only one of the ions with a corresponding change in its direction of electrophoretic migration. Bril, Bril, and Krumholz[4] achieved partial separation of rare earth mixtures by limited complexing with EDTA and subsequent electrodialysis to remove excess cations from complexed anions.

In the present unit, continuous separation is brought about by electrophoretic migration of excess rare earth ions across a transverse laminar flow of complexing agent in a packed bed. Selective complex formation of the ion mixture, with a resultant marked mobility change for the complexed species, causes the net electrophoretic migration rates to differ for each component, and hence to produce a separation. The Ligand is introduced as a complex with retainer ion, which has an affinity for ligand that is lower than any feed-component affinities. Next to the ligand-retainer mixture, the feed mixture to be separated is introduced and in turn this is followed by a chaser-ion species which has an affinity

for ligand that is higher than any of the feed-component affinities. Such input streams assure an excess of complexable ions at each point, relative to the supply of ligand, so that the ligand remains almost entirely complexed and immobile relative to the electric field. (Thus complexing agent travels only in the direction of fluid flow, with the velocity U_c of the continuing fluid.)

Physical Description of the Method

In this new type of electrochromatograph, the complexing agent or "ligand" (complexed with metal ion) enters the bed at the left end and moves through the bed with a convective velocity U_c, as shown in Fig. 1. The feed of rare earths is introduced either along part of the left end (FP 1) when partly complexed, or along part of the anode side (FP 2) when uncomplexed, and is moved by the imposed electric field transversely across the bed which uniformly contains complexing agent.

Initially the ligand is complexed with an ion for which it has a lower affinity than for the mixture of rare earths, and the feed or rare earths is followed by an ion for which complexant has an even greater affinity. In such cases sharp transitions will in general be maintained as the ions migrate through the bed of complexing agent; this result is analogous to displacement development in ion exchange.

The electrochromatographic bed can be represented by two distance variables (as in Fig. 1): z_e, the distance in the direction of electrophoretic migration, and z_c, the distance in the direction of convective flow. The steady-state migration path of any transition can readily be

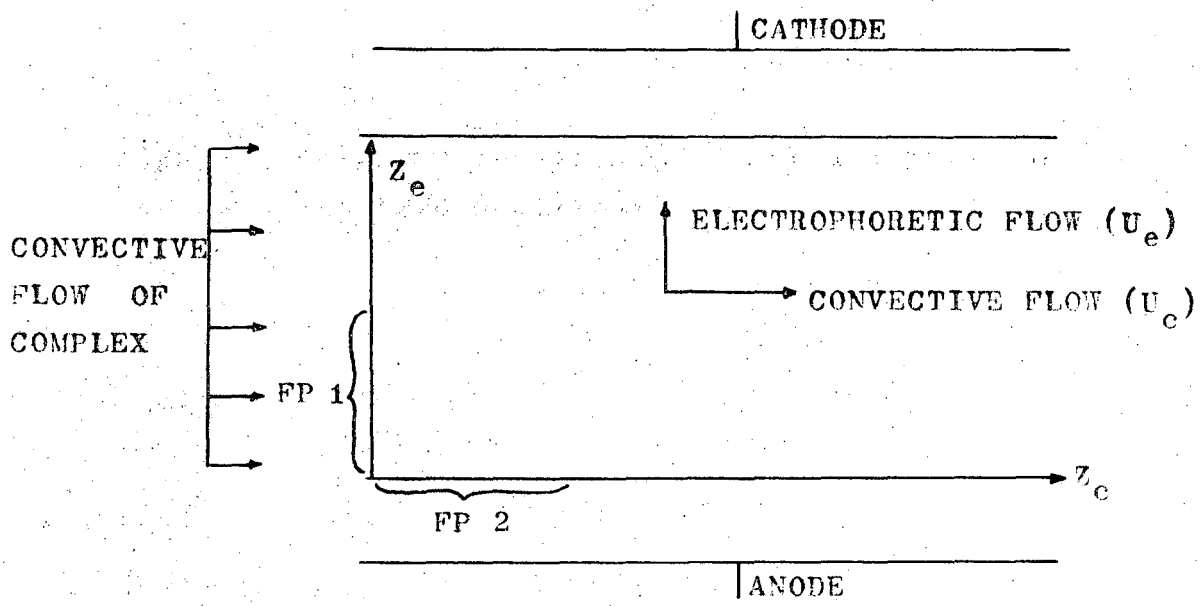

Fig. 1. Ligand electrochromatography. FP 1 and FP 2 are the two possible feed positions.

plotted on Fig. 1, once the electrophoretic and convective velocities of the transitions (that is, of the ions located at the boundaries) are known.

The electrophoretic velocity for a zone of pure component is given by the electrophoretic mobility of excess uncomplexed ions times the fraction of the total amount of that species present that is uncomplexed, $U_e\ C/(C_o + C_o^*)$. C_o is the concentration of uncomplexed ions, and C_o^* the concentration of complexed ions. Defining the ratio of uncomplexed to complexed ions as $S=C_o/C_o^*$, the net zone velocity becomes $U_eS/(S+1)$.

For a steady-state system, the transitions between zones of pure components must migrate at the same velocity as the pure zones. The direction of migration for a transition between pure components can be expressed by the distance migrated for a given time Δt in the direction of electrophoretic flow and the distance in the convective direction.

$$Z_e = U_e\ \Delta t$$

$$Z_c = U_c\ \Delta t \quad . \tag{1}$$

The transition paths for all values of U_e/U_c and S can be superimposed on a single graph by replacing Z_c by the normalized convective distance $Z_c(U_e/U_c)S/(S+1)$. Thus, on a plot of Z_e vs. $Z_c(U_e/U_c)S/(S+1)$, all transitions between pure components will have a slope of 45°, as in Fig. 2. In Fig. 2, components R and A are shown as being brought into the bed along with the complex, and B and C are introduced from the anode side. The order of increasing preference for the ion by the complexing agent is: R, A, B, C.

If a mixture of components A and B is fed to the bed from the left end, the transitions between component R and mixture and between mixture and component C occur along paths shown in Fig. 3. As components A and B of the feed mixture migrate through the ligand environment, separation occurs between them. Since B is the ion preferred by the ligand, a zone of pure A forms and expands ahead (downstream) of the mixture, and one of pure B appears behind (upstream) of the mixture. Beyond the intersection of these zones, where separation becomes complete, B transition will parallel the R-A and B-C transitions, all three having a 45° vector when plotted on these coordinates.

The time-dependent behavior of a differential one-dimensional chromatographic column can be used to represent the steady-state behavior of the two-dimensional electrochromatograph, as shown in Fig. 4. The displacement development occurring in this analogous column will trace out the steady-state behavior resulting in the ligand electrochromatograph.

Transitions Between Single-Component Regions

To calculate the slopes of the transitions of interest, between the zones of pure A and of mixture A-B, and between the zones of mixture A-B and pure B, it is necessary to determine the transverse velocity component for each transition. This can be done easily, if the following assumptions are made: (1) all species (both complex and free ions) move axially with the same convective velocity. (2) There is no mass transfer due to longitudinal dispersion or diffusion. (3) Uncomplexed ions, only, move in the electrophoretic direction. (4) Sharp transitions are maintained between separated components and the mixture which is still

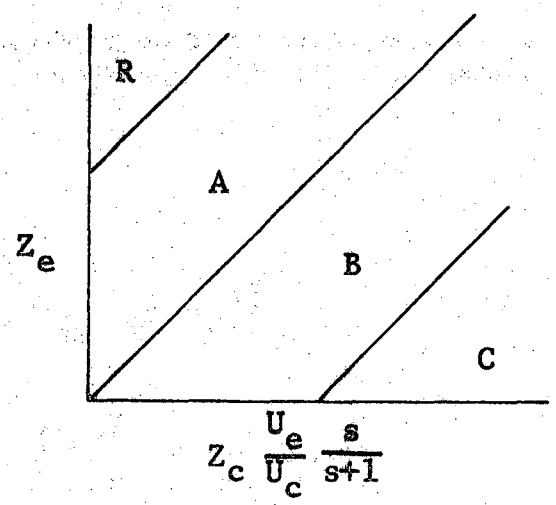

Fig. 2. Transition paths between zones of pure components on normalized coordinates. Order of increasing affinity for complexant: R, A, B, C.

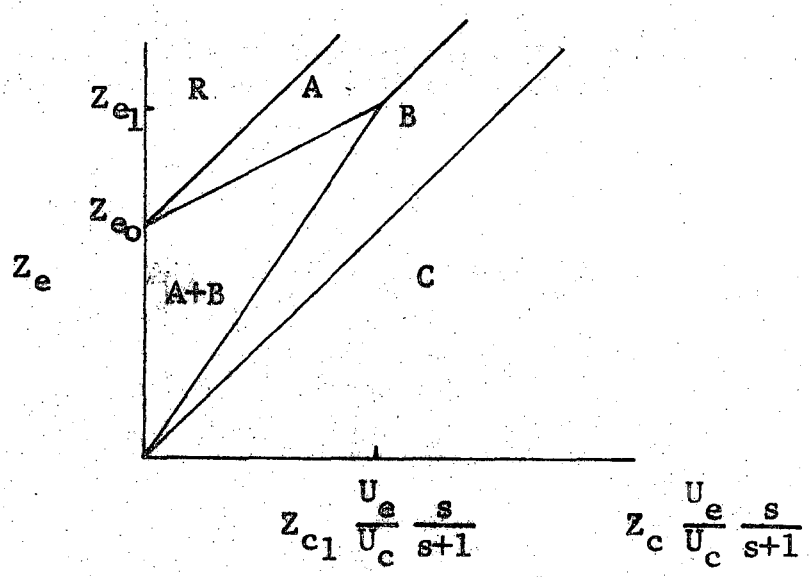

Fig. 3. Transition paths between zones of pure components and mixtures of components. Order of increasing affinity for complexant: R, A, B, C.

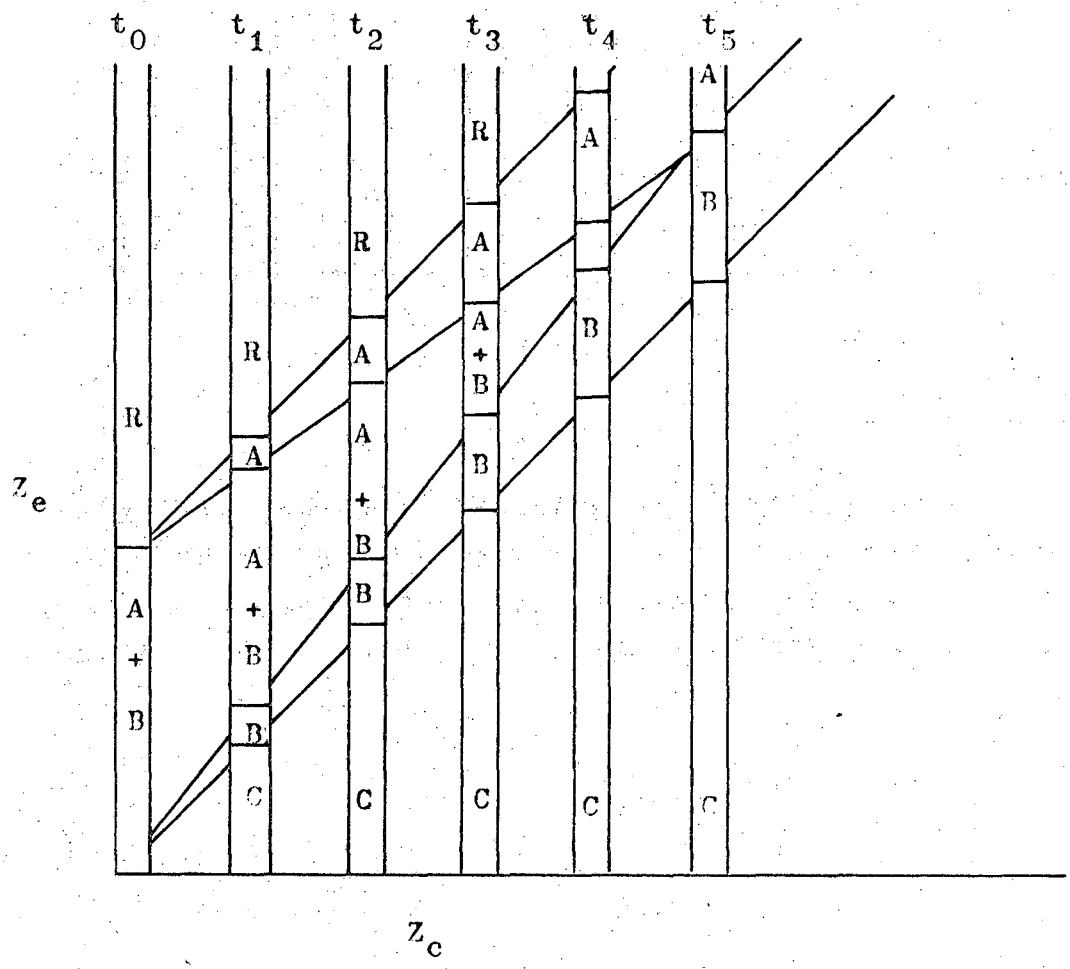

Fig. 4. The time dependent behavior of a differential unidimensional chromatograph column superimposed on on the normalized ligand electrochromatograph unit coordinates. Order of increasing affinity for resin: R, A, B, C.

separating. With these assumptions, still using the analogy of a differential one-dimensional column, a mass balance made for any component across the transition of interest will give the transition velocity. This velocity applies to the electrophoretic-migration direction, in the continuous electrochromatograph.

Sillen's derivation of transition migration velocities for one-dimensional chromatographic columns[7] has been modified for the present case. For any i-ij transition, the net transport of component i across the i-ij transition (N^i_{ij}) is given by

$$N^i_{ij} = U_e C_o(\Delta X_i) \quad , \tag{2}$$

where $X_i = C_i/C_o$, the equivalent fraction of species i among the total free ions, and ΔX_i is the difference in X_i between the two sides of the transition. In the steps to follow, $Y_i = C^*_i/C^*_o$ will represent the equivalent fraction of species i among all complexes.

Since the concentration of species i and j change only at the transition, the net-transport relation will be valid over a segment of the column, of any arbitrary size but containing only this transition, shown in Fig. 5a by dotted lines. In a given time Δt, migration of the transition will trace out a net accumulation of species shown by the shaded area in Fig. 5b. This accumulation term is given by

$$\text{Accumulation} = U^i_{ij}\, C^*_o(\Delta Y_i) + U^i_{ij}\, C_o(\Delta X_i) \quad . \tag{3}$$

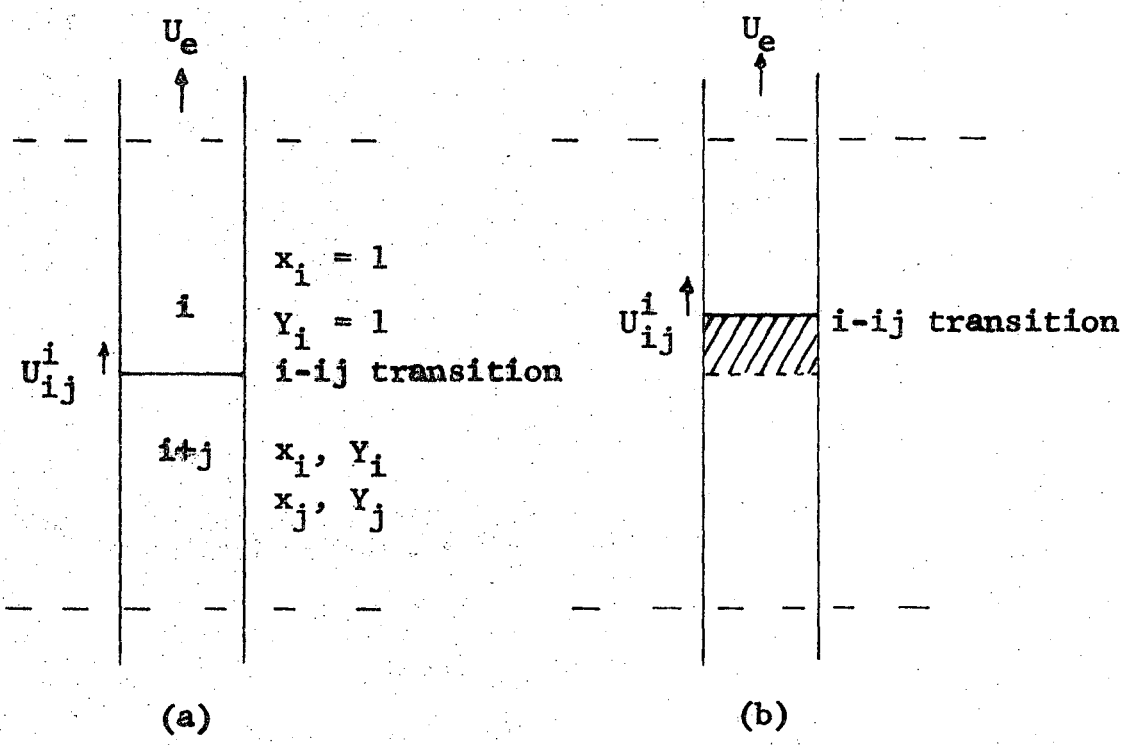

Fig. 5. Migration of i-ij transition for differential unidimensional chromatographic column.

The net material balance, across the dashed lines of the column, thus becomes

$$U_e C_o(\Delta X_i) = U_{ij}^i \ (C_o^* \Delta Y_i + C_o \Delta X_i) \quad . \tag{4}$$

Referring to Fig. 1 representing the electrochromatographic bed, the slope for the transition between pure i and the mixture of i and j is given by the ratio of the electrophoretic migration to the convective migration. The distance-velocity relations are

$$\Delta Z_e = U_{ij}^i \Delta t$$

$$\Delta Z_c = U_c \Delta t \quad . \tag{5}$$

Thus the slope of the transition i-ij in the bed becomes

$$(\Delta Z_e/\Delta Z_c)_{ij}^i = (U_{ij}^i/U_e)(S+1)/S \quad . \tag{6}$$

Equation (4) can be used to eliminate U_{ij}^i/U_e. The resulting slope for a transition is then

$$(\Delta Z_e/\Delta Z_c)_{ij}^i = \frac{\Delta X_i}{\Delta Y_i + S\Delta X_i}(S+1) \quad . \tag{7}$$

Introducing the variable ϕ_i for the point-value equivalent fraction of i (in both complexed and free-ion form) gives

$$\phi_i = \frac{Y_i C_o^* + X_i C_o}{C_o^* + C_o} = \frac{Y_i + SX_i}{S + 1} \quad , \tag{8}$$

with $\Sigma\phi_i = 1$. The equation for the slope of a transition is then expressed simply as:

$$\left(\frac{\Delta Z_e}{\Delta Z_c}\right)^i_{ij} = \frac{\Delta X_i}{\Delta \phi_i} = \frac{\Delta X_j}{\Delta \phi_j} \quad , \tag{9}$$

with $X_i = 1$ on one side, and $1-X_j$ on the other side of the transition; and similarly for ϕ. That is, the migration slope of species i is given by

$$\left(\frac{\Delta Z_e}{\Delta Z_c}\right)^i_{ij} = \frac{X_j}{\phi_j} \quad , \tag{10}$$

where j is the component which disappears at the transition.

Transition Intersections for End Feed

The feed is introduced at the end with the complex over a distance Z_{e_o}, as shown in Fig. 3. The slopes of the i-ij and ij-j transitions are each given by Eq. (9). The two transition slopes between pure component and mixture can then be written.

$$\text{Slope A-AB} = \frac{X_B}{\phi_B} = \frac{Z_{e_1} - Z_{e_o}}{Z_{c_1} \frac{U_e}{U_c} \frac{S}{S+1}} \tag{11}$$

$$\text{Slope AB-B} = \frac{X_A}{\phi_A} = \frac{Z_{e_1}}{Z_{c_1} \frac{U_e}{U_c} \frac{S}{S+1}} \quad . \tag{12}$$

A new equilibrium parameter R^i_j can be defined:

$$R^i_j = \frac{X_j \phi_i}{X_i \phi_j} \quad . \tag{13}$$

(In contrast, the usual equilibrium constant would be $X_j Y_i / X_i Y_j$.) Now Eqs. (11) - (13) can be combined to solve for the electrophoretic coordinate of the intersection point between the two transitions; that is, the value Z_{e1} required to achieve separation of a mixture fed over the interval $Z_e = 0$ to $Z_e = Z_e$.

$$\frac{Z_{e1}}{Z_{e_o}} = \frac{1}{1 - R^A_B} \quad . \tag{14}$$

The equations can also be solved for the convective distance needed for separation

$$\frac{Z_{c_i} \frac{U_e}{U_c} \frac{S}{S+1}}{Z_{e_o}} = \frac{R^A_B}{1 - R^A_B} + \phi_A = \frac{R^B_A}{R^B_A - 1} - \phi_B \quad . \tag{15}$$

Transition Intersections for Side Feed

For the case where feed is introduced from the side, as shown in Fig. 6, the same approach is followed. The resulting convective-direction distance Z_{c1} required to separate a mixture fed between $Z_c = 0$ and $Z_c = Z_{c_o}$ is found to be:

$$\frac{Z_{c1}}{Z_{c_o}} = \frac{1}{1 - R^A_B} \quad . \tag{16}$$

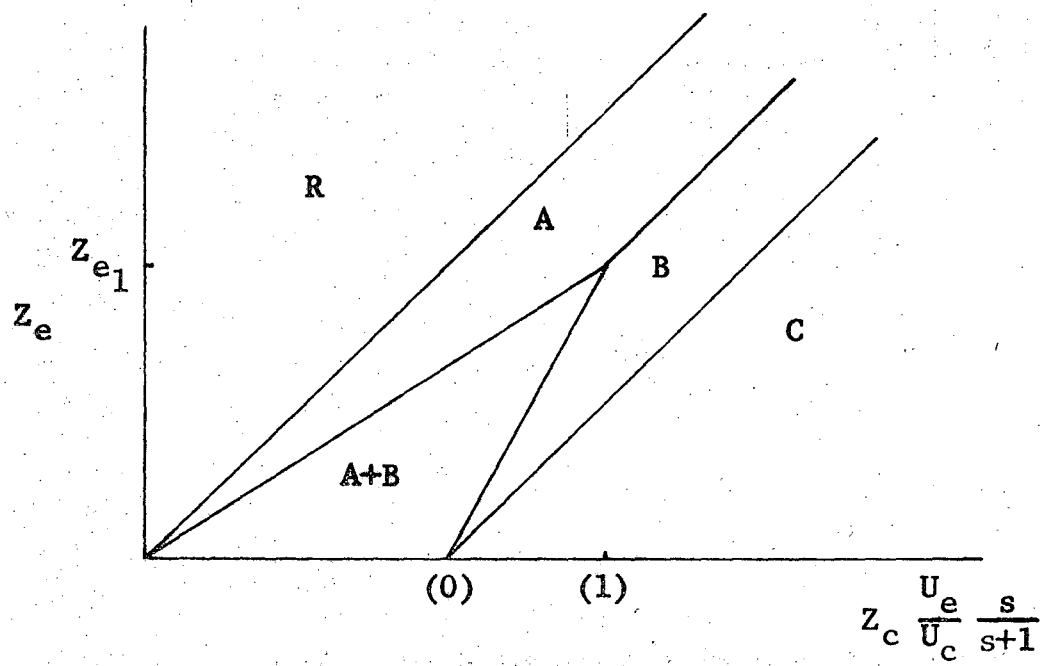

Fig. 6. Side feed of A-B mixture to normalized ligand electrochromatograph unit. Order of increasing affinity for complexant: R, A, B, C.

The electrophoretic distance required for separation for this case is

$$\frac{Z_{e_1}}{Z_{c_o} \frac{U_e}{U_c} \frac{S}{S+1}} = \frac{R_B^A}{1 - R_B^A} + X_B = \frac{R_A^B}{R_A^B - 1} - X_A \quad . \qquad (17)$$

Dimensionless Framework

Dimensionless distances can be defined by dividing the previous normalized distances by the appropriate feed distance. The new coordinates then become;

$\tilde{Z}_e = \frac{Z_e}{Z_f}$ dimensionless electrophoretic distance

$\tilde{Z}_c = \frac{Z_c}{Z_f} \frac{U_e}{U_c} \frac{S}{S+1}$ dimensionless convective distance.

The feed distance Z_f is given by

$Z_f = Z_{e_o}$ for end feed

$Z_f = Z_{c_o} \frac{U_e}{U_c} \frac{S}{S+1}$ for side feed.

Feed and Offtake Locations

The resulting intersections of the transitions are shown in Fig. 7 as a function of the modified equilibrium parameter R_B^A and of the feed ratio of the ion mixture. This graph can be used to select the conditions

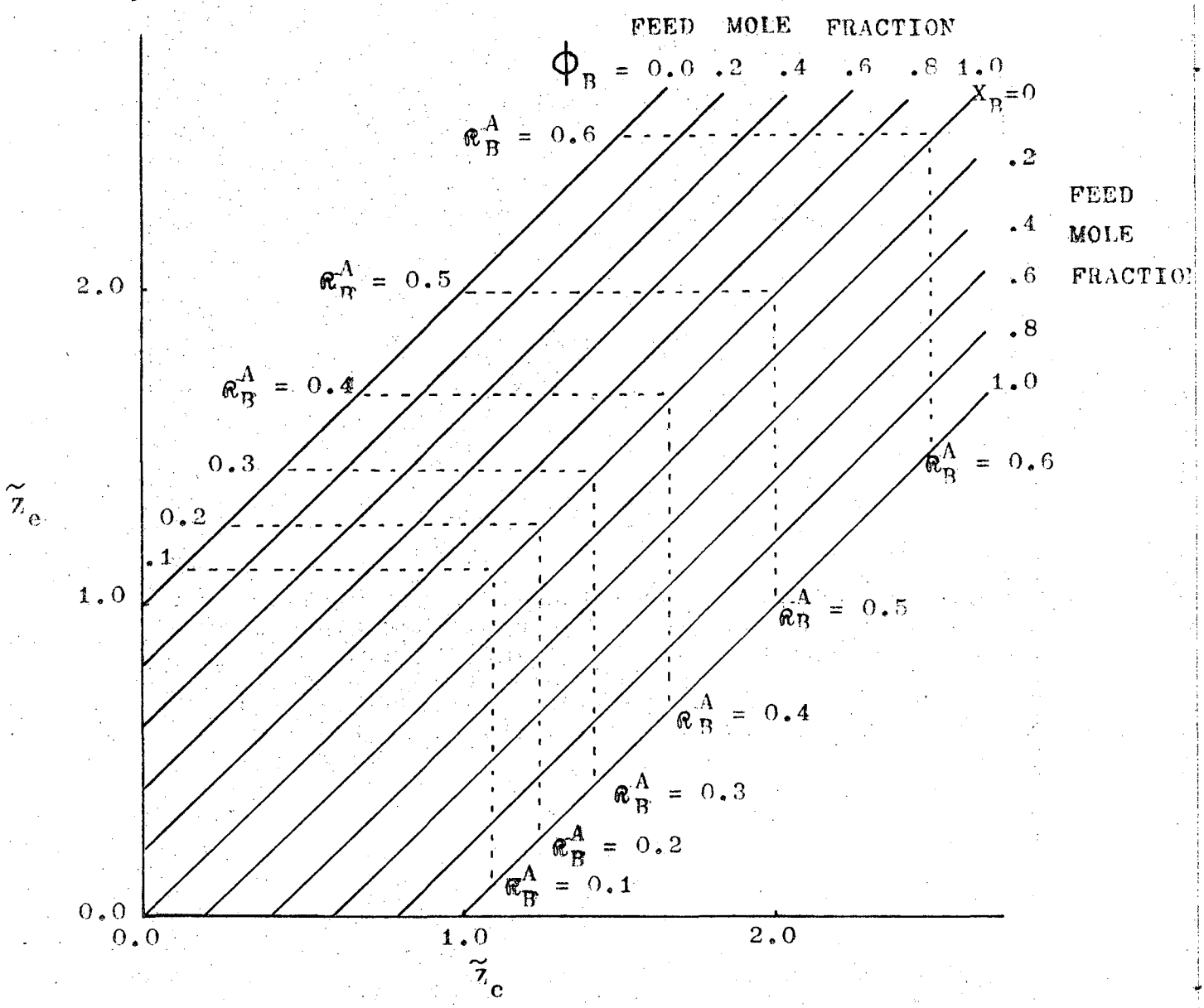

Fig. 7. Intersection of transitions for the separation of A-B mixtures on a dimensionless, normalized graph representing the ligand electrochromatograph unit. The horizontal dashed lines represent the transition intersections for end feed; the vertical lines represent the intersections for side feed.

to give the most efficient separation, that is, to determine where the feed should be introduced and where the various products should be collected.

The two possible feed positions are shown in Fig. 1. The feed may be fed to the unit with the complexing agent, or it may be introduced electrophoretically through the diaphragm along the side of the unit.

The separated components may be collected from the column in one of three ways, as shown in Fig. 8. Both components may be collected along the side of the unit (through the diaphragm), both at the end of the column, or one component may be collected along the side and the other at the end. It is generally desirable to operate at the smallest ratio of power consumption (IE) to throughput. Collecting both species along the side or at the end results in a sizable expenditure for excess power, as indicated in Fig. 9. This immediately favors setting the offtake position so that one component is collected along the side and the other at the exit end.

The practicable operating conditions are thus reduced to one offtake pattern and two possible feed positions. The choice of feed position is made with the help of Fig. 7. The electrical power required to operate the unit is given by IE, the product of current and voltage. At a given value of S the voltage will be proportional to $\tilde{Z}_e$; hence the current will be proportional to the cross-sectional area for electrophoretic flow, or in other words proportional to $\tilde{Z}_c$. The power required for a given separation will be proportional to the area of the unit on the normalized graph, that is, to the area bounded by the appropriate $\tilde{Z}_e$ and $\tilde{Z}_c$ that just give

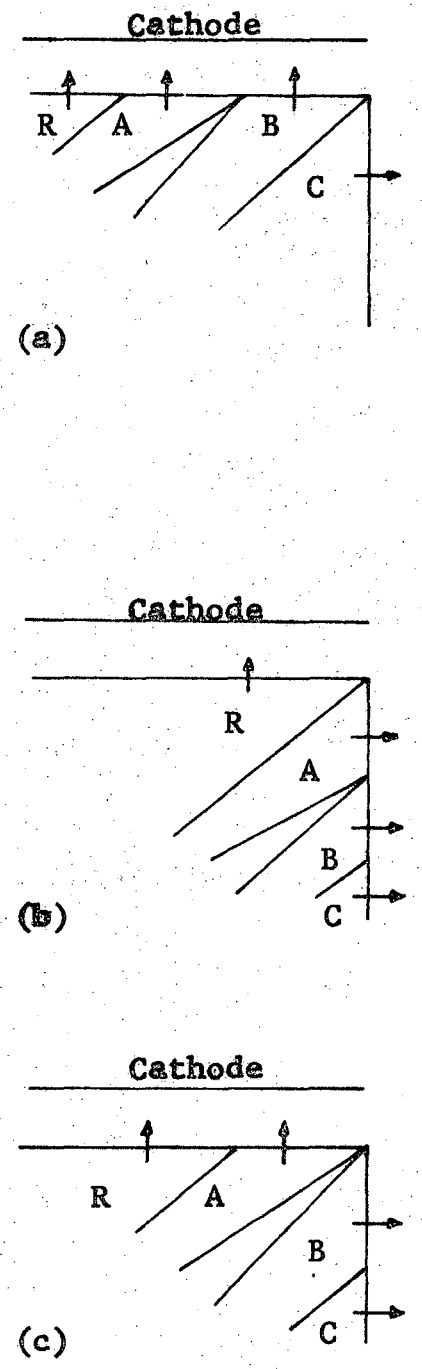

Fig. 8. Possible offtake patterns for ligand electrochromatograph operation.

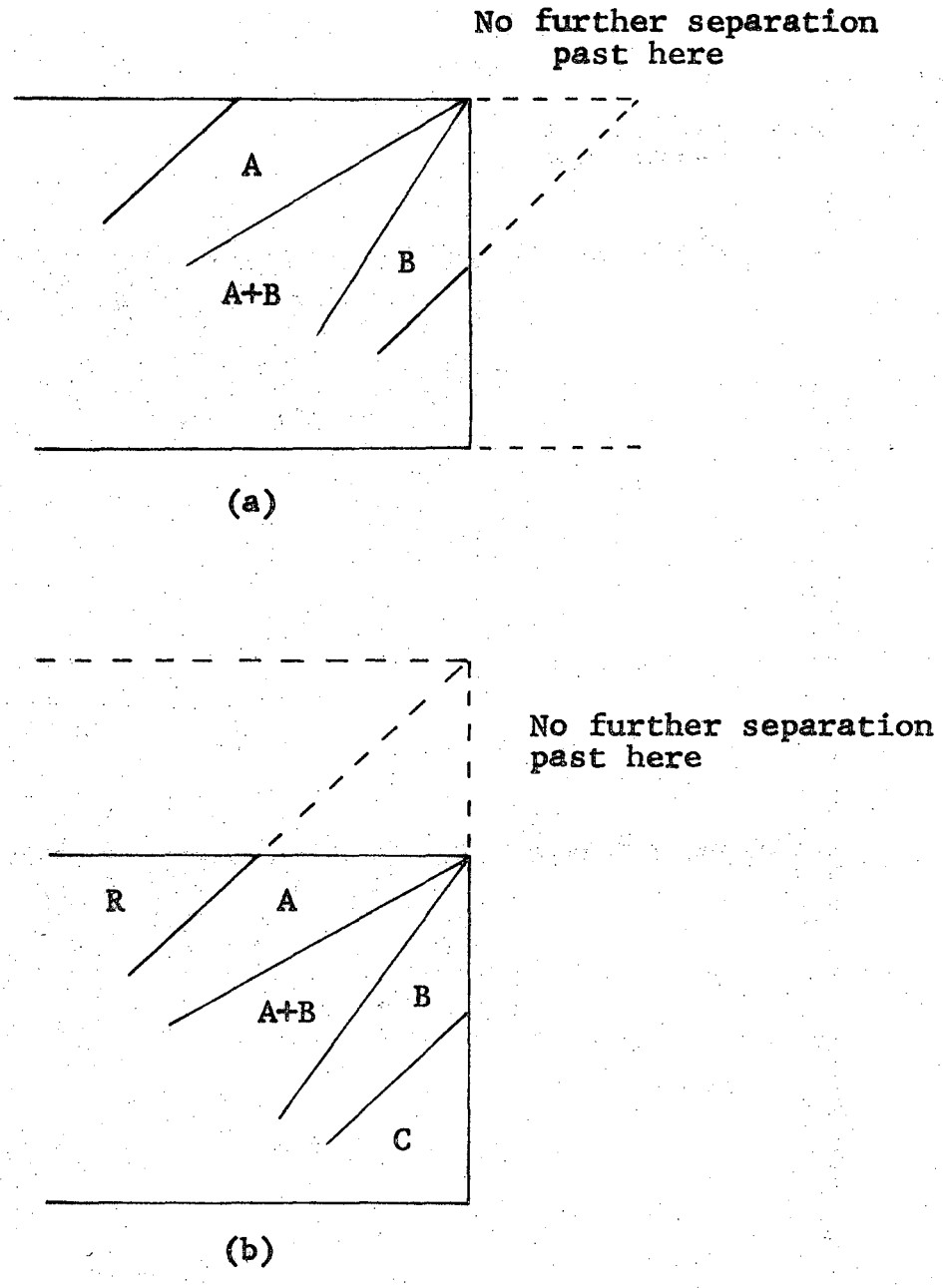

Fig. 9. Inefficiency resulting if (a) both components are taken off along the side or (b) both at the end.

separation. The area can thus be determined for each alternative feed position, and the one that results in the smaller area can be adopted for actual operation.

For a given equilibrium parameter R_B^A and a feed mixture lean in the less strongly complexed component ($\phi_A = 0.1$, or $X_A = 0.1$, depending on feed position) the corresponding power requirements for each feed position are represented in Fig. 10 by the corresponding areas. For this case it can be seen that feeding at the end would require only about half the power compared to feeding at the side. Likewise it can be shown that for a feed rich in the less desired component ($\phi_a > 0.5$ or $X_A > 0.5$) feeding along the side becomes advantageous. Thus the general rule is recorded in the following table:

Feed Mixture	Feed Position
Rich in high-affinity component	End feed
Rich in low-a-finity component	Side feed

Departures from Ideal Conditions

Heat-Transfer

The rise in temperature due to the passage of current places serious limitations on the design and operating conditions of electrochromatographic units. The use of coolant streams on the faces or the sides (that is, in the electrode chambers) of a unit can significantly reduce such temperature effects. Nevertheless it is necessary to be able

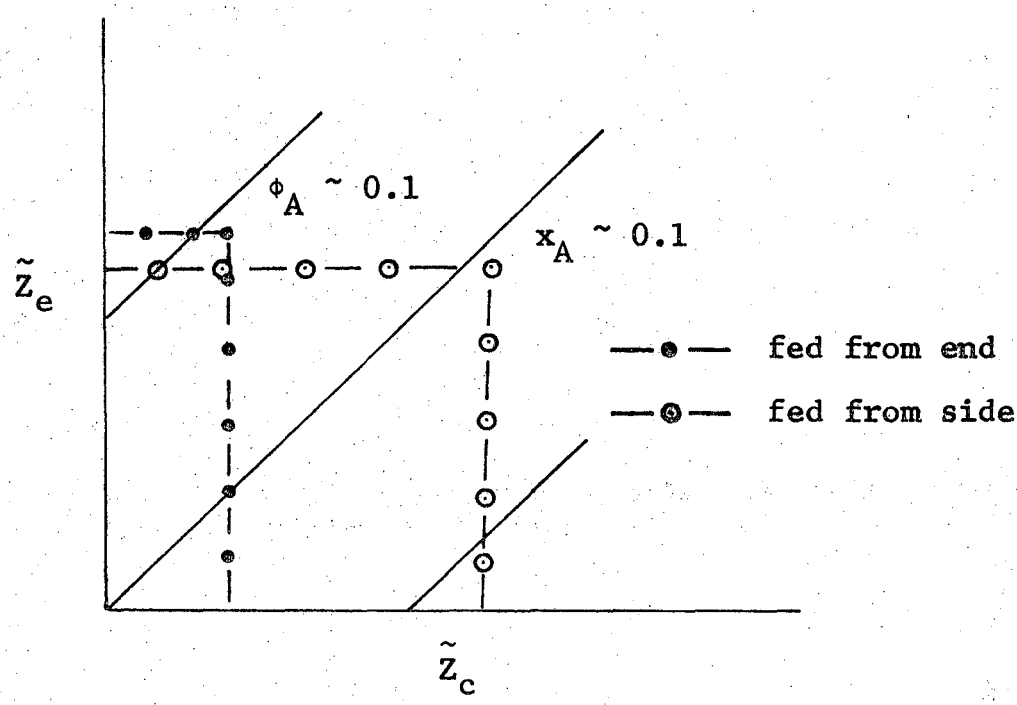

Fig. 10. Normalized dimensionless area required to separate A-B mixture lean in A, for side feed and for end feed.

to predict the maximum temperature rise in the center of the unit. Such calculations will place limits on applied voltage, solution concentration levels, residence time, feed temperature, and perhaps other factors. Failure to properly account for the temperature rise caused by Joule heating can have the following harmful effects:

(1) Gas evolution from the process stream with subsequent disruption of flows.

(2) Boiling of the liquid.

(3) Damage to membranes, diaphragms, or housing caused by uneven thermal expansion.

(4) Variation in physical properties such as mobilities, equilibrium constants, and viscosities which may have adverse effects on separations.

The maximum temperature rise in a unit has been previously solved for three cases,[8] as shown in Fig. 11:

(1) Cooling at the electrode-faces of the bed only.

(2) Cooling at the two lateral faces perpendicular to the electrode-faces.

(3) Cooling at all four faces.

The third mode of cooling is not generally employed, and will not be reviewed here.

If the physical properties are the same in all directions, and the voltage gradient is constant across the bed, then the solution to the first two cases will be the same, except for a change in coordinates.

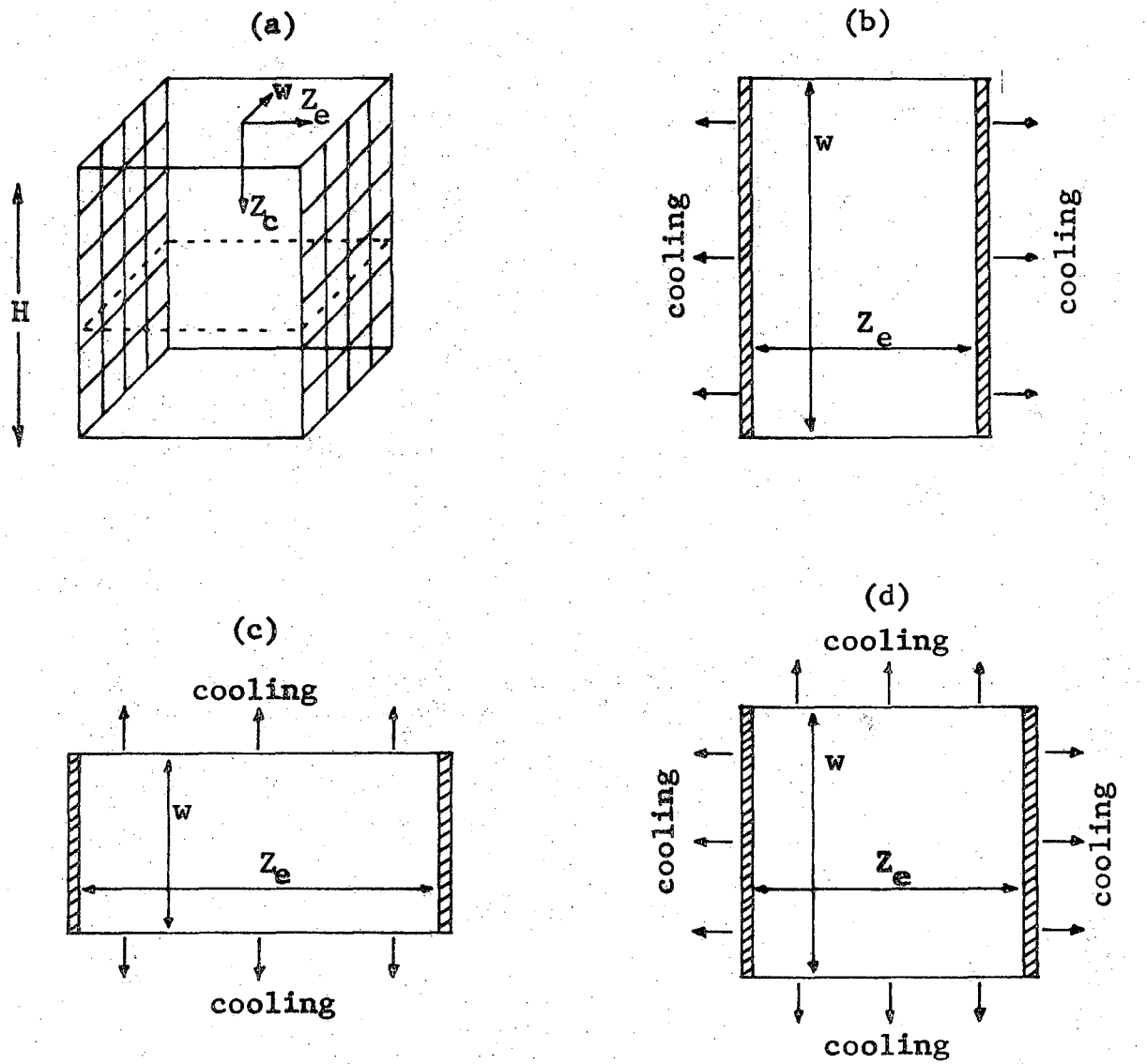

Fig. 11. Rectangular models of electrophoresis units with lateral cooling. (a) General model (b) Case 1 (c) Case 2 (d) Case 3.

For the case where cooling occurs at $Z_e = 0$ and $Z_e = Z_e$, the general heat transfer equation can be written

$$\frac{\partial}{\partial Z_e}\left(k_n \frac{\partial T}{\partial Z_e}\right) + \frac{\partial}{\partial Z_c}\left(k_h \frac{\partial T}{\partial Z_c}\right) - \frac{\partial}{\partial Z_e}\left(U_e^w \rho C_p T\right)$$

$$- \frac{\partial}{\partial Z_c}\left(U_c \rho C_p T\right) + \frac{dp}{dv} = \frac{\partial}{\partial t}\left(\rho C_p T\right) \quad , \tag{18}$$

where k_n = effective thermal conductivity, ρ = density, T = temperature, U_c = plug-glow velocity in Z_c-direction, U_e^w = electro-osmotic flow in Z_e-direction, and C_p = heat capacity. The power density is $\frac{dp}{dv} = k_b(\nabla E)^2$, where k_b = effective specific electrical conductivity, and E = electrostatic potential.

The following reduced variables are adopted: $T' = T - T_o$ $z_e' = z_e/Z_e$, $E' = E/E_{z_e}$, $\tau = H/U_c$, $\alpha_h = k_h/\rho c_p$, $W = k_b/k_h$. T_o is the temperature at the cooled wall and H is the column length.

The heat-transfer equation can be simplified by the following assumptions:

(1) Steady-state operation, for which the heat-accumulation term vanishes.

(2) Negligible convection due to electro-osmosis and axial conduction.

(3) The potential gradient is in the x-direction only.

(4) Plug flow through the packing.

With the above assumptions, Eq. (18) becomes

$$\frac{\partial}{\partial z_e}\left(k_h \frac{\partial T}{\partial z_e}\right) - \rho C_p \frac{\partial T}{\partial \tau} + k_b \left(\frac{dE}{dz_e}\right)^2 = 0 \quad , \tag{19}$$

with the reduced variables just defined, this equation becomes

$$\frac{\partial^2 T'}{\partial z_e'^2} + \frac{1}{k_h}\frac{\partial T'}{\partial z_e'}\frac{\partial k_h}{\partial z_e'} - \frac{x^2}{\alpha_h}\frac{\partial T'}{\partial \tau} + WE_{Z_e}^2\left(\frac{dE}{dz_e'}\right)^2 = 0 \quad , \qquad (20)$$

with the initial conditions: $0 \leqslant z_e' \leqslant 1 \qquad T' = 0$

and the boundary conditions: $z_e' = 0 \qquad T' = 0,\ E' = 1$

$z_e' = 1 \qquad t' = 0,\ E' = 0$

The maximum temperature rise is given analytically by

$$T'_{max} = \frac{(\Delta E/\Delta Z_e)^2}{2}\ell^2 W\left\{1 - 1.032\sum_{n=0}^{\infty}\frac{(-1)^n}{(2n+1)^3}\exp\left[-\frac{(2n+1)^2\pi^2\alpha_h\tau}{4\ell^2}\right]\right\} \quad ,(21)$$

where 2ℓ is the distance between cooling compartments. Thus this equation is valid for the case of cooling at the electrodes ($\Delta Z_e = 2\ell$) or cooling at the two faces ($\Delta W = 2\ell$). For most cases of interest $\pi^2\alpha\tau/4e^2 > 0.1$ and only the first exponential term need be retained of the series.

For a given voltage gradient, the relation between the maximum temperature rise T'_{max} is given as a function of the distance between cooling plates (21) and the residence time τ, as shown in Fig. 12. It can be seen that for large values of ℓ, T'_{max} becomes a constant and independent of ℓ. This corresponds to the situation where most of the Joule heating is absorbed as sensible heat by the liquid and transported out of the unit with the process liquid. The 45° asymptote corresponds to the steady-state condition where the Joule heating is conducted away via the cooling surfaces. The latter situation is desirable for operating since it gives the maximum throughput for a given temperature rise. The design relation for operation thus becomes

$$T'_{max} = \frac{1}{2}\left(\frac{\Delta E}{\Delta z_e}\right)^2 W\ell^2 \quad . \qquad (22)$$

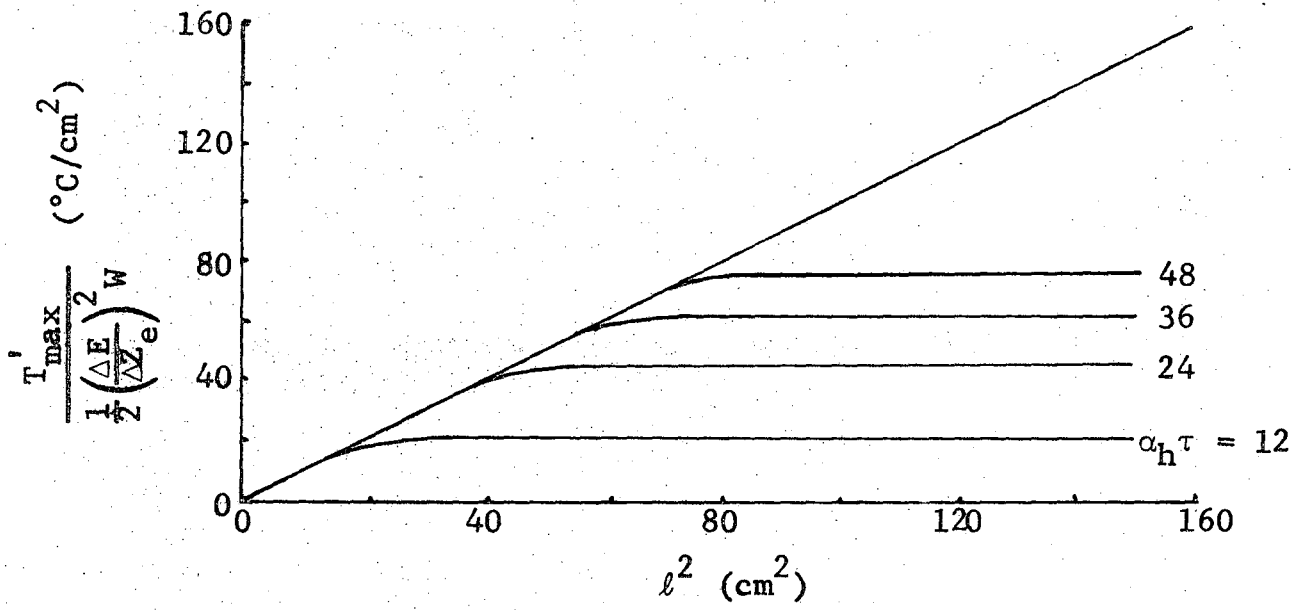

Fig. 12. Maximum temperature rise as a function of distance between cooling faces and fluid residence time.

Dispersion

Theoretical concentration profiles for transitions between components should be abrupt (discontinuous) jumps from one component to the adjacent one; in practice such boundaries do tend to approach the theoretical prediction and exhibit "self-sharpening." Axial and radial dispersion, however, cause mass transfer between zones of pure component, and result in finite overlap regions. The overlap zones between components will decrease till the self-sharpening tendency of the zone equals the disruptive dispersive mechanisms. Once this balance is reached, the boundary remains stable, getting neither sharper nor broader.

The overlap region between components (in going from 5% to 95% of one of the components) can be predicted as a function of the flowrate, particle diameter, and selectivity of the complexing agent between components.

The effect of dispersion on self-sharpening boundaries in ion exchange has been developed mathematically.[6] Because of the great similarity between the ion exchange case and the present system, adaption of the mathematics for the former has proven possible. In the former, the movement of the front is shown in Fig. 13a. Figure 13b shows the established front in the present unit. This front can be interpreted in terms of a unidimensional column of stabilized fluid as shown in Fig. 13c in dotted lines. As the fluid moves from left to right the front in our column moves from bottom to top.

The general equations for one of the species in the overlap region is given by

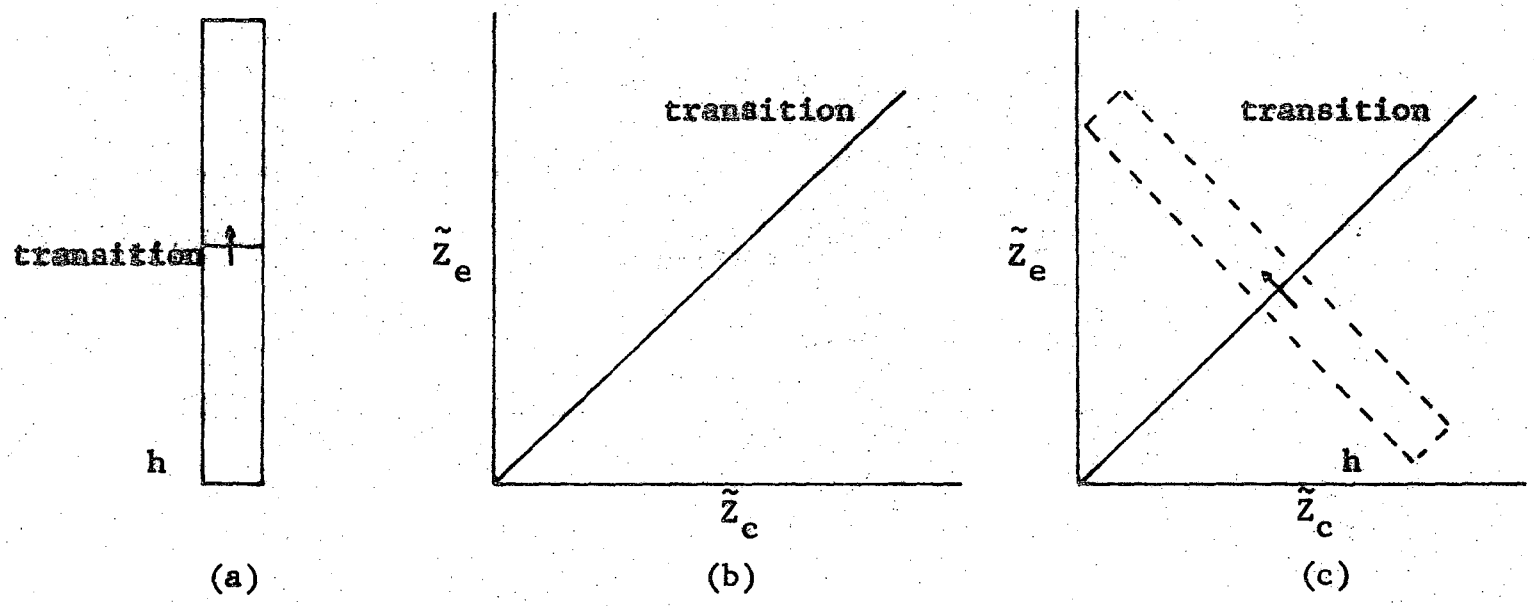

Fig. 13. Analogy of transition in continuous ligand electrochromatograph (b) with transition in a unidimensional column (a); (c) indicates how the mathematics of case (a) can be applied for solving case (b).

$$D\frac{\partial^2 C}{\partial h^2} + D\frac{\partial^2 C^c}{\partial h^2} = U_p\frac{\partial C}{\partial h} + \frac{\partial C}{\partial t} + \frac{\partial C^c}{\partial t} \quad , \tag{23}$$

where C = concentration in equivalents per unit volume of the excess uncomplexed species, C^c = concentration in equivalents per unit volume of the complexed species, D = effective dispersion coefficient (assumed to be the same for uncomplexed and complexed species), U_p = net velocity of uncomplexed species perpendicular to the transition zone, h = distance along unidimensional column (perpendicular to transition), t = time.

This equation differs from the analogous case in ion exchange, in that it has an additional term to account for the dispersion of the complexed species.

The following substitution can be made

$$\xi = \frac{U_p}{D}\cdot\frac{C_o^c}{C_o + C_o^c}\left[h - \frac{U_p C_o t}{C_o + C_o^c}\right] \quad , \tag{24}$$

where the subscript zero refers to total concentrations. It is found that for large values of ξ the concentration profile will asymptotically approach a profile that has following characteristics: (1) $C = C(\xi)$; (2) no net flow of cations relative to a cross-section of the column at constant ξ. From these two conditions it follows that the accumulation terms $(\partial C/\partial t) + (\partial C^c/\partial t)$ become zero and can be dropped.

With the additional definition $X_1 = C_1/C_o$ and $Y_i = C_1^c/C_o^c$, the equation can be reduced to

$$\frac{\partial^2 X}{\partial \xi^2} + \frac{C_o^c}{C_o} \frac{\partial^2 Y}{\partial \xi^2} = \frac{\partial X}{\partial \xi} - \frac{\partial Y}{\partial \xi} \quad . \tag{25}$$

This can be integrated to get

$$\frac{\partial X}{\partial \xi} + \frac{C_o^c}{C_o} \frac{\partial Y}{\partial \xi} = X - Y \quad . \tag{26}$$

From the boundary conditions

$$\xi = -\alpha \qquad X_i = Y_i = 1$$

$$\xi = \alpha \qquad X_i = Y_i = 0 \quad ,$$

it can immediately be seen that the constant of integration for Eq. (26) is zero.

The equilibrium relation can be used to express Y_i in terms of X_i.

$$r_j^i = r = \frac{X_i}{Y_i} \frac{Y_j}{X_j} \quad . \tag{27}$$

Equation (26) becomes

$$\int_{\xi_1}^{\xi_2} d\xi = \frac{1}{1-r} \int_{X_1}^{X_2} \frac{r^2 + 2r(1-r)X + (1-r)^2X^2 + \frac{C_o^c}{C_o} r}{[r + (1-r)X]\ X\ [X-1]} dX \quad . \tag{28}$$

This equation can be integrated readily and the terms combined to yield

$$\xi_2 - \xi_1 = \left(\frac{r+1}{1-r}\right)\left[\frac{C_o^c}{C_o} + 1\right] \log_e \frac{X_2 - 1}{X_1 - 1} + \frac{C_o^c}{C_o} \log_e \frac{(1-r)X_2 + r}{(1-r)X_1 + r} \quad . \qquad (29)$$

The analogous case for ion exchange (Eq. (23) without the dispersion term for the complexant) can be solved with the same substitution (Eq. (24)) to give

$$\xi_2 - \xi_1 = \frac{1+r}{1-r} \log \frac{X_1}{X_2} \quad . \qquad (30)$$

The results of Eq. (29) and (30) are plotted in Fig. 14.

The dispersion term is the sum of the radial and axial dispersion contributions. The Peclet numbers for each give the relation between the velocity and the appropriate dispersion coefficient.

$$Pe_{axial} = \frac{Ud_p}{D_A} = 0.5$$

$$Pe_{radial} = \frac{Ud_p}{D_r} = 12 \quad . \qquad (31)$$

Radial dispersion for complexed species and free ions occurs as a result of convective flow (in the $\tilde{Z}_e$ direction), and for free ions as a result of electrophoretic flow (in the $\tilde{Z}_c$ direction). The latter, however, will generally be small compared to the axial dispersion in this direction for both species (resulting from convective flow) and will be neglected. The net dispersion for each mechanism resulting from convective flow, shown in Fig. 15, is given by

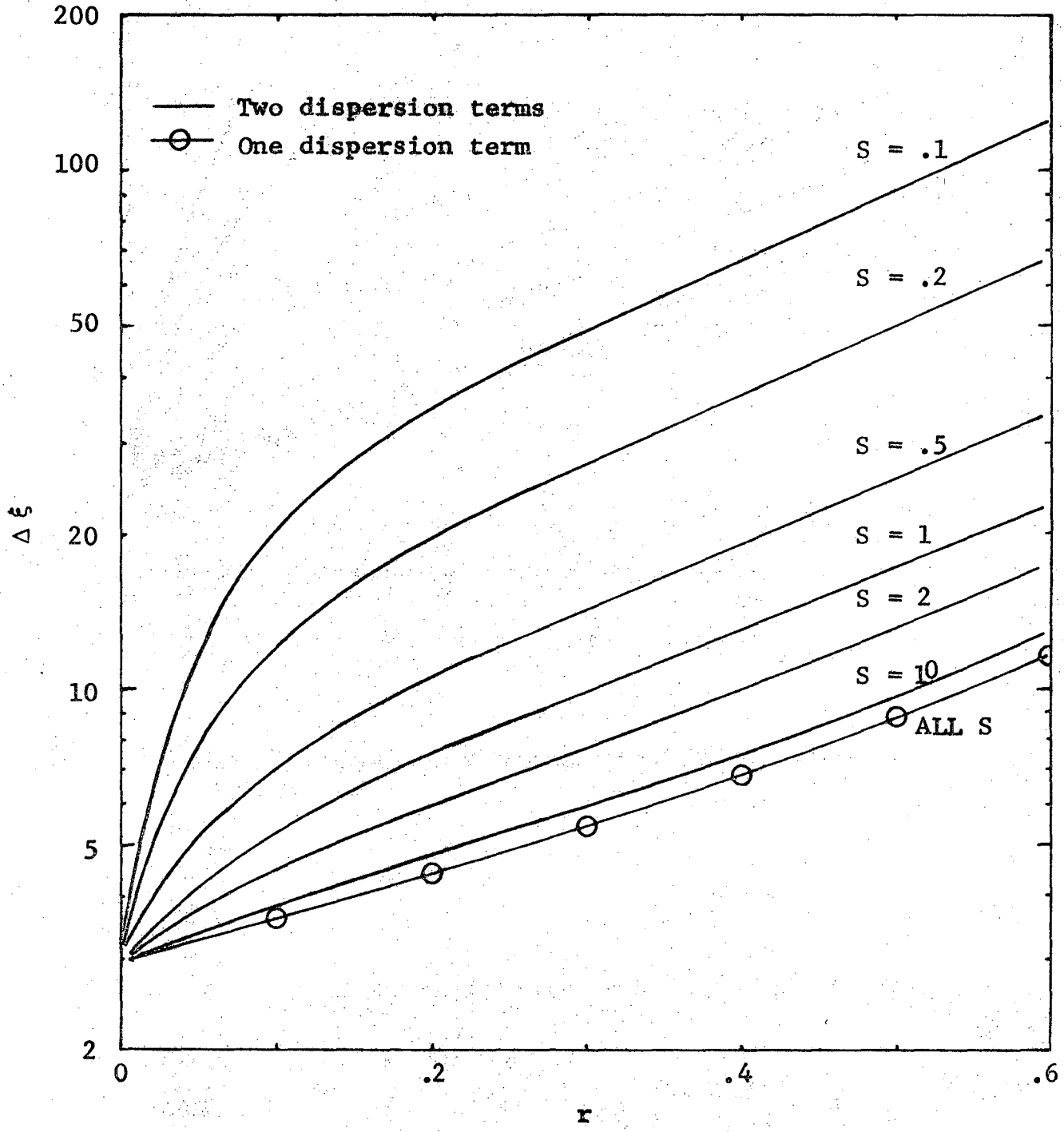

Fig. 14. Dimensionless overlap distance, for one and two dispersion terms.

Fig. 15. Radial and axial dispersion resulting from convective flow.

$$D = D_R \cos\theta + D_A \sin\theta$$

$$= \frac{1}{12} U_c\, d_p \cos\theta + 2U_c\, d_p \sin\theta \quad , \tag{32}$$

where θ is the angle between the transition path in the unit and the coordinate in the direction of convective flow. In the unit this angle is given by $\tan\theta = (U_e/U_c)\, S/(S+1)$.

The transformation relation, Eq. (24), gives the dependence of the overlap distance h on the dispersion term, the ratio of excess free ions to complex, the equilibrium parameter (through ξ), and the migration velocity perpendicular to the interface. The velocity in the direction perpendicular to the transition can be expressed in terms of the electrophoretic velocity

$$U_p = U_e \cos\theta \quad . \tag{33}$$

Substituting Eq. (32) and (33) into (24), and simplifying, yields

$$\frac{\Delta h}{d_p} = \Delta\xi(S+1)\left[\frac{1}{12U_e/U_c} + 2\,\frac{U_e/U_c S}{S+1}\right] \quad . \tag{34}$$

Figure 14 and Eq. (34) are used to calculate overlap distances between zones of pure components.

Equation (34) can be minimized with respect to (U_e/U_c) to give

$$\left(\frac{U_e}{U_c}\right)_{min} = \left(\frac{S+1}{24S}\right)^{1/2} \quad . \tag{35}$$

Figure 16 shows $\Delta h/d_p$ plotted as a function of r and S for $(U_e/U_c)_{min}$ values. Optimum operating conditions (in terms of minimum overlap distance) are found in the range $0.2 \leqslant S \leqslant 1.0$. This corresponds to $(U_e/U_c)_{min}$ values from 0.5 (at S = 0.2) to 0.29 (at S = 1). This gives a convective velocity two to three times the electrophoretic velocity.

Apparatus

General Description

The "ligand" electrochromatograph and its auxiliary components are shown in Fig. 17. Figure 18 is a schematic flow sheet for this unit. Figure 19 is a schematic drawing of the central unit.

As shown in Fig. 18, six different solutions potentially can be fed to various parts of the central unit. Retainer-complex solution and feed-complex solution can be fed to the top end of the packed bed. Feed, chaser, and wash solutions can be fed through manually operated constant-displacement pumps into the various side compartments. The separating-system output consists of four streams emerging from the unit via offtake grooves at the bottom of the packed bed, and exit streams from each of the side compartments through the previously mentioned pumps. Independently electrolyte is fed into, and out of, each electrode chamber.

The solutions fed to the top of the packed bed are kept at 50-60°C to minimize their dissolved-air content, and are cooled to room temperature by a water jacket immediately before they enter the bed. Prior to operation, the solutions are degased by applying a vacuum until the liquid boils; then styrofoam floats are placed on top of the liquid to hinder re-absorption of air.

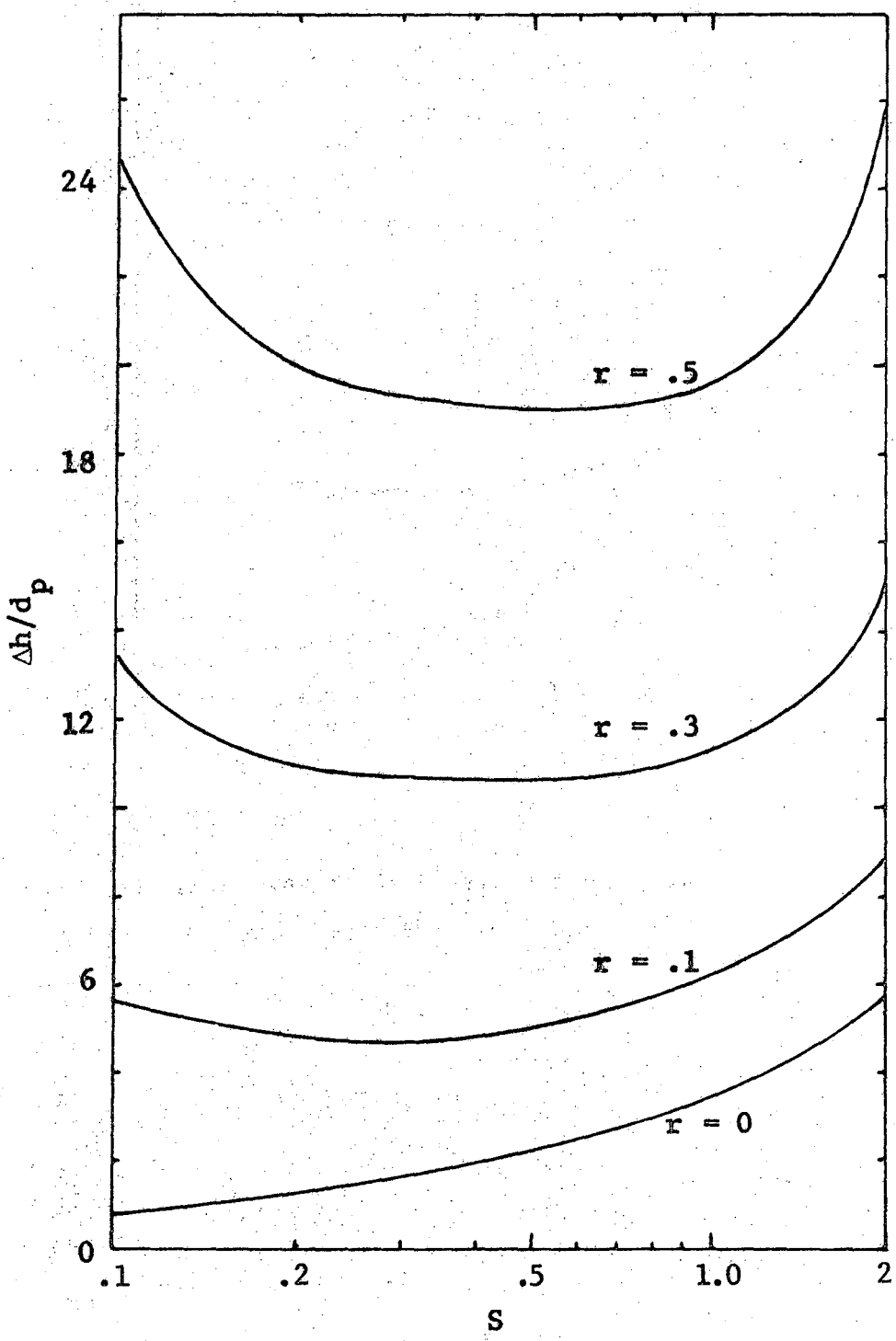

Fig. 16. Overlap distance as a function of r and s for $(U_e/U_c)_{min} = [(S+1)/24S]^{1/2}$.

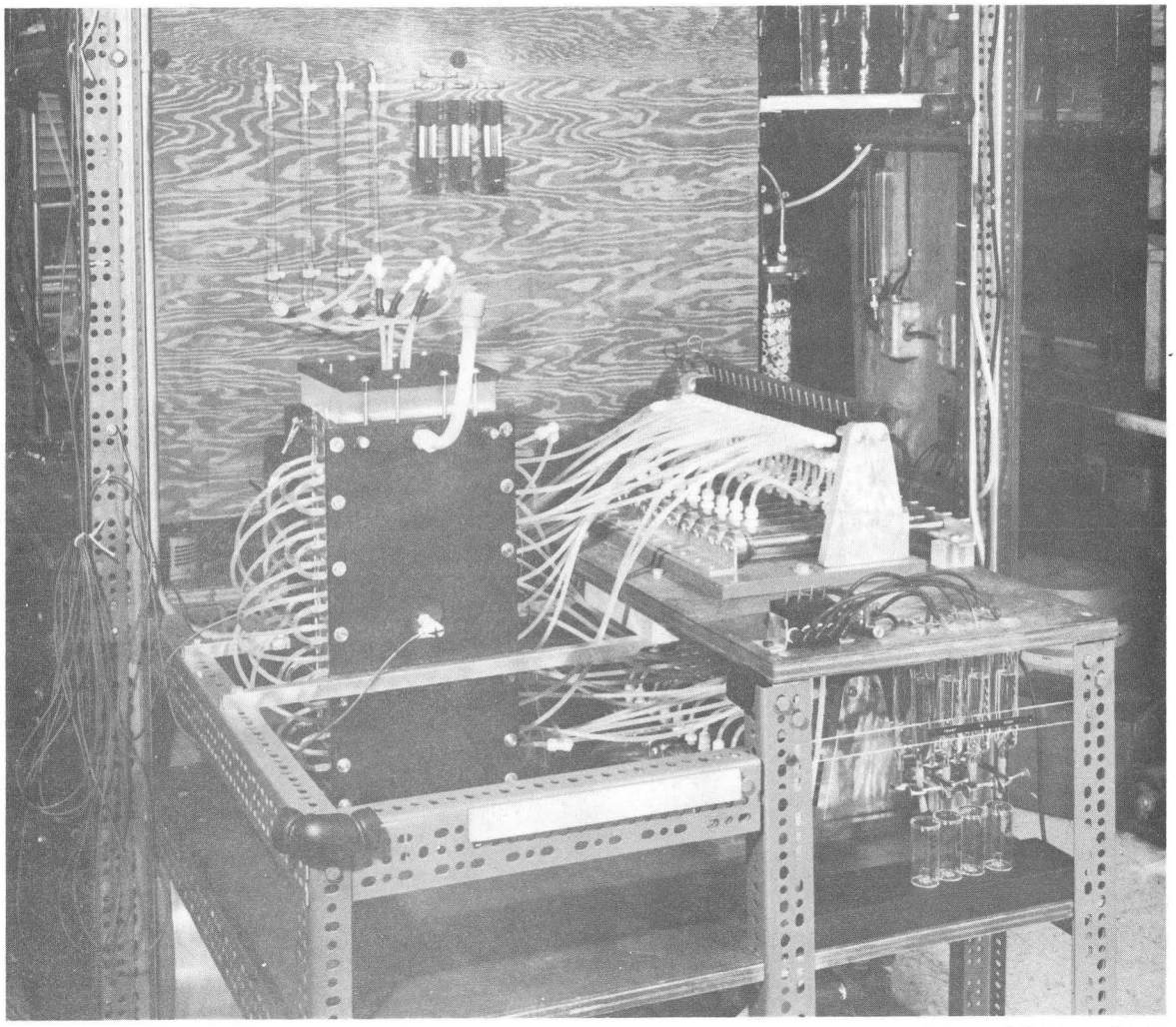

CBB 6912-7688

Fig. 17. "Ligand" electrochromatograph and its auxiliary components.

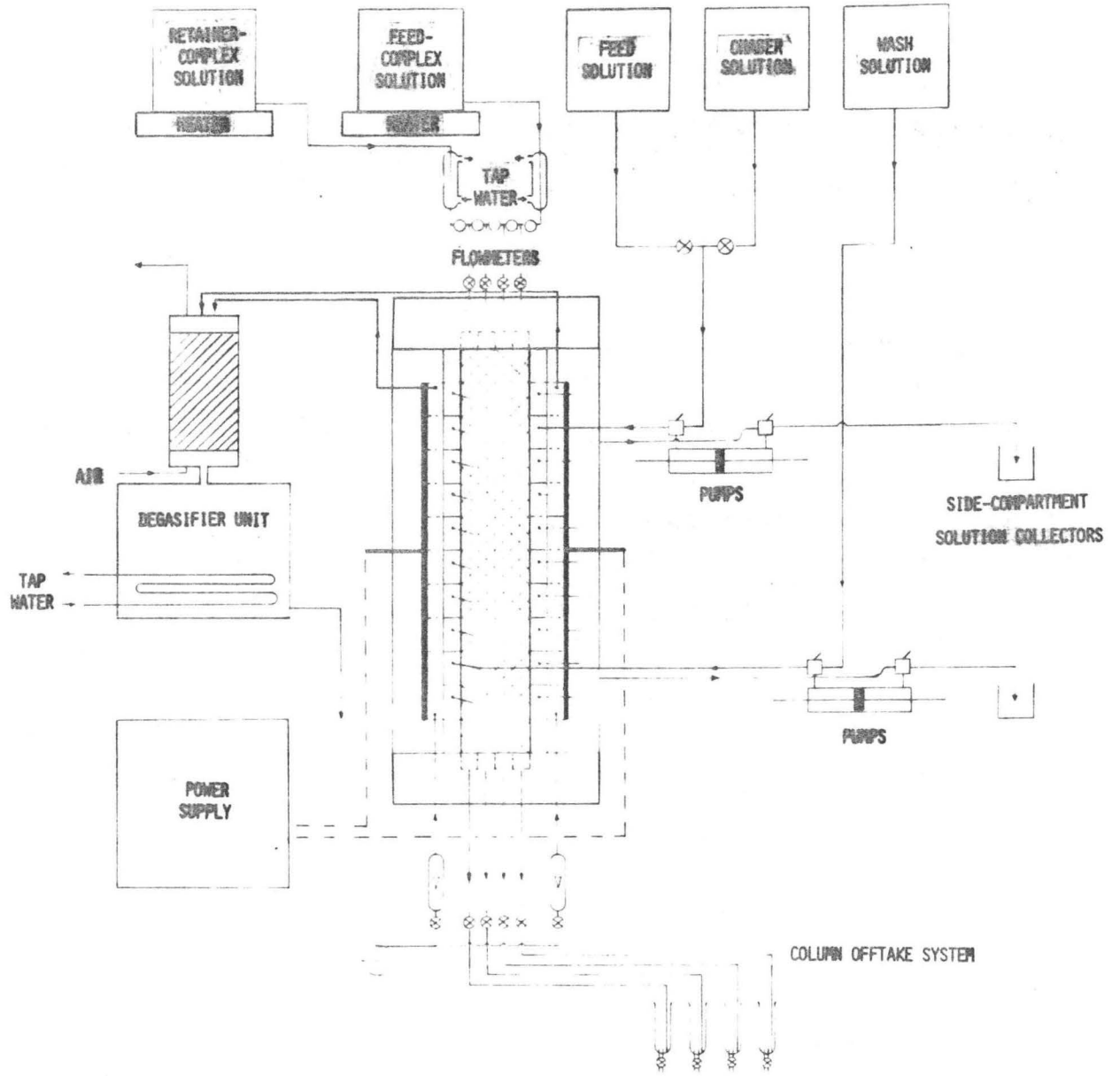

Fig. 18. Flow sheet for ligand electrochromatograph.

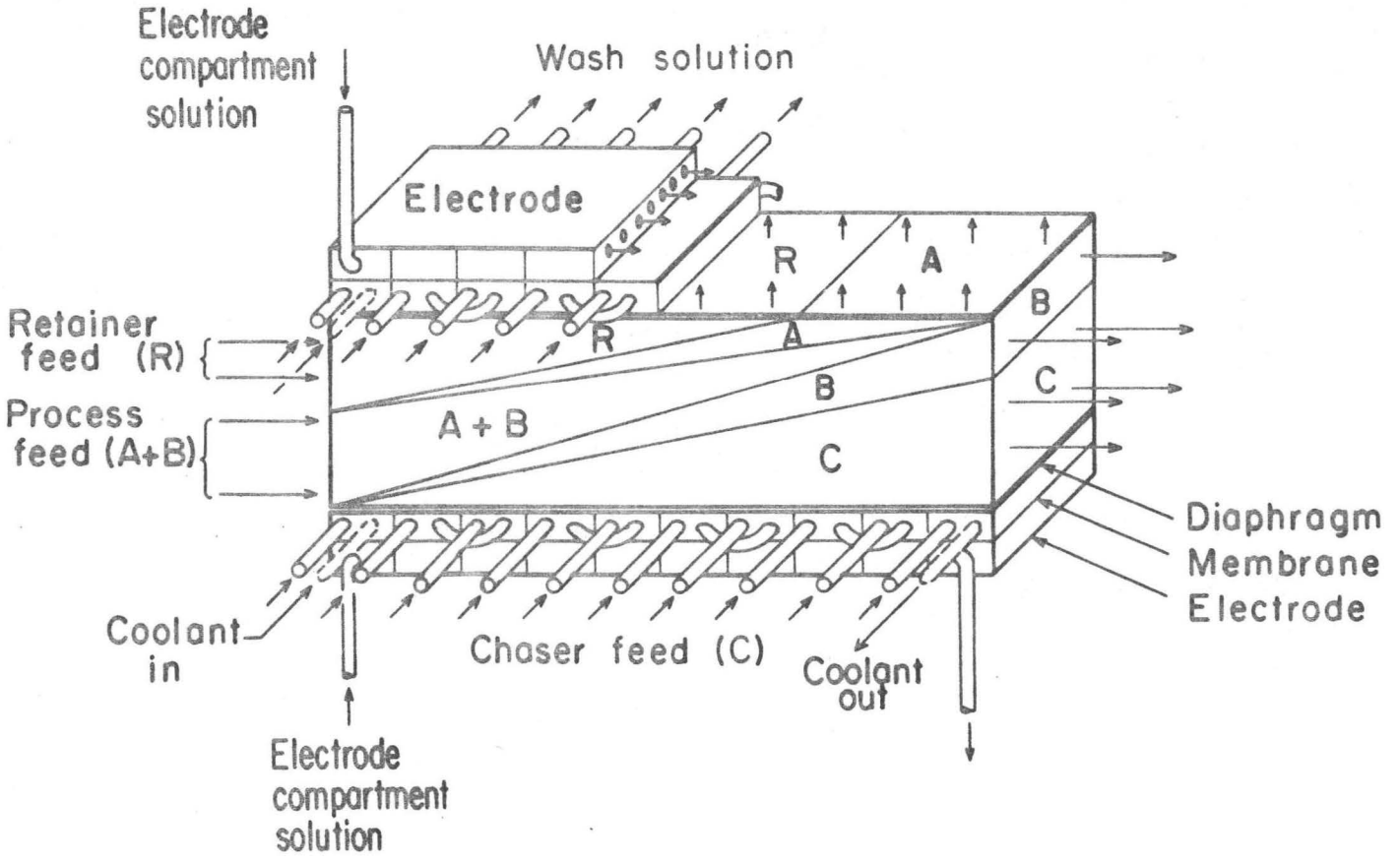

Fig. 19. Schematic diagram showing construction and operation of the ligand electrochromatograph.

A set of on-off valves makes it possible to vary the number of inlet lines containing retainer-complex solution and feed-complex solution. The flowrate of each inlet stream is metered by a Fischer and Porter Predictability flowmeter #36-541-07 and a Fischer and Porter glass-and-Teflon needle valve.

For the case where only retainer-complex solution is fed to the bed, feed solution can also be fed to any number of compartments on the anode side. Chaser solution is fed to the remaining compartments on that side. Wash solution is fed to all the compartments on the cathode side of the bed.

The electrolyte solution for the two electrode compartments is contained in the degasifier unit. Cooling coils maintain the solution temperature at room temperature. The electrolyte stream passes through a centrifugal pump and is split into two. The streams are each sent through a Schutte & Koerting purge meter #58-G-056-M-1 and introduced one to each electrode compartment. The streams leave the electrode compartments at the top, and flow to the top of the degasifier; there they are stripped of H_2 by aeration and are then recombined in a container beneath the degasifier column.

Power for the central unit is provided by a silicon rectifier (model #S-100-50 from Rapid Electric Co.), capable of providing 100 amperes at a constant voltage up to 50 volts.

Electrochromatograph Unit

The unit consists of a sandwich assembly of Lucite-block sections clamped between 1/2 in. aluminum plates. The sandwich consists of two

long rectangular-block spacers serving as the sides for the central chamber, with pairs of sections housing the side compartments and the electrode compartment placed symmetrically above and below the central chamber. Lucite end plates are placed at each end of the unit and attached to the aluminum frame. A schematic drawing of the primary unit is shown in Fig. 19. Figure 20 is an end view of this sandwich construction, with the outlet end plate removed, which shows the central chamber and the slotted feed or offtake segments. Figure 21 is an exploded cross-sectional drawing of the unit. An ion-exchange membrane is placed between each electrode compartment sheet and side compartment sheet.

Electrode-Compartment Section

Figure 22 shows the electrode-compartment section and the electrode. The electrode (10 cm × 40 cm in extent) consists of a sheet of graphite 1/4 in. thick bolted to a sheet of copper 1/16 in. thick, with a 1/4-in.-diameter copper rod soldered to the center of the copper plate. Insulating epoxy resin is applied to all the copper not touching the graphite, so that only the graphite can make contact with the solution. Figure 23 is a photograph, and Fig. 24 a scale drawing, of the assembled electrode-compartment section. Spacers, supported in grooves above the electrode, line up with corresponding supports on the side-compartment section and thus provide support for the ion-exchange membrane which lies between the two sections. Clearance between the spacers and the electrode, along with 1/8 in. perforations through the spacers, allow readily for electrolyte flow lengthwise through the electrode compartment. This electrolyte enters and leaves at opposite ends of the compartment through

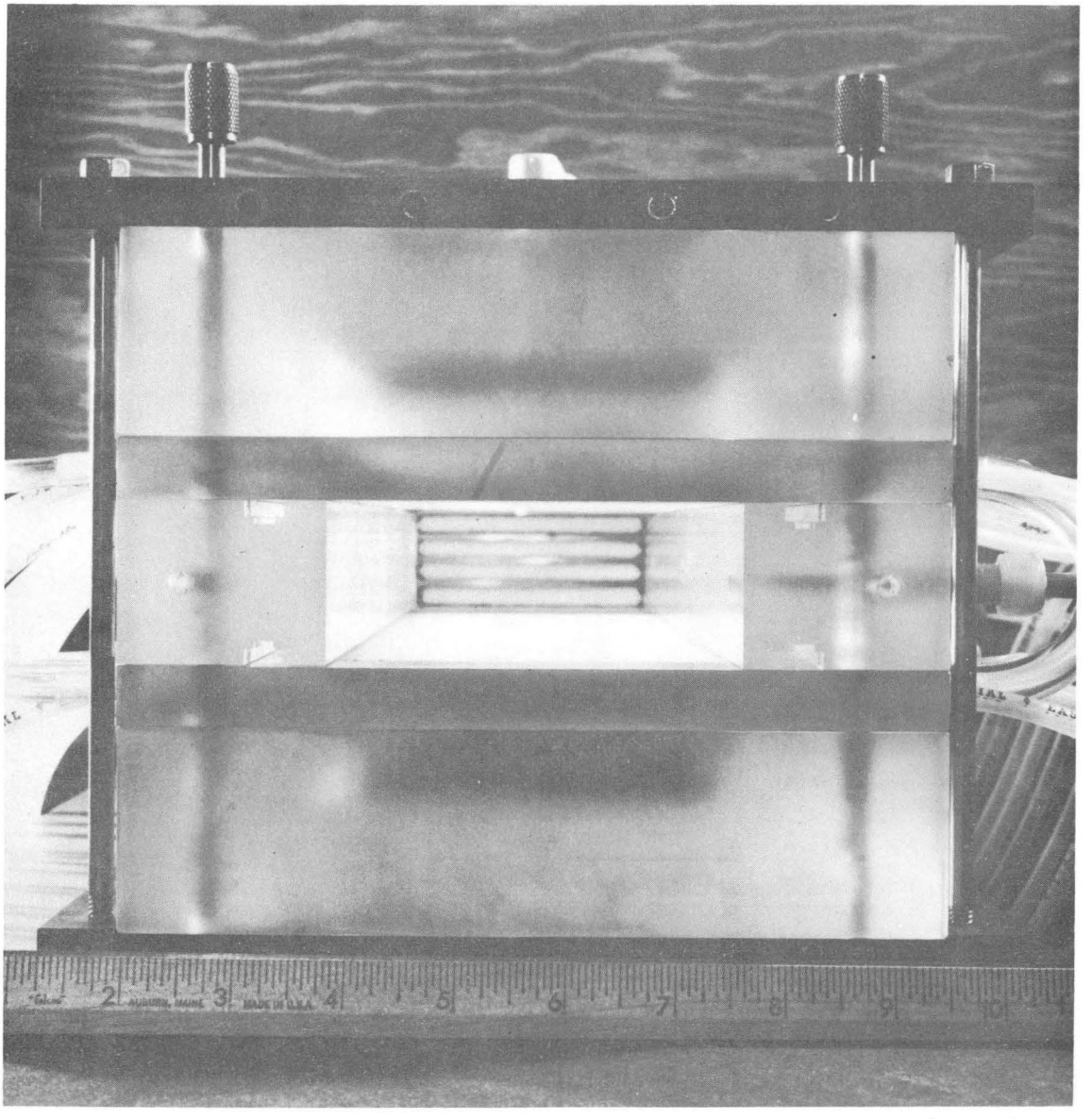

CBB 698-5659

Fig. 20. View of central chamber of electrochromatograph unit, with one end plate removed.

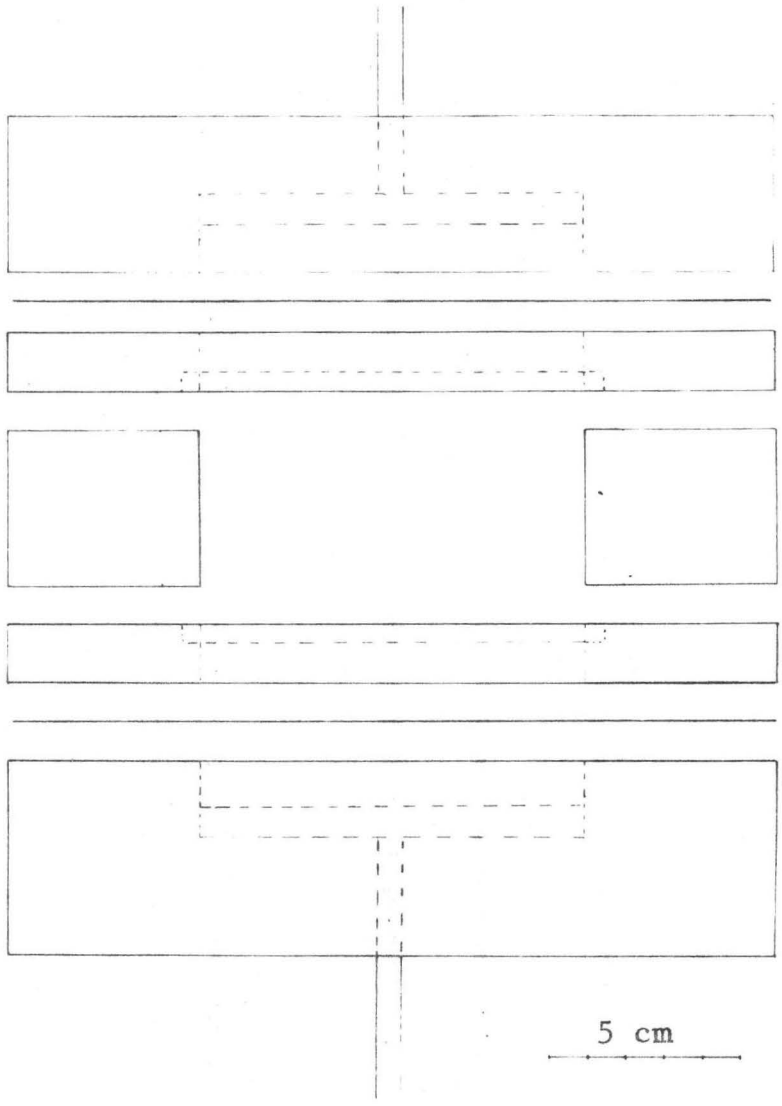

Fig. 21. Exploded cross-sectional drawing of ligand electrochromatograph (end view).

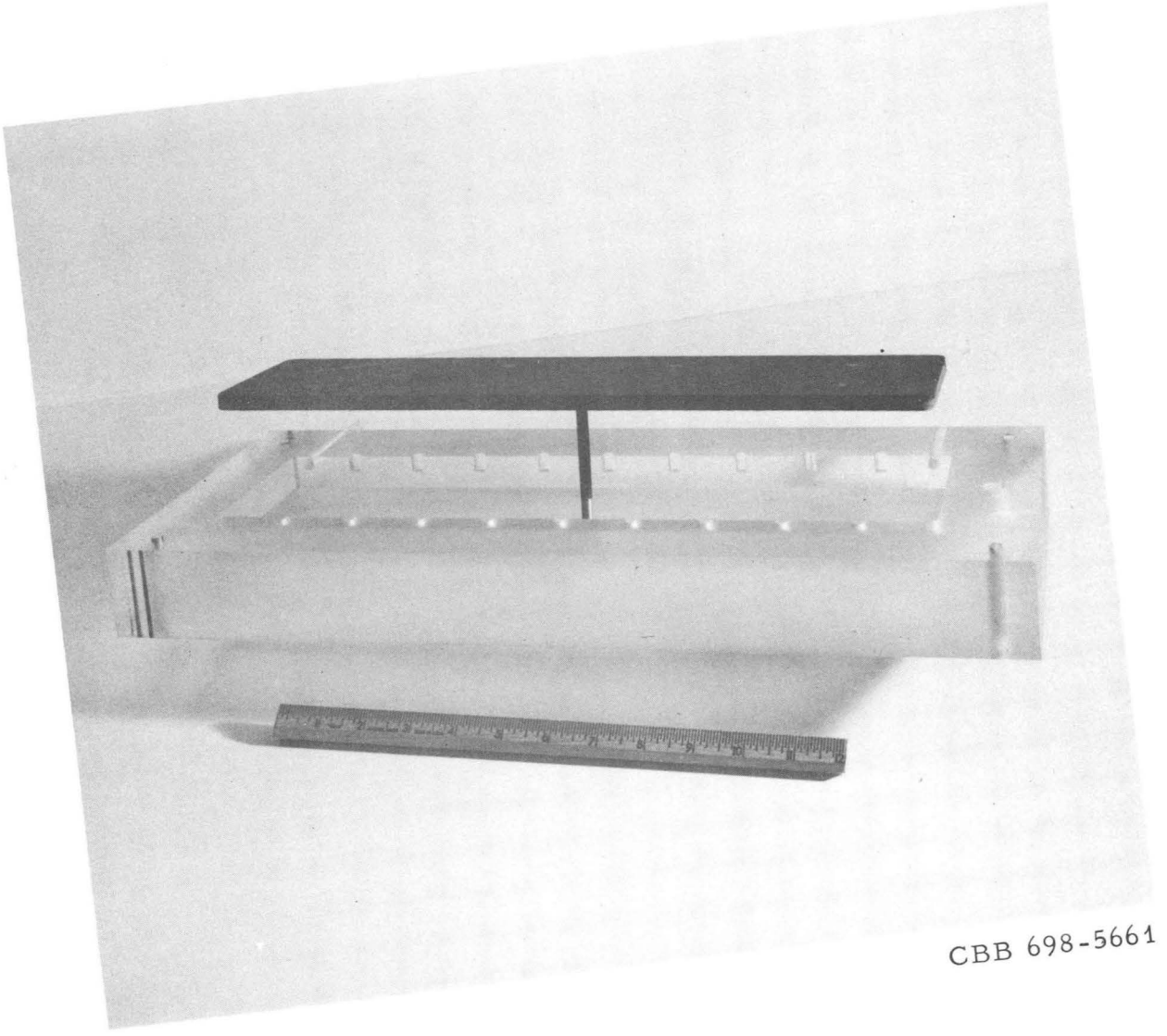

CBB 698-5661

Fig. 22. Electrode and electrode-compartment section prior to assembly.

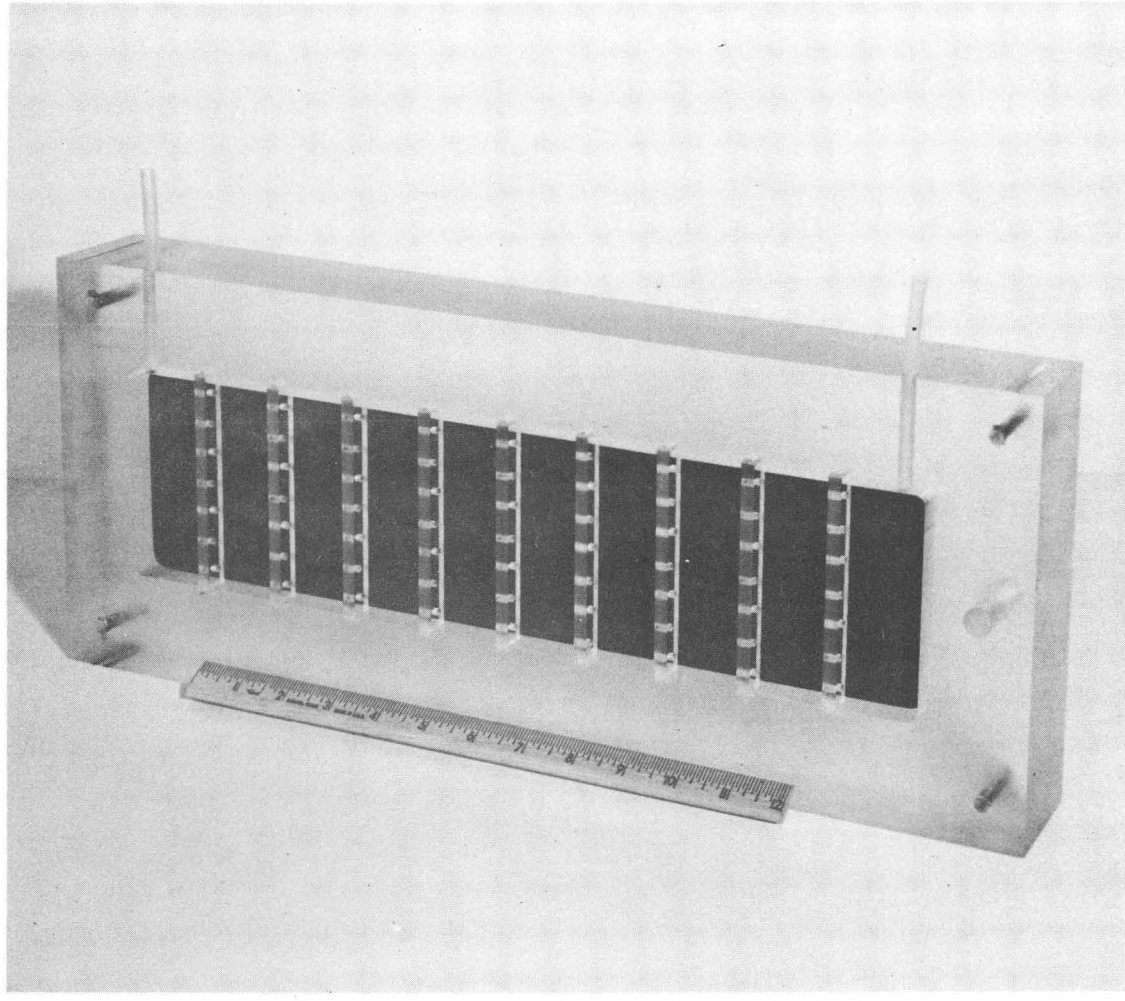

CBB 698-5671

Fig. 23. Electrode and electrode-compartment section in assembled form.

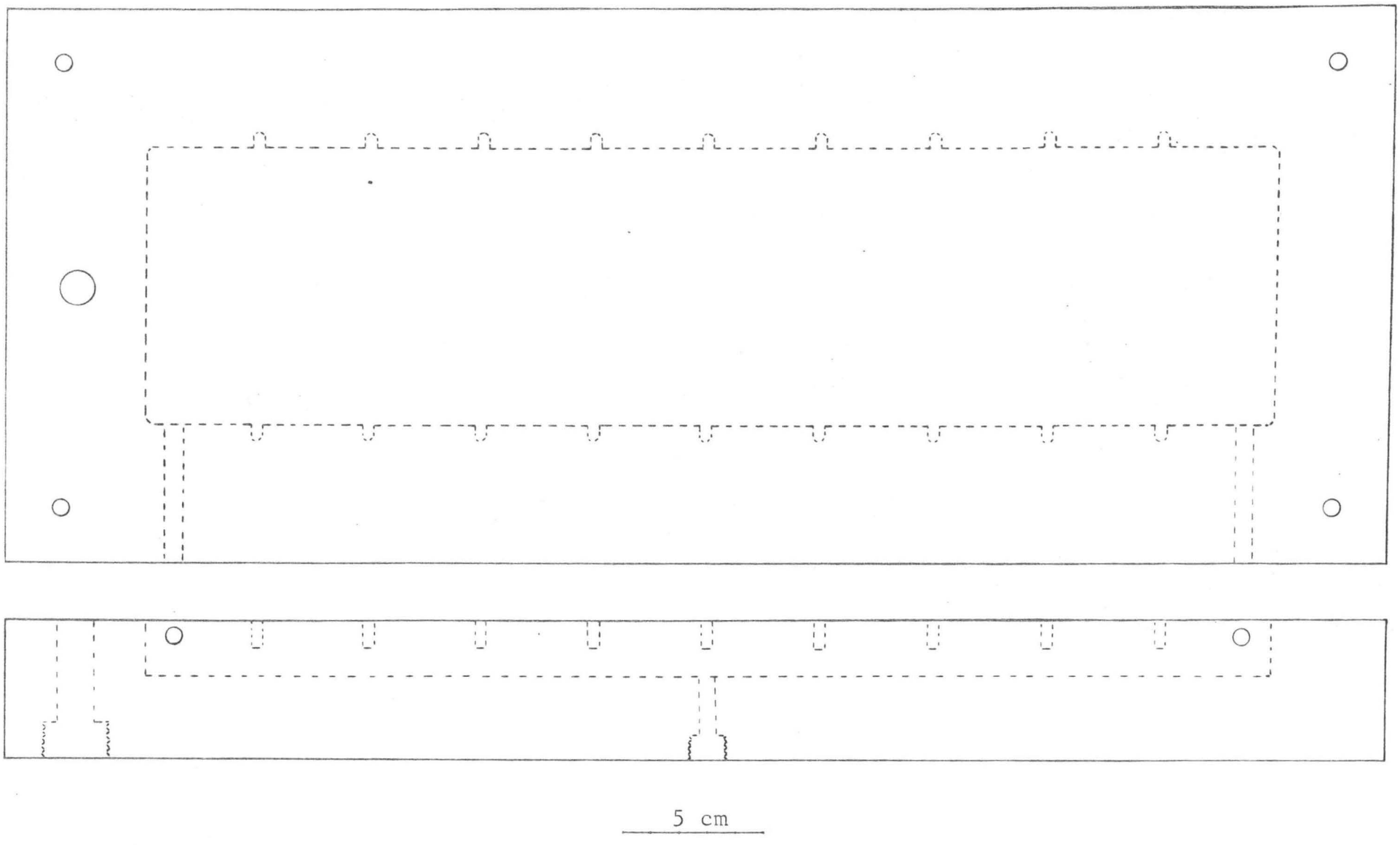

Fig. 24. Scale drawing of electrode-compartment section.

1/4 in. O.D. polyethylene tubing epoxied into 1/4-in. access holes. A 1/2-in. port giving access to the central packed bed is located along the centerline 2.5 cm from the top end. Guide holes, 1/4 in. in diameter, for unit assembly are located at each corner, 2 cm from each side.

Side-Compartment Section

This section, drawn to scale in Fig. 25, consists of a flat rectangular Lucite block (20 × 49 × 1.5 cm) with 10 rectangular openings (the side compartments). The opening at each end is 10 × 3.68 cm, the remaining eight being each 10 × 3.33 cm. The whole central section of the block (11 × 41 cm, contained inside the dotted line), which contains these openings, is milled down 0.5 cm. A siliceous diaphragm (Filtros Electrolytic-35, 11 × 41 × 0.318 cm) is glued with epoxy resin into the milled-out space. Each of the two opposite narrow sides has 20 1/4 in. access ports; so that four ports, two on each side, connect to each compartment. Two of these ports (one on each side) are fitted with 1/4-in. polyethylene tubes opening into the compartment and epoxied into place; these tubes, connected to a positive-displacement pump, are used to exchange the liquid in the compartment. An intact 1/4-in. O.D. polyethylene tube, epoxied into place, crosses each compartment between the remaining two ports; these tubes are joined together in series to serve as a cooling line through which tap water is circulated. Guide holes (1/4-in.) are located at the four corners. A 1/2-in. access port at one end (with a similar one for the electrode compartment sheet) allows access to the bed. The bed can be packed using a slurry, or unpacked with a vacuum line via this port. Figure 26 shows the open side-compartment

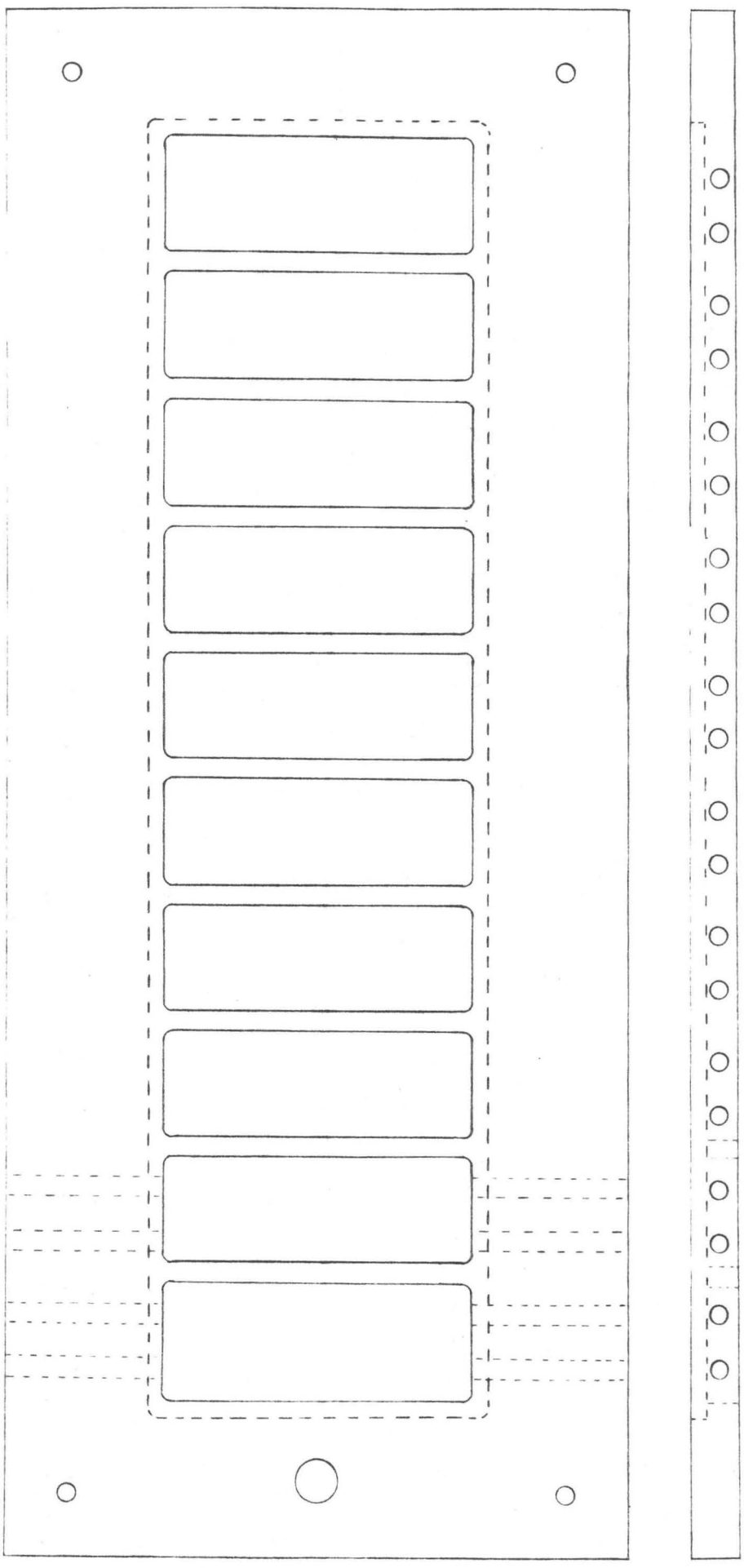

Fig. 25. Scale drawing of side-compartment section.

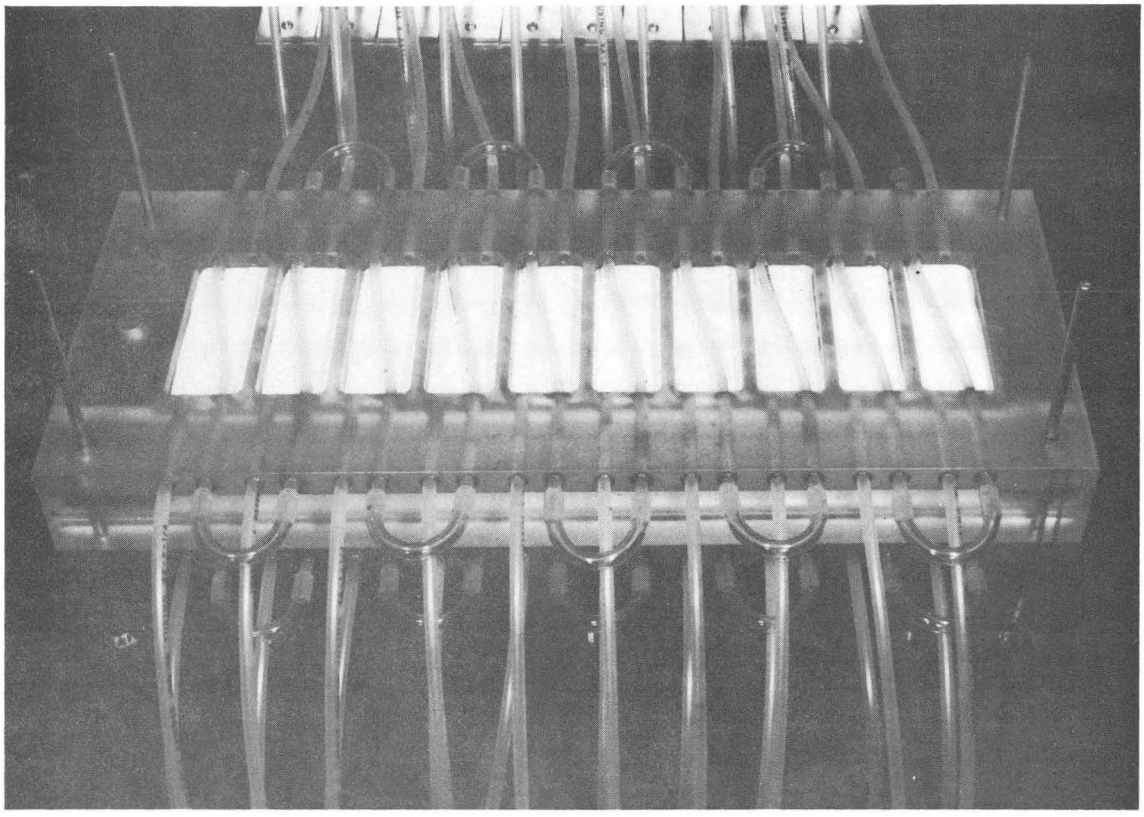

CBB 698-5665

Fig. 26. Side-compartment section viewed from the outside.

section as viewed from the outside; the second side-compartment section can be seen below the main bed. Figure 27 shows one such section in place, from the inside, with the diaphragm covering the compartments. The continuous tubing connected to all the compartments is the cooling line.

Bed Spacers

These are two rectangular Lucite blocks, each 5 × 4 × 49 cm (see Figs. 21 and 26), which become the containing outer walls for the main bed. Grooves for a 3/16 × 9/32-in. port gasket are located 1 cm from the inner edge on the wider face and run the length of the block. One of the blocks has three temperature-probe holes, 3/16-in. in diameter, at 5 cm, 25 cm, and 45 cm along the centerline of the 4-cm face. One-quarter-in. guide holes for unit assembly are located at two outer corners of each block. Additional 1/4-in. guide holes (1.5 cm deep) are provided at the ends, 1.5 cm from the side and 2 cm from the top and bottom, to line up the end plates.

End Plates

These are made from Lucite blocks 17 × 20 × 4 cm, as shown in Figs. 28 and 29. Four feed or offtake grooves are provided to handle the flows to and from the packed bed; the outer grooves are each 0.85 cm wide and the inner grooves 0.7 cm wide. These grooves are all 1 cm deep with a 0.5 cm step at each end. Packing-retainer strips, cut from 1/8-in. thick Vyon porous polyethylene, are positioned on these steps, in the grooves, and glued into place by epoxy resin. The process streams enter or leave these grooves through 1/4-in. polyethylene tubes epoxied into

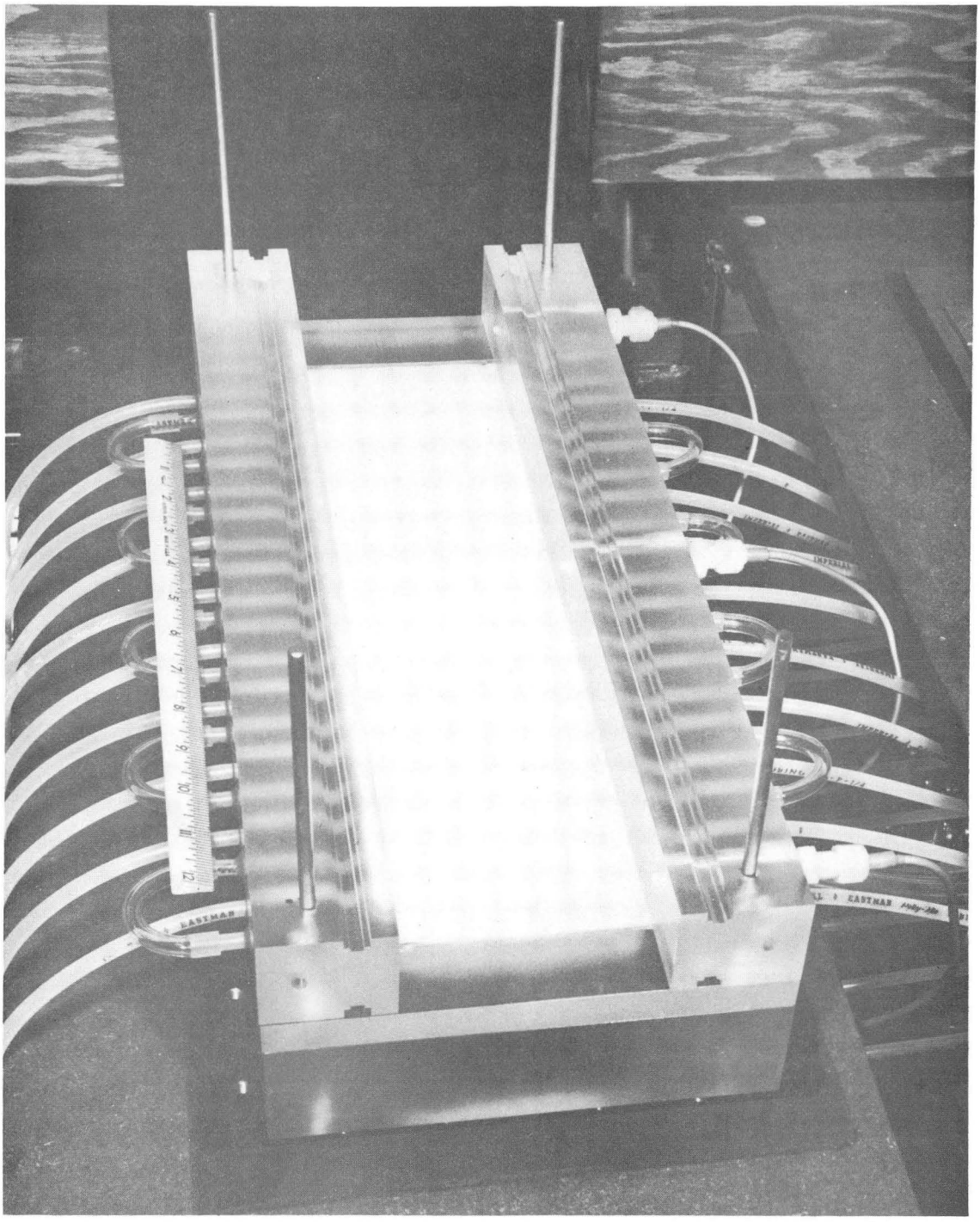

CBB 698-5669

Fig. 27. Bedside view of side-compartment section, with bed spacers in position.

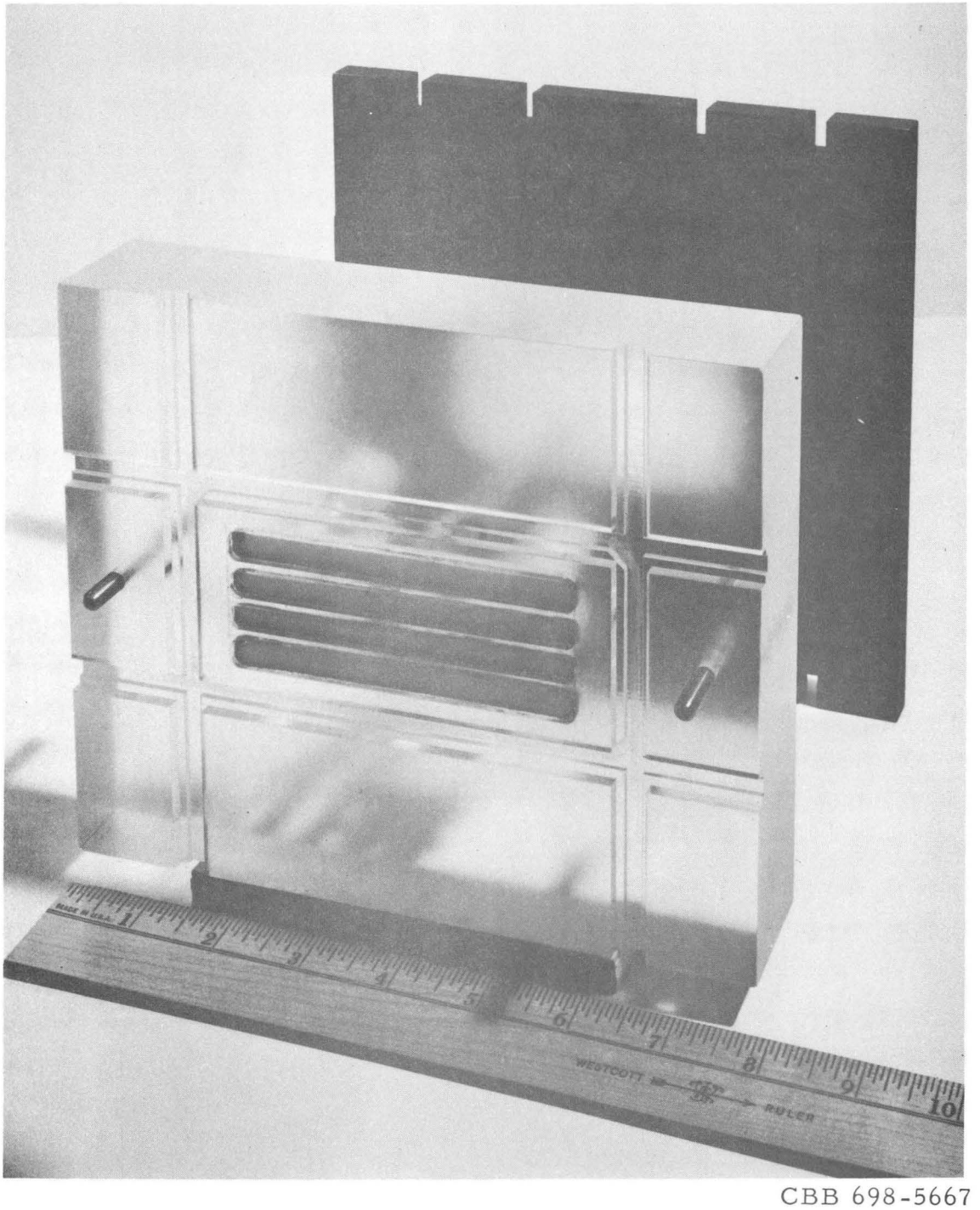

CBB 698-5667

Fig. 28. End plate for "ligand" electrochromatograph unit.

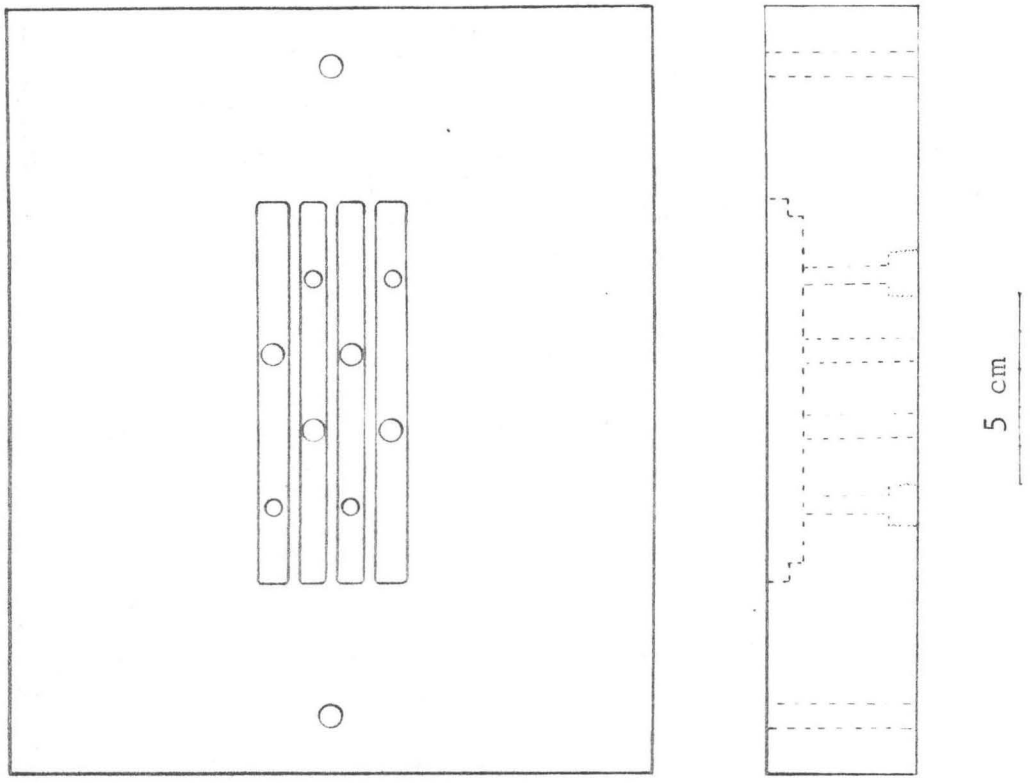

Fig. 29. Scale drawing for end plate.

1/4-in. holes located alternately 4 and 6 cm from the right end of the grooves. The outlet (bottom) end plate has additional 3/16-in. thermometer probe holes located alternately 8 and 2 cm from the right end of the grooves. Two 1/4-in. guide holes for unit assembly are provided along the center line 1.5 cm from each side.

Constant-Pressure and Displacement Pumps

The pumps were designed to allow for the discontinuous replacement of the side-compartment solutions without appreciable alteration of the static pressure in that compartment. The porous ceramic diaphragms used in the side-compartment sections are known to cause electro-osmotic flows. By keeping the fluid stagnant in the compartment and allowing an electro-osmotic pressure to build up instead, the disruptive electro-osmotic flows can be eliminated.

Figure 30 gives the positive-displacement pump and its accessory lines and valves. Twenty such units are used, one for each side compartment. The pump consists of a 7.5-in.-long Lucite tube 1.5 in. in O.D. and 1.0 in. in I.D., with a 3/8-in. stainless steel rod silver-soldered to a brass plunger. The liquid on each side of the plunger is connected (through two three-way valves) either to two lines connected across a side compartment, or to two elbows connected respectively to wash solution and to a collection vessel. When the pump is connected to the compartment, forward movement of the plunger causes the liquid in front of the plunger (space A) to replace the liquid in the side-compartment, which in turn moves to fill the volume behind the plunger (space B). The valves are then switched to connect the pump to the two elbows. As the

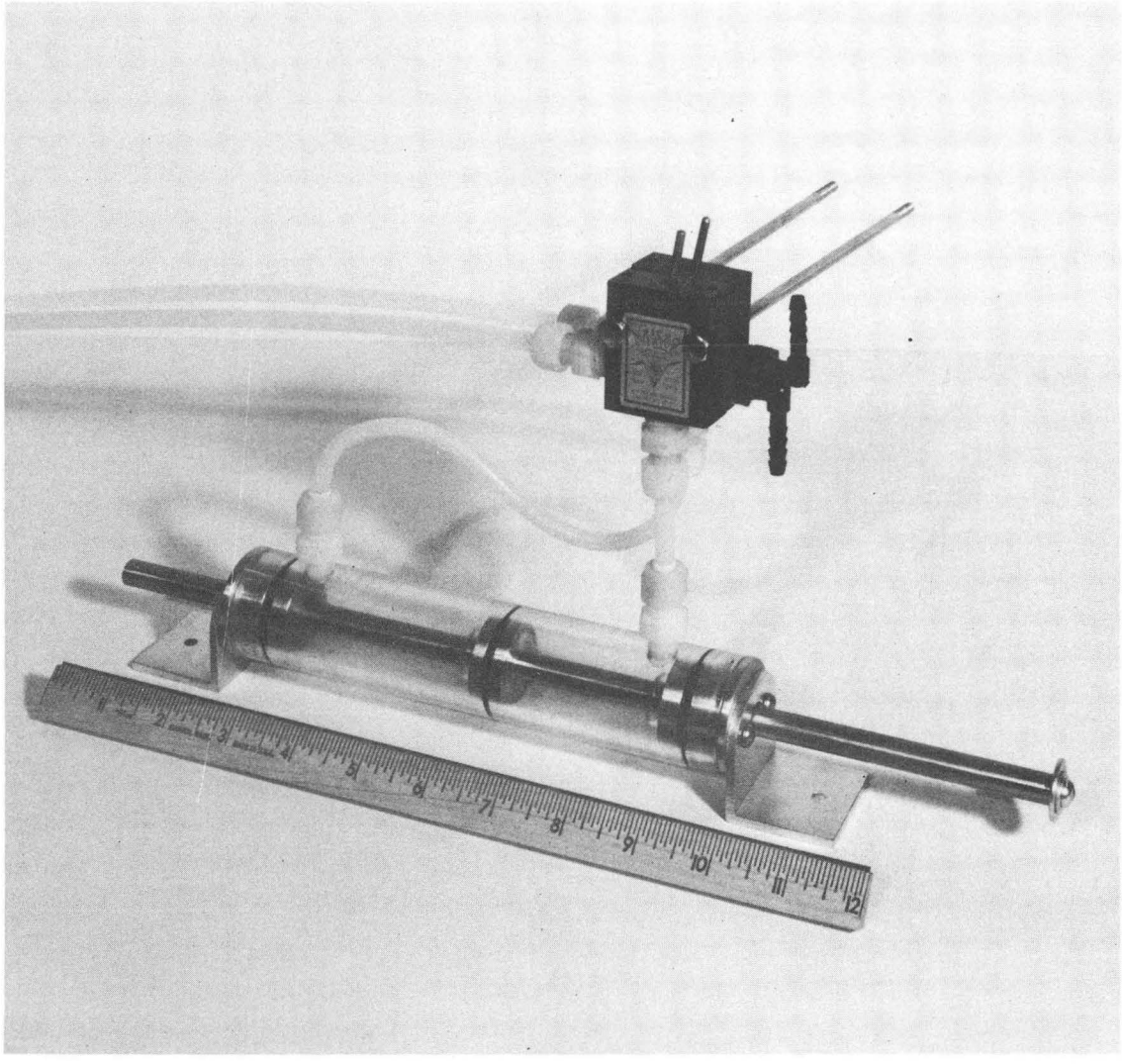

CBB 698-5663

Fig. 30. Constant-pressure and displacement pump and its accessory lines and valves.

plunger moves back, the liquid in space B is forced downward into the collection vessel.

In this manner, wash solution is introduced to the side compartment, and the side-compartment product solution is collected. The distance the plunger is moved determines the amount of liquid replaced. Up to 65 cc of liquid (or about twice the volume of each side compartment) may be displaced in this manner.

Offtake System

Uniform flowrates for all four offtake lines are achieved with the collection system shown in Fig. 31. The four offtake streams first pass through four on-off valves, then into four 2.5-cm-I.D. 15-cm long test tubes fitted with bottom drain valves. As intake fluid enters the test tubes, the drain valves being closed, the liquid level in each test tube rises; the result is to equalize the flowrates hydrostatically. If the flow in one stream is initially faster, that fluid level will rise faster; this pressure-head difference between the test tubes then slows down the faster flow to the point where all flows are even. When the test tubes are filled, the drain valves are opened, and the test tubes drain quickly to the drain-pipe level with minimum disruption to the column offtake flows.

Temperature Probes

Eight Telethermometer probes #61248-000 (from Van Waters & Rogers) monitor the temperatures. Seven measure the temperatures in the packed bed, three at the centerline along the length of the bed and four at the

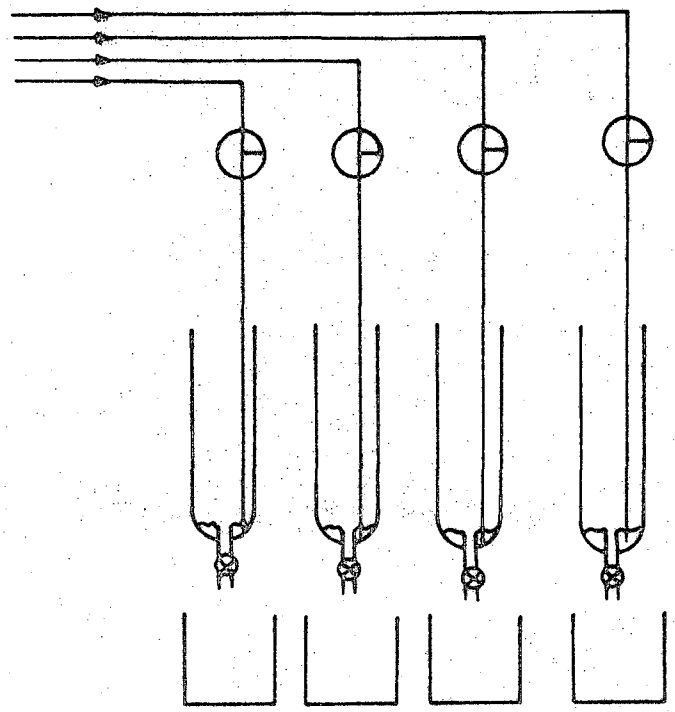

Fig. 31. Offtake flow regulating system.

offtake end (one in each offtake groove). The remaining probe monitors the temperature of the electrolyte entering the electrode compartments.

Voltage Probes

Two stainless steel rods, 6 cm long and 0.1 cm in diameter, are sealed into holes drilled through one of the bed spacers, 7.5 cm from the inlet line and 1.5 cm from each diaphragm; i.e., 1 cm apart. The rods penetrate the bed 0.1 cm and are used to measure the voltage gradient in the bed. In the side compartments adjacent to the bed probes, stainless steel wires, inserted through the polyethylene feed and outlet lines, protrude a few mm.

Membranes

Anion exchange membranes (A-100, courtesy of American Machine & Foundry Co.) are used.

Bed Packing

Polystyrene beads (Bio-Beads -X2, 150-200 mesh, supplied by Bio-Rad) are used as column packing.

Apparatus Assembly

To prepare each separate column section for assembly, all process lines are attached to the sections. The diaphragms are epoxied to the side-compartment sections. The electrodes are placed in the electrode-compartment section, and the spacers are put in place above the electrode surface (see Fig. 23). The unit is assembled in the horizontal position, and after assembly, tilted into the vertical operating position.

Two sets of alignment rods (four each) are used for sandwich assembly. Brass rods 23 cm long with a diameter of about 0.23 in. are used initially, to allow quick assembly. When the sandwich is together, before the bolts are tightened, the brass rods are replaced by 1/4-in. diameter stainless steel rods that fit snugly into the holes and give exact alignment.

Sandwich assembly, which is best performed by two people, is begun by placing an electrode compartment section on one of the aluminum support plates, and putting the brass alignment rods in place. The ion-exchange membrane, 18 × 17 cm in size, is taken from its water bath, excess surface water being removed by wiping with a dry cloth. Care is taken that the membrane is never allowed to dry, as this causes shrinking and possible cracking; this requires that the entire sandwich assembly-procedure, from the time the first membrane is removed from the bath until water can be introduced to the electrode chamber and the side compartments, must be accomplished in 10 to 15 minutes. The fresh membrane is placed upon the electrode-chamber section. Silastic 892-RTV adhesive sealant is applied to the 1 cm exposed strip of Lucite around the membrane (the block is 20 × 49 cm). A side-compartment section is placed over the membrane. The two bed spacers fitted with port gaskets are put into place. Next the other side-compartment section is placed over the bed spacers. The second membrane is put on top, and sealant again applied to exposed Lucite. Finally the remaining electrode-chamber section and the aluminum support are put into place.

The temporary brass alignment rods are now removed, and the stainless steel rods inserted in their place. The bolts clamping together the sandwich construction are tightened, starting in the middle and alternately tightening the bolts on each side while working toward the ends. As soon as the bolts are secured, water is introduced into all the side compartments and the electrode chambers to wet the membrane. Since the process lines are not yet connected to the constant-displacement pumps, temporary rubber stoppers are fastened to the lines to keep the water in the compartments. The unit is checked visually for leaks and for proper membrane seating. If water is leaking, other than by seepage through the porous diaphragm, the unit is taken apart and reassembled.

Once this part of the unit is successfully assembled, the end plates are bolted on. This is done by putting the port gaskets in place, applying Silastic 892-RTV sealant on each side of the port gasket, lining up the end plates with the bed spacers by means of two aligning posts, and bolting the end plates to the main unit. The main chamber is filled with water, and the end plates checked for leaks. If the unit is leak-free, it is tilted vertically and placed into position. The lines are then unstoppered and attached to the support systems.

A curved 1/2-in.-O.D. polyethylene line, reaching above the top of the unit, is fastened to the 1/2-in. access port. The column is packed by feeding a slurry into a funnel connected to the top of this curved pipe. While slurry is being introduced at the top, water is allowed to drain from the offtake lines. This gives uniform packing in a relatively short time.

Once the column is filled with polystyrene beads, the offtake lines and the access tube are closed. The column is now ready for operation.

Selection of Operating Conditions

General Procedure

To determine operating conditions for a potential separation, Fig. 7 is used. From available equilibrium data for the feed ions with the ligand to be used, modified equilibrium parameters are calculated for various values of S (ratio of uncomplexed to complexed ions) using Eqs. (8) and (13); values of S between 0.25 and 1.0 give the minimum overlap distance between components. The feed position is chosen (either end feed, or side feed) and the dimensionless values of $\tilde{Z}_e$ and $\tilde{Z}_c$ that just give separation are read from the graph.

For each trial combination of S, $\tilde{Z}_e$, and $\tilde{Z}_c$, the contributing physical variables Z_e, Z_c, Z_{eo} (or Z_{co}), and the ratio U_e/U_c must now be found. For a given apparatus, Z_e and Z_c are fixed by the overall dimensions. The feed distance (either Z_{eo} or Z_{co}) is usually set at as large a value as will still give the desired separation, in order to maximize the production rate. This then sets U_e/U_c; so, if either U_e or U_c is specified, the other one is automatically specified. Since $U_c = Z_c/\tau$ and U_e = (cation mobility) $\times (\Delta E)_{bed}/Z_e$, either τ or $(\Delta E)_{bed}$ can be selected.

In the preliminary runs on the present unit the residence time was generally set between 0.5 to 2 hours, and the required bed voltage

calculated. This voltage was then used to calculate the highest allowable solution concentrations that could be used without producing more than 20 to 40-degree temperature rise in the bed.

Actual operation of the present unit has shown that two additional factors must be taken into account for successful operation: electrophoretic migration of the ligand, and the kinetics of equilibration between complexed and uncomplexed species.

Ligand Electromigration

In the theoretical development complexed ligand has been assumed to have zero electrophoretic mobility, and thus to migrate only in the convective direction as shown in Fig. 32a. In general, the mobility of rare earths complexed with various ligands is a function of pH.[9] An "isoelectric" pH can usually be found that will result in a zero electrophoretic mobility. Since this isoelectric point is not always the optimum operating pH, the electromigration of metal-ligand complex must be taken into account.

In preliminary investigations EDTA (ethylene-diaminetetraacetic acid) was used as the ligand, primarily because it has good selectivity between rare earth ions and because its physical and chemical properties have been investigated extensively. EDTA has four ionizable anionic groups. Above a pH of 2, at least to pH 10, the rare earth-EDTA complex behaves as an anionic species with a constant mobility.[9] Below a pH of 2 the mobility decreases. The isoelectric point occurs close to a pH of 1, and below this point the complex begins to behave as a cation.

The operating pH is between 2 and 5. Below around pH 2.5, gradual precipitation of uncomplexed EDTA becomes a problem. At pH values greater than 5, the rare earth hydroxides begin to precipitate.

The effect of ligand electrophoretic migration on the ligand streamline is shown in Fig. 32b. Complexed ligand enters at the feed end, moves at an angle across the unit, and leaves partially at the exit end and partially at the side. Such a situation has two adverse consequences:

1) No separation occurs in the ligand-free region of the bed. This can result in incomplete separation of the ion mixture.

2) Overlap regions between zones will tend to diffuse and broaden in the ligand-free part of the bed. Self-sharpening between zones occurs only in the presence of ligand.

These effects can be overcome by introducing ligand to the bed from the side compartments in addition to the entrance end. The streamlines for this case are shown in Fig. 32c. Operating in this manner has the advantage over operating with zero ligand mobility, in that it increases the effective electrophoretic separation distance without increasing the size of the apparatus. Rare earth ions migrating through a given distance in the electrophoretic direction pass through more complexing agent, because the ligand is migrating in the other direction, and are consequently separated in a shorter distance.

Such an increase in the effective electrophoretic distance parameter may make it possible to feed over the entire entrance-end cross-section (and still get the desired separation). The qualitative effect of ligand migration on the design graph (Fig. 7) is indicated by Fig. 33.

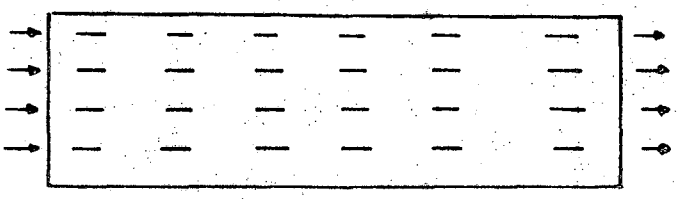

a) Ligand introduced at entrance end; zero ligand electrophoretic mobility.

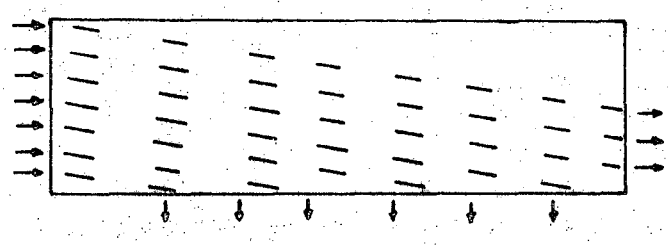

b) Ligand introduced at entrance end; finite ligand electrophoretic mobility.

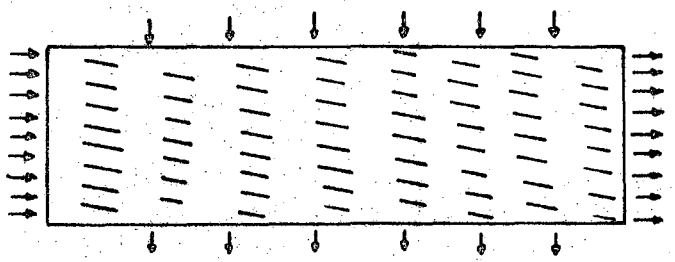

c) Ligand introduced at entrance end and side; finite ligand electrophoretic mobility.

Fig. 32. Ligand streamlines.

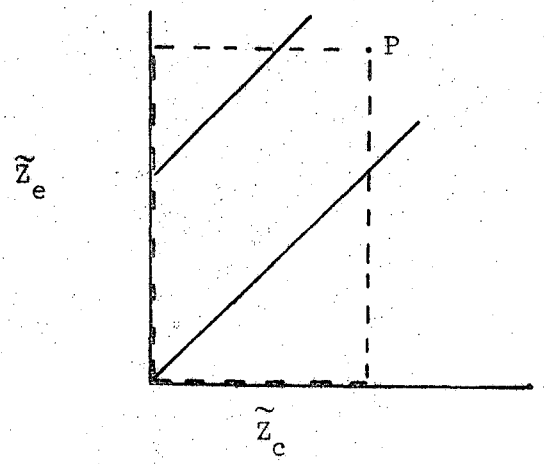

a) No ligand electromigration.

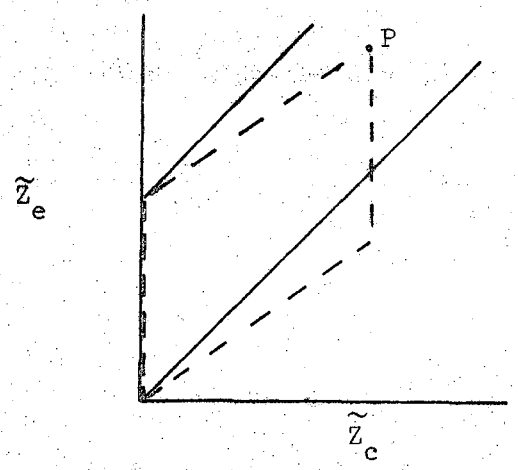

b) Effect of ligand electromigration

Fig. 33. Effect of ligand electromigration on the design graph.

Figure 33a shows the intersection point P for separation and the column boundaries (in dashed lines), when there is no electromigration of ligand. Ligand migration has the effect of tilting the column sides upward on the design graph, as shown in Fig. 33b. Thus complete separation is achieved in a column with feed being fed to the entire entrance end.

Reaction Kinetics

The design theory assumes that the exchange reaction for a rare earth ion with a second complexed rare earth is instantaneous. Although the exchange reaction for divalent cations such as Fe^{++} is almost instantaneous, it is known[10] that the exchange for the trivalent cation Fe^{+++} is very slow (5 hours for 50% exchange at a pH of 1).. For the rare earths, the rate of complex formation with EDTA is almost instantaneous, but decomplexing may be rather slow. Equilibrium studies to determine rare earth-EDTA stability constants using binary mixtures of rare earths are run for up to 24 hours in order to assure complete solution equilibrium.[11]

In this study operation at low feed concentrations (10^{-3} M in rare earth) and low temperature (20°C) resulted in very little separation. Attempts to speed up the kinetics by increased concentrations (to $\sim 10^{-2}$ M in rare earth, which may or may not have an effect), increased temperatures (up to 60°C in the bed), and low pHs (between 2 and 3) resulted in more satisfactory results.

Temperature Rise in the Bed

The theoretical treatment for the temperature rise given above assumes a rectangular packed bed with cooling at the two (equipotential)

bed walls. In the present unit the packed bed is separated from the cooled electrode chambers by the additional side-compartment sections, each of which is partially cooled by a coolant line running through it. The distance from the center of the bed to the coolant lines is about 2.5 cm; to the membrane, 3.5 cm. As a measure for design purposes, 3.0 cm can be taken as the effective distance from the center of the bed to a cooling surface for determining limiting concentrations, with the further assumption that the total voltage at the electrode applies across this $2 \times 3 = 6$ cm hypothetical bed. The problem arises that only the voltage drop across the bed required for separation is predicted from the design theory, but the total voltage across the bed plus the adjacent compartments, diaphragms, and membranes enters into the temperature rise predictions. Generally about 50% of the applied voltage will be across the bed, although this percentage will vary somewhat with solution concentrations in the various compartments.

In attempting to speed up the kinetics by using higher concentrations and higher voltages that will result in bed temperatures up to 60°C, difficulties can arise. One difficulty is that the temperature rise is not uniform axially. Each change in voltage and in temperature profile requires adjustment of the flow rate; also, the total available voltage is limited. If the concentration is slightly too high, or if the fraction of the total voltage that is dissipated across the bed changes, requiring a higher voltage, the temperature rise becomes too large and the bed dries out locally. When this happens, channelling occurs; the overlap distance tends to spread across the entire bed. A frequent repacking of the bed appears the only way to overcome this difficulty.

Experimental Runs

Preliminary runs on the ligand electrochromatograph were performed using feed mixture [$La(NO_3)_3$ and $Ce(NO_3)_3$], complexing agent [$(EDTA)Na_2$], chaser ion [$Cu(NO_3)_2$], and wash solution ($NaNO_3$). Solutions were analyzed by X-ray fluorescence analysis for La^{+++}, Ce^{+++}, and Cu^{++}. The procedure has been previously reported.[12,13,14] Feed mixture was introduced with the ligand over the entire entrance end of the bed. Chaser ion was fed to the bed from all the side compartments on the anode side; wash solution was introduced to all side compartments on the cathode side.

When no retainer is used, only a zone containing the more tightly complexed component develops out of the mixture zone. This zone will appear between the mixture zone and the chaser zone. The mixture zone emerging from the end of the column will have the same concentration ratio as the feed; the mixture solution will contain both free and complexed rare earths. Since only uncomplexed ions from the mixture zone can migrate to the side compartments (complexed species will migrate in the opposite direction), the product collected in the side compartments will be rich in the less tightly complexed ions.

Results and Discussion

Offtake patterns for a break-in run are shown in Fig. 34. The column boundaries for the conditions of this run are imposed on the theoretical design graph and shown in Fig. 35. This run served mainly to check flowrate stability. No effect was made to change conditions during the run to give a better separation. Nonetheless the resulting offtake

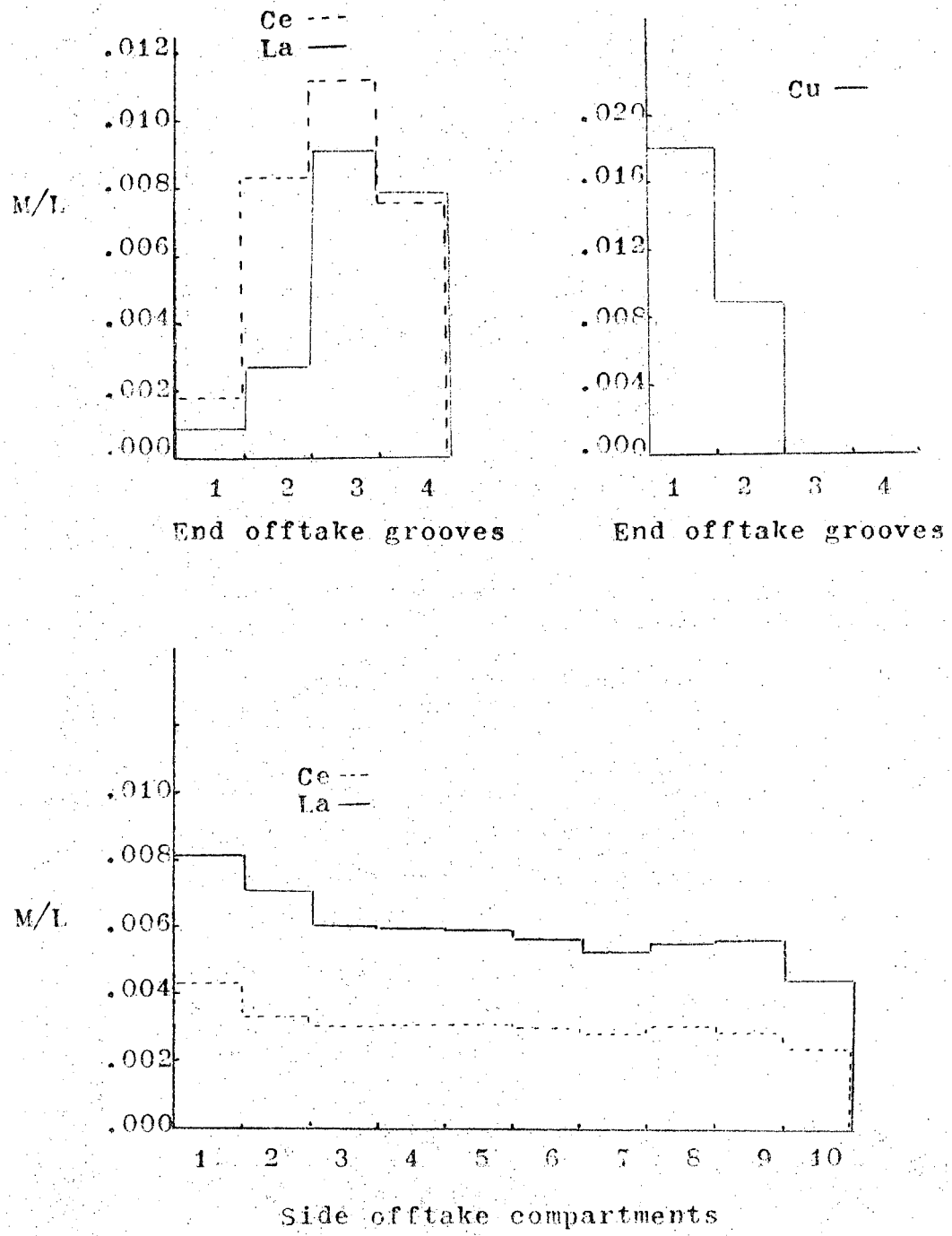

Fig. 34. Offtake patterns after 2τ for S = 1. End feed: 0.01 M $La(NO_3)_3$, 0.01 M $Ce(NO_3)_3$, 0.01 M $(EDTA)Na_2$. Chaser feed at anode side side compartments: 0.03 M $Cu(NO_3)_2$, 0.06 M $NaNO_3$. Wash solution: 0.01 M $NaNO_3$. Electrode compartment solution: 0.1 M $NaNO_3$. Applied 20 volts. Bed voltage = 8 volts. τ = 1 hour.

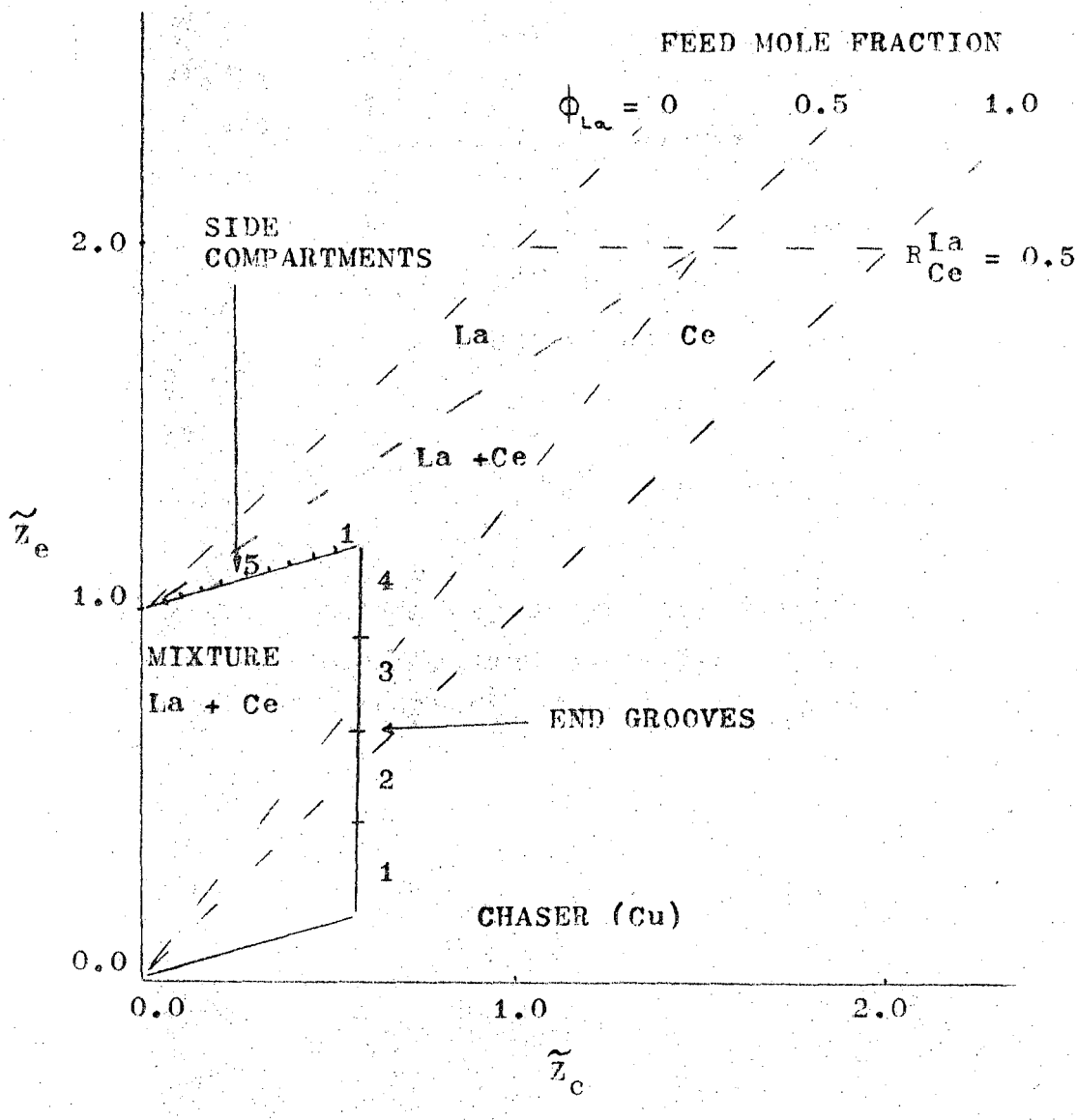

Fig. 35. Column boundaries for conditions in Fig. 34 superimposed on design graph, for (rare earth mobility)/(complexed ion mobility) = -4.

patterns in Fig. 34 do follow the pattern predicted from Fig. 35. Figure 35 predicts chaser ion in end offtake grooves 1 and 2, and Cu^{++} is found only in those two. Ion preferred by the ligand is expected in groove 2 along with chaser, and mixture is expected in grooves 3 and 4 and in all the side compartments. Offtake groove 2 is found to be rich in Ce^{+++}, the preferred ion. The side compartments, containing the uncomplexed ions from the mixture zone, are found to be rich in the less tightly complexed ion (La^{+++}), as expected.

The end offtake concentrations for the rare earths are of the same order as the feed concentrations; those for the side compartments are roughly one-half the feed concentrations. These side-compartment concentrations correspond to the ions collected in these compartments during intervals of one residence time. By exchanging these side-compartment solutions only every two or three residence times, a corresponding two- or three-fold increase in concentrations could have been obtained. Conversely, more frequent sampling of these compartments would result in more dilute concentrations.

In the succeeding run, column conditions were readjusted early in the run to give more complete separation of one component. Figure 36 shows the resulting offtake patterns. Figure 37 shows the column boundaries for this run superimposed on the theoretical design graph; almost complete separation of Ce^{+++} is expected. In practice, as Fig. 36 shows, a nearly complete separation was achieved; however, some trailing of La^{+++} into grooves 2 and 3 did occur. The inlet column temperature for this run was 26°C; the maximum temperature reached downstream was 33°C. It is believed

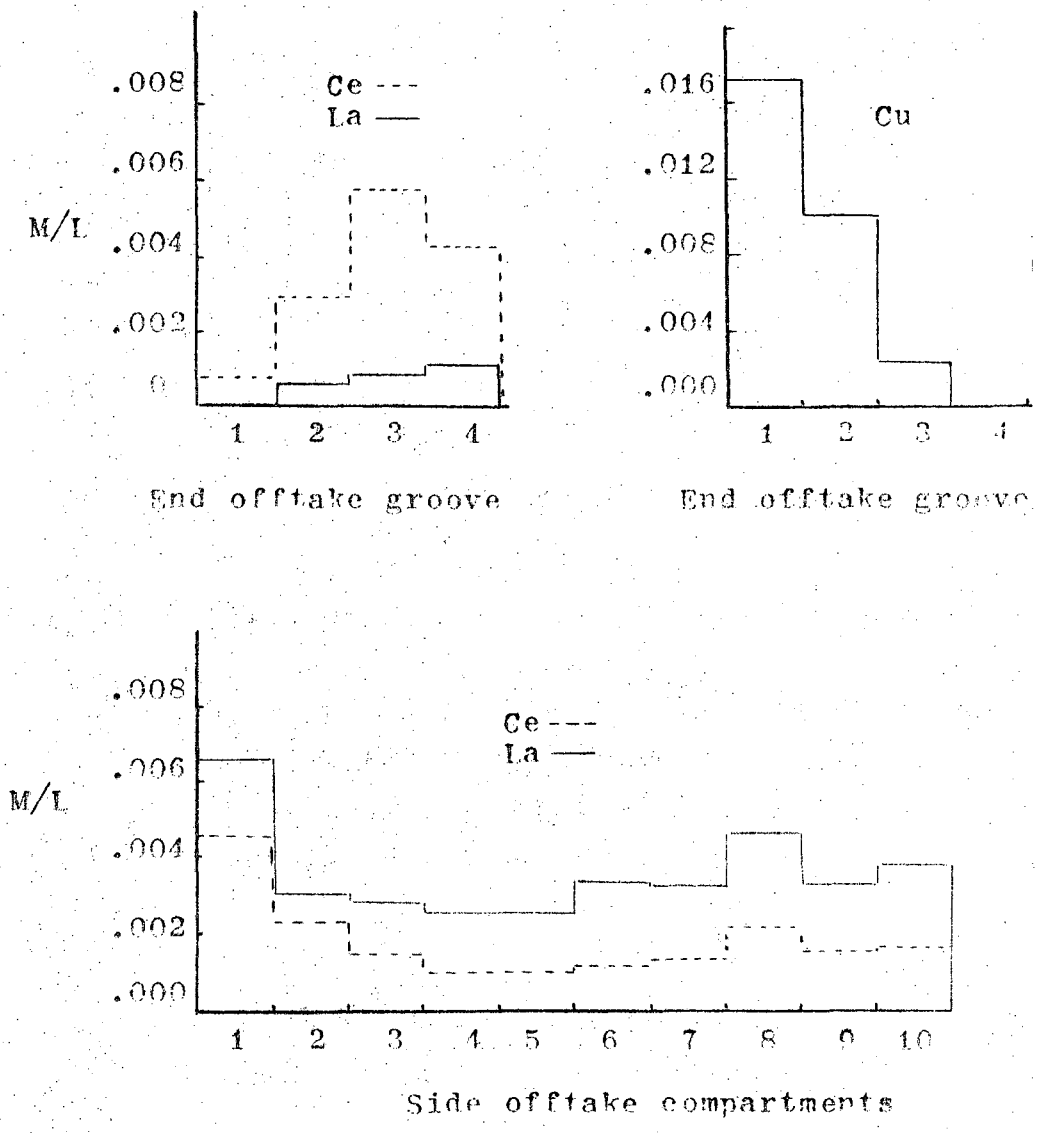

Fig. 34 Offtake patterns after 1τ for S = 0.5. End feed: 0.0075 M $La(NO_3)_3$, 0.0075 M $Ce(NO_3)_3$, 0.01 m $(EDTA)Na_2$. Chaser feed at anode side compartments: 0.03 M $Cu(NO_3)_2$, 0.12 M $NaNO_3$. Wash solution: 0.2 M $NaNO_3$. Applied voltage: 20 volts. Bed voltage: 12 volts. τ = 2 hours.

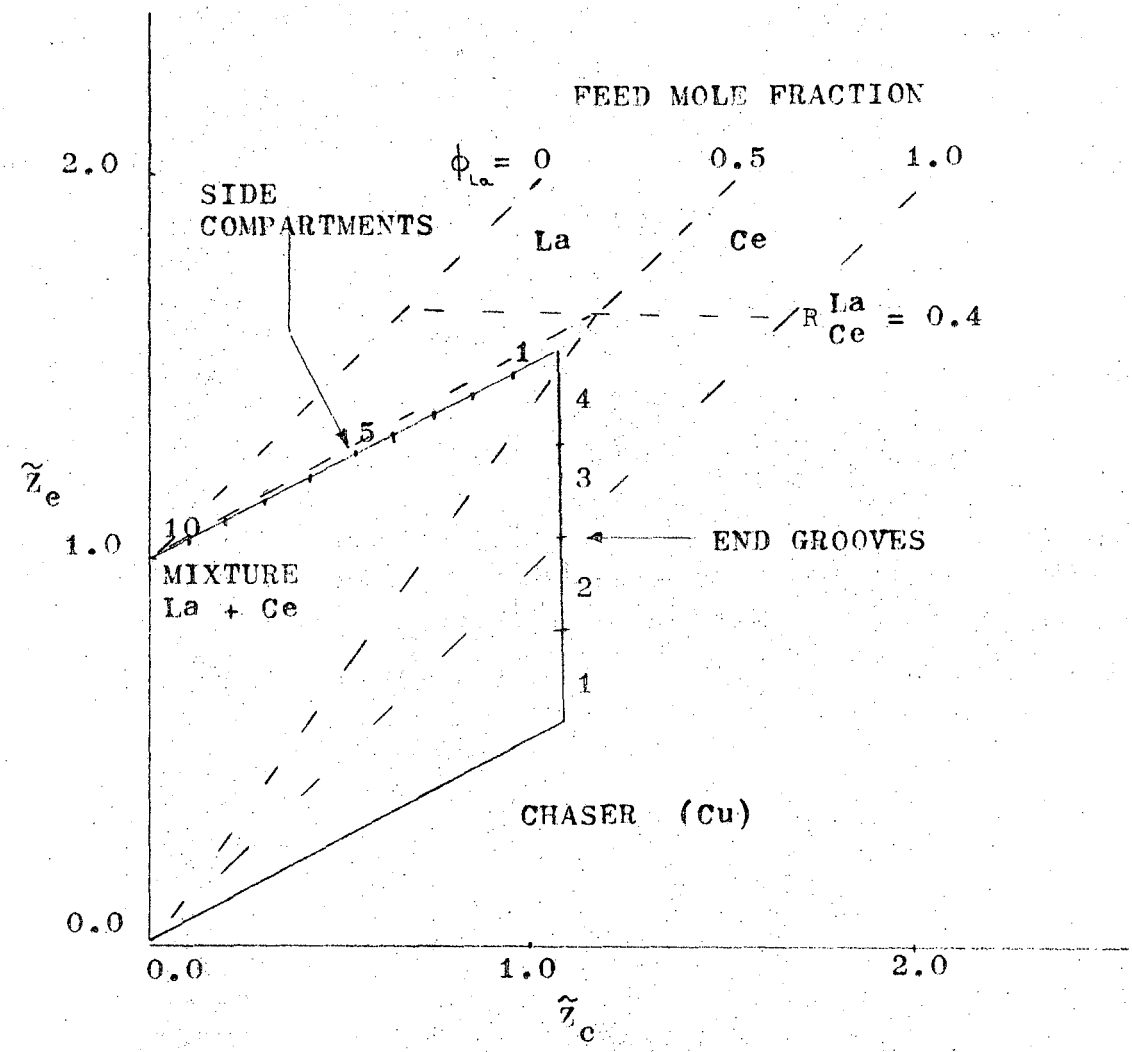

Fig. 37. Column boundaries for conditions in Fig. 36 superimposed on design graph, for the case (rare earth mobility)/(complexed ion mobility) = -4.

that trailing was caused by slow kinetics of exchange of uncomplexed rare earth ions with the complexed species. The side-compartment solutions, again representing the concentrations accumulated in one residence time, show higher ratios of La^{+++} to Ce^{+++} than in the run in Fig. 34. This is due to the lower ratio of uncomplexed to complexed rare earths used in this run (S = 0.5 instead of 1.0).

In both runs reported above (for S = 1.0 and 0.5), the wash solution fed to the cathode side compartments contained only $NaNO_3$. Consequently the complexed ligand was partially diverted away from end off-take groove 4 for S = 1.0 and partially away from 3 and 4 for S = 0.5 by its electromigration. To remedy this situation, $(EDTA)Na_2$ was used in the side-compartment wash solution, to help insure the presence of ligand throughout the bed. To keep the flow of ligand into the bed from the side compartment steady, frequent exchange of the wash solution in the stagnant side compartments was required, leading to lower concentrations of rare earths in these compartments.

The next run used disodium EDTA in the side compartment, with the effect that sodium served as a retainer ion. Thus, with use of a low value of S (about 0.25), it was expected that the cathode side boundary of the column (superimposed on the design graph) would shift into the pure lanthanum-ion zone, and that complete separation of both components would become theoretically possible.

Figure 38 gives the result of this trial. To raise the bed temperature up to about 50°C, so as to help the kinetics, higher concentrations and voltages (up to 60V) were employed. The subsequent rapid

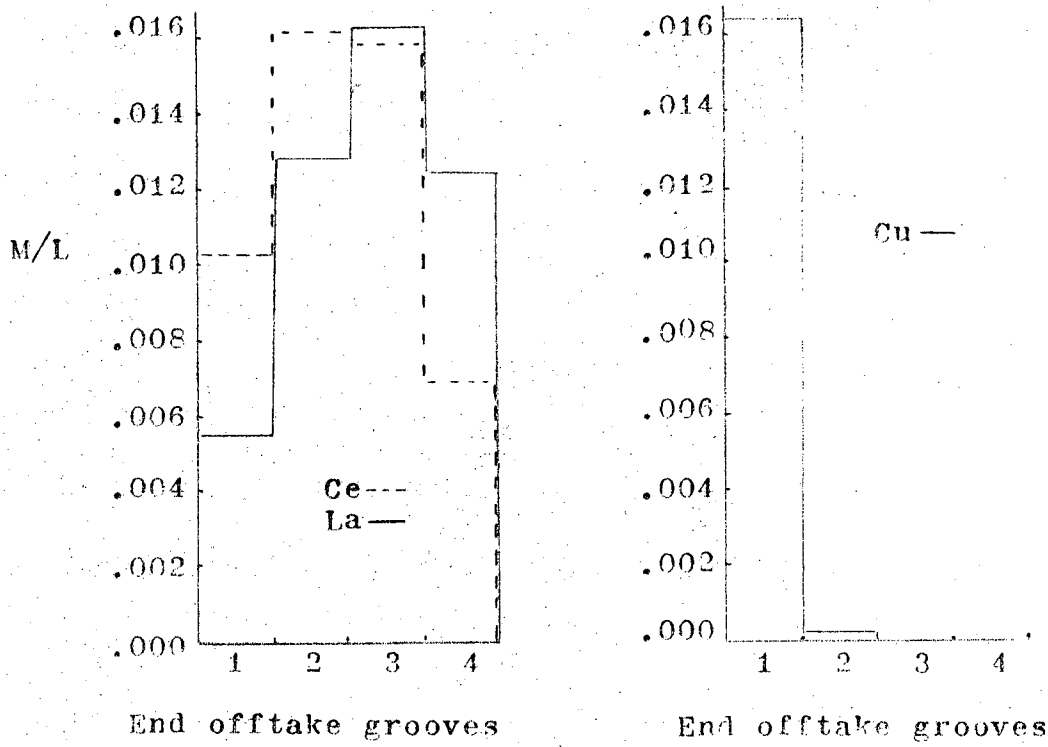

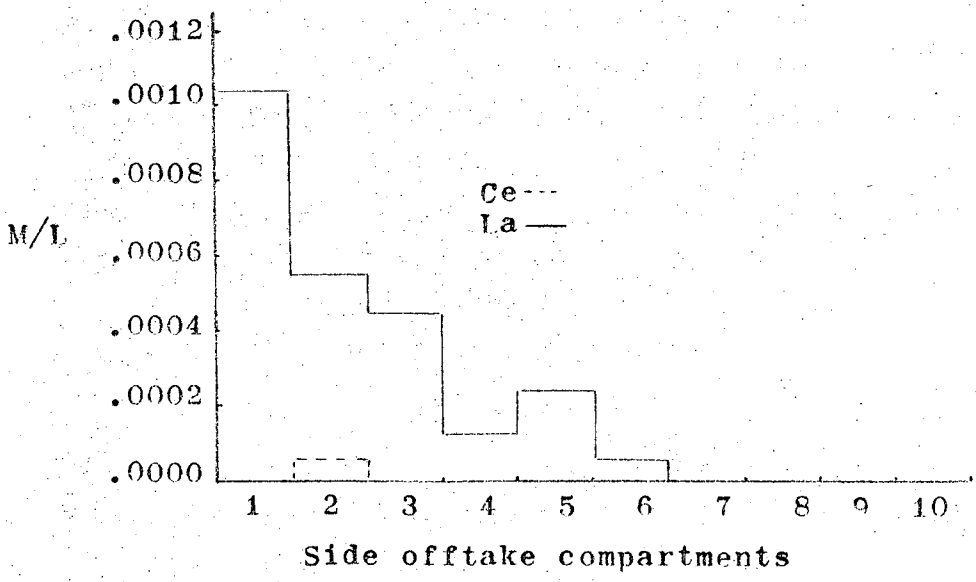

Fig. 38 . Offtake patterns after 2τ for S = 0.25. End Feed: 0.0125 M $La(NO_3)_3$, 0.0125 M $Ce(NO_3)_3$, 0.02 M $(EDTA)Na_2$ Chaser feed: 0.03 M $Cu(NO_3)_2$, 0.24 M $NaNO_3$. Wash solution: 0.01 M $(EDTA)Na_2$, 0.02 M $NaNO_3$. Electrode compartment solution: 0.3 M $NaNO_3$. Applied 40 volts. Bed voltage = 20 volts. τ = 0.5 hours.

increase in temperature forced a reduction in applied voltage to 40 volts. To keep the bed from drying out, it was cooled quickly by halving the residence time. For the resulting operating conditions, the calculated column boundaries are drawn on the design graph shown in Fig. 39, which show that separation of La^{+++} into the side compartments is expected. The results in Fig. 38 bear this out; Ce^{+++} is just beginning to separate from the mixture in grooves 1 and 2, while La^{+++}, pure except for a trace of Ce^{+++}, is obtained in the side compartments. Dut to the low fraction of uncomplexed rare earths (S = 0.25), and since the side-compartment solution was changed every ten minutes, the concentrations of rare earths in the side compartment are much lower than the feed concentrations.

In all three runs reported here, the transitions between rare earths and chaser ion are fairly sharp. The overlap distance in all cases is roughly 1 cm, somewhat more than the 0.5 cm predicted. Slow kinetics of exchange, or partial drying of the bed resulting in channelling, could account for this.

Recommended Future Work

The further study needed can be projected along three theoretical and six experimental lines.

1) Extend design predictions for separation to more than two components.

2) Incorporate metal-ligand complex mobility (for anionic and for cationic migration) into the design graph. It may be possible to combine the two alternate feed positions (end and side) by use of a

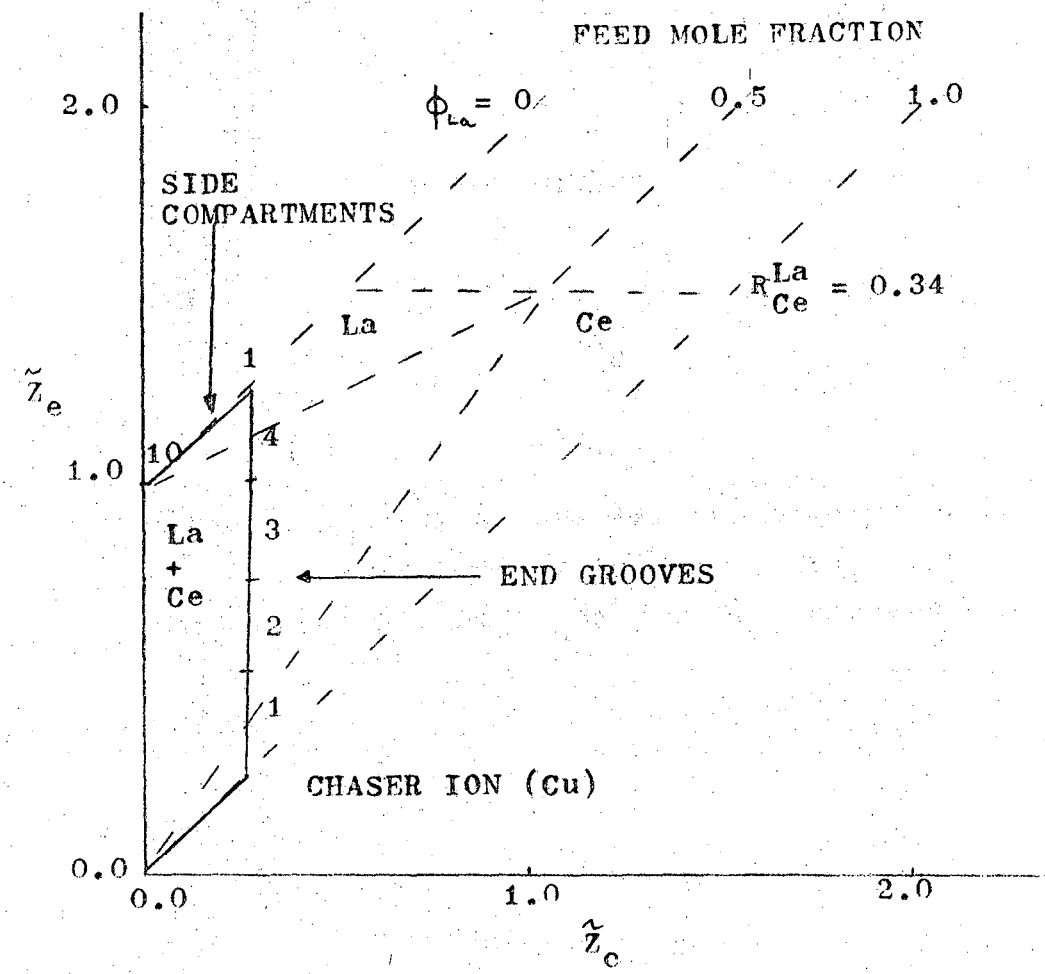

Fig. 39. Column boundaries for conditions in Fig. 38 superimposed on design graph, for (rare earth mobility)/(complexed ion mobility) = -4.

composite algebraic term. This would then result in only one set of parameters and one set of feed fractions in the design graph.

3) Investigate modifications to or adjustments of the equilibrium theory, to account for possible slow kinetics and subsequent lack of equilibrium at each point in the column.

4) Investigate other ligands such as HEDTA and DPTA in regard to selectivity and reaction rates.

5) Investigate other packing materials such as glass beads. The polystyrene beads used tends to dry out as the temperature rises, and to clump.

6) Incorporate additional voltage probes so as to measure voltage-gradient uniformity along the entire length. Local changes in gradient would provide immediate evidence of drying-out or other operational difficulties.

7) Searth for other possible anion-exchange membranes with reduced tendency to shrink or crack upon drying.

8) Investigate alternate diaphragm materials, possibly of sandwich construction, to provide equivalent physical strength with higher permeability.

9) Investigate the steady-state boundary sharpening (or width of overlap zone), as between two initially separated feeds, in relation to metal-ligand ratio, ligand selectivity, mobility of complexed species, and differences in mobility of the uncomplexed metal ions (for example, between ions of different valence).

References

1. K. Marek and R. Pribil, Collection Czechoslov. Chem. Commun. 20, 715 (1955).
2. H. C. Hershey, R. D. Mitchell, and W. H. Wobb, J. Inorg. Nucl. Chem. 28, 645 (1966).
3. M. Lederer, J. of Chromatography 1, 86 (1958).
4. K. Bril, S. Bril, and P. Krumholz, J. Phys. Chem. 63, 256 (1959).
5. H. H. Strain and J. C. Sullivan, Anal. Chem. 23 (6), 816 (1951).
6. E. N. Lightfoot, J. Phys. Chem. 61, 1868 (1957).
7. L. G. Sillen, Arkiv. for Kemi. 2, 477 (1950).
8. E. Ravoo, P. J. Gellings, and T. Vermeulen, T. Analytica. Chimica. Acta. 38, 219 (1967).
9. R. A. Bailey and A. Steiger, J. of Chromatography 25, 442 (1966).
10. S. S. Jones and F. A. Long, J. Phys. Chem. 56, 26 (1952).
11. I. V. Tananaev and G. V. Shevchenko, Russian J. of Inorganic Chem. 6, 974 (1961).
12. J. R. Rhodes, Analyst 91, 683 (1966).
13. H. R. Bowman, E. K. Hyde, S. G. Thompson, and R. C. Jared, Science 151, 562 (1966).
14. R. D. Giauque, Analytical Chem. 40, 2075 (1968).

TECHNICAL INFORMATION DIVISION
LAWRENCE RADIATION LABORATORY
UNIVERSITY OF CALIFORNIA
BERKELEY, CALIFORNIA 94720